CAPITAL UNIVERSITY OF SCIENCE AND
TECHNOLOGY, ISLAMABAD

Orthogonal and Non Orthogonal Stagnation Point Flows

by

Yasir Mehmood

A thesis submitted in partial fulfillment for the
degree of Doctor of Philosophy

in the

Faculty of Computing
Department of Mathematics

2018

Orthogonal and Non Orthogonal Stagnation Point Flows

By

Yasir Mehmood

(PA131004)

Foreign Evaluator No. 1

Dr. Bengisen Pekmen Geridnmez

TED University, Kolej ankaya Ankara Turkey

Foreign Evaluator No. 2

Dr. Abderrahim Ouazzi

Technische Universitt Dortmund Fakultt fr Mathematik, Dortmund, Germany

Prof. Dr. Muhammad Sagheer

(Thesis Supervisor)

Prof. Dr. Muhammad Sagheer

(Head, Department of Mathematics)

Prof. Dr. Muhammad Abdul Qadir

(Dean, Faculty of Computing)

DEPARTMENT OF MATHEMATICS

CAPITAL UNIVERSITY OF SCIENCE AND TECHNOLOGY

ISLAMABAD

2018

To my Beloved Family and Respected Teachers

CAPITAL UNIVERSITY OF SCIENCE & TECHNOLOGY
ISLAMABAD
Expressway, Kahuta Road, Zone-V, Islamabad
Phone:+92-51-111-555-666 Fax: +92-51-4486705
Email: info@cust.edu.pk Website: https://www.cust.edu.pk

CERTIFICATE OF APPROVAL

This is to certify that the research work presented in the thesis, entitled "**Orthogonal and Non Orthogonal Stagnation Point Flows**" was conducted under the supervision of **Dr. Muhammad Sagheer**. No part of this thesis has been submitted anywhere else for any other degree. This thesis is submitted to the **Department of Mathematics, Capital University of Science and Technology** in partial fulfillment of the requirements for the degree of Doctor in Philosophy in the field of **Mathematics**. The open defence of the thesis was conducted on **18 July, 2018.**

Student Name : Mr. Yasir Mehmood (PA131004) Yasir

The Examining Committee unanimously agrees to award PhD degree in the mentioned field.

Examination Committee :

(a) External Examiner 1: Dr. Amir Rasheed
Assistant Professor
LUMS, Lahore

(b) External Examiner 2: Dr. Muhammad Kamran,
Assistant Professor
COMSATS University,
Wah Cantt Campus

(c) Internal Examiner : Dr. Javed Iqbal Siddiqui
Associate Professor
Capital University of Science & Technology, Islamabad

Supervisor Name : Dr. Muhammad Sagheer
Professor
Capital University of Science & Technology, Islamabad

Name of HoD : Dr. Muhammad Sagheer
Professor
Capital University of Science & Technology, Islamabad

Name of Dean : Dr. Muhammad Abdul Qadir
Professor
Capital University of Science & Technology, Islamabad

AUTHOR'S DECLARATION

I, **Mr. Yasir Mehmood (Registration No. PA131004)**, hereby state that my PhD thesis titled, '**Orthogonal and Non Orthogonal Stagnation Point Flows**' is my own work and has not been submitted previously by me for taking any degree from Capital University of Science and Technology, Islamabad or anywhere else in the country/ world.

At any time, if my statement is found to be incorrect even after my graduation, the University has the right to withdraw my PhD Degree.

(**Mr. Yasir Mehmood**)

Dated: July 18, 2018

Registration No : PA131004

PLAGIARISM UNDERTAKING

I solemnly declare that research work presented in the thesis titled "**Orthogonal and Non Orthogonal Stagnation Point Flows**" is solely my research work with no significant contribution from any other person. Small contribution/ help wherever taken has been duly acknowledged and that complete thesis has been written by me.

I understand the zero tolerance policy of the HEC and Capital University of Science and Technology towards plagiarism. Therefore, I as an author of the above titled thesis declare that no portion of my thesis has been plagiarized and any material used as reference is properly referred/ cited.

I undertake that if I am found guilty of any formal plagiarism in the above titled thesis even after award of PhD Degree, the University reserves the right to withdraw/ revoke my PhD degree and that HEC and the University have the right to publish my name on the HEC/ University Website on which names of students are placed who submitted plagiarized thesis.

(Mr. Yasir Mehmood)
Registration No. PA131004

Dated: 18 July, 2018

Acknowledgements

Veneration for **Allah** almighty, who created us among the humans, the supreme beings, the Muslims and bestowed with the discernment to distinguish the right from wrong. Obeisance to the Omniscient who adorned the Universe with the Holy Prophet, **HAZRAT MUHAMMAD (Sallallahu Alaihay Wa'alihi wasalam)** the prime cause of the creation of macrocosm, the one who transformed the twilight of the deserts of ignorance into the illuminated oasis of knowledge and directed humanity towards the path of heaven. I would like to express my sincere gratitude to **Dr. Muhammad Sagheer** for his persistent, continuous, dedicated and pertinent guidance that kept me motivated to complete thesis. During my studies **Dr. Muhammad Sagheer** not only helped me in resolving the mysteries of fluid dynamics but also made me realize the importance of dedication, consistency and time management. It has been an honor to have him as my supervisor for my PhD thesis. He has always encouraged my research work and has advised me patiently by providing insightful suggestions. I would also like to thank all the faculty members of Mathematics department of the Capital University of Science and Technology especially **Dr. Shafqat Hussain**, for that they provided an environment, which was conducive for honing my theoretical knowledge and enhancing my skills. In addition, they ensured me that I have learnt how to utilize the concepts and skills in solving active research problems. I also want to thank all the members of computational fluid dynamics research group especially **Khalid Mehmood, Sajid Shah** who have always provided me a pleasant environment to think of innovative ideas and continue research. I would like to express my gratitude especially to **Muhammad Bilal** for his brotherly advice and timely support; whenever I needed it the most. He was always the beacon of hope for me and lifted my spirits, when I was affected by research blues. I dedicate this PhD thesis to my friends and family, especially my sweet wife, lovely child, Abdul Wasay who is the pride and joy of my life. Finally, I wish to thank my parents, brothers and sister for their love and encouragement, without whom I would never have enjoyed so many opportunities.

List of Publications

1. **Y. Mehmood**, M. Sagheer, S. Hussain and M. Bilal, "MHD stagnation point flow and heat transfer in viscoelastic fluid with Cattaneo-Christov heat flux model", *Neural Computing & Applications*, http://doi.org/ 10.1007/s00521-017-2902-2, 2017.

2. M. Bilal, M. Sagheer, S. Hussain, and **Y. Mehmood**, "MHD stagnation point flow of Williamson fluid over a stretching cylinder with variable thermal conductivity and homogeneous/heterogeneous reaction", *Communications in Theoratical Physics*, 67, 688-696, 2017.

3. **Y. Mehmood**, M. Sagheer and S. Hussain, "MHD oblique stagnation point flow of nanofluid over a convective stretching surface", *Journal of Computational and Theoretical Nanoscience*, 14, 1724-1734(11), 2017.

Abstract

In this dissertation, the orthogonal and non orthogonal stagnation point flows for different types of fluids have been investigated. We analyze the heat and mass transfer effects on magnetohydrodynamics (MHD) orthogonal stagnation point flow in viscoelastic fluid with Cattaneo-Christov heat flux model. Furthermore MHD orthogonal stagnation point flow of Williamson fluid over a stretching cylinder with variable thermal conductivity and homogeneous/heterogeneous reaction is studied. The MHD oblique stagnation point flow of nanofluid over a convective stretching surface has also been presented. To model the system of partial differential equations, different emerging laws of Physics are used. To convert the system of partial differential equations into the ordinary differential equations, some suitable transformations named as the similarity transformations are utilized. Further, the system of ordinary differential equations is tackled by the classical shooting method to obtain the numerical solution of the proposed problems. Tables are constructed and graphs are plotted to observe the trend of those parameters for which the significant effects are observed. To validate the numerical solution, the MATLAB built-in function bvp4c is also implemented. An excellent agreement is observed in the results obtained by two different ways i. e. shooting method and built-in function bvp4c. A comparison with the previously available literature in limiting cases is also performed to strengthen the reliability of the code. It is analyzed that in case of the non orthogonal stagnation point flows for the Newtonian fluid, the point of zero skin friction along the wall undergoes a shift in the position with the variations in the magnetic parameter, angle of incidence and sretching ratio parameter.

Contents

List of Figures

List of Tables

Symbols

a, c	constants
b	slip coefficient
C	concentration field
D	mass diffusion
e	stretching ratio parameter
k	thermal conductivity
l	characteristic length
m, n	dimensionless concentration
M	magnetic parameter
p	pressure
Q	heat generation coefficient
R	radius of cylinder
s, t	dimensional constants
T	temperature of fluid
(u, v)	velocity components
(x, y)	coordinate axis
A_1, B_1	chemical species
a_1, b_1	concentration of A_1, B_1
B_0	magnetic field strength
C_f	skin friction coefficient
C_W	concentration at stretching surface
C_∞	ambient concentration
c_p	specific heat
D_{A_1}	diffusion species coeff. of A_1
D_{B_1}	diffusion species coeff. of B_1
D_B	Brownian diffusion coefficient
D_T	thermophoretic diffusion coefficient

f'	dimensionless velocity
k_1	reaction rate
l_s	heterogeneous reaction rate constant
L_1	strength of homogeneous reaction
L_s	strength of heterogeneous reaction
l_1	homogeneous reaction rate constant
Nt	thermophoresis parameter
Nb	Brownian motion parameter
Nu	Nusselt number
Pr	Prandtl number
q_w	heat flux
Re	Reynolds number
r_1	stretching parameter in normal direction
r_2	Biot number
Sc	Schmidt number
T_w	wall temperature
T_∞	ambient temperature
u_e	ambient velocity
U_0, V_0	constants
U_w	stretching velocity along x-axis
$\mathbf{q}$	heat flux
$\mathbf{V}$	velocity vector
$(\rho c)_f$	heat capacity of the fluid
$(\rho c)_p$	heat capacity of the nano particles
α	thermal diffusivity
β	elasticity number
λ	Weissenberg number
η	similarity variable
ρ	density of fluid
ν	kinematic viscosity
σ	electrical conductivity
θ	dimensionless temperature
ϕ	dimensionless concentration
γ	thermal relaxation time
Γ	Williamson parameter
ψ	stream function

ε	thermal conductivity parameter
λ_0	free path of molecular mean
λ_1	relaxation time of the fluid
λ_2	relaxation time of heat flux
σ_v	tangential momentum accommodation
γ_1	chemical reaction parameter
γ_2	angle of incidence
γ_3	curvature parameter
β_1	heat generation coefficient
τ_w	wall shear stress
δ_1	rate of mass diffusion coefficient
ϕ_1	thermal stratification parameter

Chapter 1

Introduction

1.1 Introduction

This Chapter contains some basic study related to the non-Newtonian and Newtonian fluids over different type of geometries. A discussion related to the heat transfer mechanism is made in accordance with the Fourier's and non-Fourier's law over cylinder and stretching sheet. A brief history and importance of boundary layer rheology for an upper-convected Maxwell fluid, nanofluid, stagnation point and magnetohydrodynamic flow is presented.

1.2 History

In nature, heat transfer in a fluid has a significant effect which happens due to difference in temperature within body or between two bodies. Many researchers have worth seeing contributions in this regard like [1–8]. In various practical situations, Fourier's model provides the basis to analyze the heat transfer phenomenon. But its major drawback is that energy equation in its parabolic form which produces an initial disturbance that can alter the whole system. To counter this shortcoming, Cattaneo [9] amalgamated the thermal relaxation time within the classical Fourier's law in order to get the hyperbolic energy equation. By introducing thermal relaxation time rather than diffusion in Fourier's law, heat transfer in the pattern of waves with limited speed is observed. In order to obtain invariant formulation of the material, Christov [10] modified the Cattaneo law with

the amalgamation of thermal relaxation time for the Oldroyd's upper-convected derivatives. The study of thermal convection in the Cattaneo-Christov model was carried by Straughan [11]. For the incompressible fluid, Tibullo and Zampoli [12] explained the uniqueness of Cattaneo-Christov heat flux model. Han et al. [13] inspected the coupled flow and heat transfer phenomenon in an upper-convected Maxwell (UCM) fluid over a stretching sheet by employing Cattaneo-Christov heat flux model. Khan et al. [14] analyzed the UCM fluid combined with heat transfer effects over an exponentially stretching surface by taking into account the Cattaneo-Christov heat flux model.

The Maxwell fluid has received a prominent consideration of researchers in the recent era. The main advantage of Maxwell fluid is that it incorporates the relaxation time for the viscoelastic fluid in the boundary layer flow. Choi et al. [15] explored the flow of Maxwell fluid in a channel, in which, by increasing the Deborah number, the viscoelasticity influenced the velocity profile in the same pattern as that of inertia in a Newtonian fluid with a constant Reynolds number. The MHD UCM fluid in relevance with the boundary-layer flow over a porous channel was studied by Abbas et al. [16], in which they considered the mutual effects of viscoelasticity, inertia and applied magnetic field to yield an analytical solution. The impact of MHD and thermal radiation on the Maxwell fluid over a stretching sheet was analyzed by Aliakbar et al. [17]. According to their observation, a boost in the magnetic parameter and elasticity number caused an enhancement in the heat transfer rate from the stretching sheet to the fluid. Mustafa [18] considered an UCM fluid for rotational type of flow and analysis of transfer of heat by employing the Cattaneo-Christov heat flux model. Kumaria and Nath [19] examined the MHD stagnation-point mixed convection flow of an UCM fluid. Kumaria and Nath [19] concluded that with an increment in the elasticity number, reduction in the surface heat transfer, surface velocity gradient and displacement thickness was experienced. Sadeghy et al. [20] explored the stagnation point flow of an UCM fluid wherein they negate the previously well-established prediction about the stagnation point flow of viscoelastic fluids, which stated that the velocity within the boundary layer may outrun from the layer that exists outside. Hayat et al. [21] explored the stagnation point flow of an UCM fluid for the process of mass transfer. The effect on the stagnation point flow of an UCM fluid for heat transfer on a stretching sheet was scrutinized by Hayat et al. [22]. Hayat et al. [23] discussed the stagnation point flow and heat flux in the Cattaneo-Christov

model over a nonlinear stretching surface of the variable thickness along with the homogeneous -heterogeneous reactions in Maxwell fluid having variable thermal conductivity.

Mass transfer phenomenon is the mechanism of mass transition from one domain to another. Many scientific mechanisms and disciplines containing atoms and molecule-transportation are based on this phenomenon. The water vaporization, separation of chemicals during distillation procedure and by using natural or artificial sources, diffusion of industrial pollution in rivers and oceans are examples of the process of mass transfer. Kendoush [24] investigated the effects of mass and heat transfer over solid surfaces near the stagnation region. Mass and heat transfer impacts on the magnetic flow for a linear stretching sheet was investigated by Liu [25]. Cortell [26] studied different phenomenon of chemical reaction over mass transfer of two categories of viscoelastic fluids over a porous stretching sheet. Sui et al. [27] recently investigated the upper-convected Maxwell nanofluid in accordance with the boundary layer flow of mass and heat transfer by using the double-diffusion Cattaneoe-Christov model with boundary slip condition for linear stretching sheet.

Heat transfer analysis over a stretching cylinder is one of the current research topics among researchers by virtue of its extensive applications in many engineering processes. Usually, the thermal conductivity is taken as constant. Heat is transferred due to difference in temperature. If there is a large temperature difference, then assumption of constant thermal conductivity will lead to a noticeable error. Thus, to minimize this type of error, it is necessary to deal with a temperature dependent variable thermal conductivity within the energy boundary layer region. Hussain et al. [28] inspected the effect of hydromagnetodynamics Jeffrey fluid flow on heat transfer along with the variable thermal conductivity. They used the inclined magnetic field on peristaltic flow and obtained the solution analytically using the perturbation method. Lin et al. [29] presented the numerical solution of unsteady pseudo-plastic nanoliquid within a thin film flow over a linearly stretching surface. They inspected the repercussion of viscous dissipation and variable thermal conductivity along with four different types of nanoparticles. The influence of variable thermal condutivity on an exponentially stretching sheet for a third grade fluid using the inclined magnetic field was explored by Hayat et al.

[30]. In another research article, Hayat et al. [31] documented the significance of variable thermal conductivity and mixed convection with heat source and sink on the viscoelastic nanofluid over a stretching cylinder. Si et al. [32] explored numerically the laminar film condensation of non-Newtonian pseudo-plastic fluid on an isothermal vertical plate with a variable thermal conductivity. Malik et al. [33] inspected the heat transfer phenomenon of Williamson fluid with heat generation/absorption and variable thermal conductivity passing over a stretching cylinder. They examined that an enlargement in the parameter of thermal conductivity intensifies the temperature. The references [34–37] include some recent work relevent to the variable thermal conductivity.

An extensive literature can be found regarding the non-Newtonian fluid flow over a stretching cylinder by virtue of its engineering and industrial applications such as metallurgical processes, extraction of petroleum, pipe industry and many others. Numerous models have been proposed to analyze the pseudo-plastic fluids e.g. Carreaus model, Power law model, Ellis model, Cross model and Williamson fluid model. A variable viscosity of larger range is considered in the Williamson fluid model. Williamson [38] introduced a model that describes the pseudo-plastic materials and fluid flow experimentally. Malik and Salahuddin [39] used the Williamson fluid model along with the effect of magnetohydrodynamics over a stretching cylinder. Solutions are achieved by the shooting method for the fluid flow. Malik et al. [40] addressed the heat transfer analysis of Williamson fluid past a stretching cylinder with homogeneous/heterogeneous reaction by using the Keller box method. In another article, Salahuddin et al. [41] numerically investigated the hydromagnetodynamics flow for Williamson fluid with Cattaneo-Christov heat flux model over a non-linear stretching surface. Explicit finite difference method is employed for the numerical solutions. Hayat et al. [42] offered an overview of the literature about the MHD boundary layer flow of Williamson fluid with Ohmic dissipation and thermal radiation. They noticed the decreasing pattern of Weissenberg number on velocity profile. A list of references concerning Williamson fluid can be found in [43–45].

A phase is claimed to be a uniform state of a system which has no observable boundary. In chemical reactions, the homogeneous reactions are categorized as a single phase reactions whereas the heterogeneous reactions are categorized as

multiphase reactions. Chemical reaction rate is enhanced by adding suitable catalyst in the reactant having lesser activation energy. Recently, a very hot area of research among the scientists in chemical reactions is the amalgamation of heterogeneous and homogeneous reactions and their complicated interactions. Hayat et al. [46] examined the Jeffrey fluid flow along with the homogeneous-heterogeneous reaction by adopting the Cattaneo-Christov heat flux model. They concluded that the concentration of molecules upturns with a raise in the Schmidt number. In another article, Hayat et al. [47] scrutinized a solution of Oldroyd-B fluid with MHD and homogeneous/heterogenenous reaction using the Cattaneo-Christov heat flux model. Reddy et al. [48] analyzed the effect of homogeneous/heterogenenous reaction on MHD and non-linear thermal radiation between rotating plates. They employed the shooting technique for solving the problem. Homogeneous/heterogenenous reaction in magneto-nanofluid in a permeable shrinking surface was inspected by Mansur et al. [49]. During the equivalent process of the diffusion coefficients and auto catalyst of the reactants, homogeneous-heterogenenous reaction in a viscous nanofluid flow past over a stretching sheet was analyzed by Kameswaran et al. [50]. Solutions for flow and heat transfer are computed numerically by the shooting method [51–55] integrated with Runge-Kutta method of order four.

The flow surrounded by a stagnation point has attained a considerable attention among considerable researchers in the course of the previous few decades by virtue of its extensive usage at industrial level, e.g. heat ex-changers situated in an unelevated-velocity profile, nuclear reactors cooling all along emergency restrain, electronic devices cooling by fans, solar central receivers unprotected to wind currents and several hydrodynamic processes. Initially Hiemenz [56] proposed the concept of the stagnation point flow. According to his theory, the stagnation point flow describes the motion of fluid particles which are adjacent to the stagnation region of a solid surface for both fixed and moving bodies. Idea of Hiemenz was further extended by Homann [57] by considering stagnation point flow for the three dimensional case. The two dimensional stagnation point flow striking on an immovable plane with an arbitrary angle of incidence was investigated by several authors [58–60]. An exact similarity solution of the Navier Stokes equations by considering 2-dimensional stagnation point flow for a viscous fluid striking non orthogonally above a stretching sheet was given by Lok et al. [61]. The idea of Lok was further extended by Singh et al. [62] for the porous media. Recently, Dash

et al. [63] provided the numerical solution of the stagnation-point boundary layer flow over a stretching/shrinking sheet. Mabood et al. [64] proposed the heat and mass transfer analysis for the stagnation point magnetic flow of nanofluid combined with viscous dissipation, radiation and chemically reactive properties for porous medium. Stagnation point flow with heterogeneous and homogeneous reactions for Cattaneo-Christov heat flux model was investigated by Hayat et al. [65], in which they detected that the bigger values of the thermal relaxation time exhibit a decay in the temperature distribution. M. Turkyilmazoglu [5] examined the stagnation point flow along with the slip effects on the magnetohydrodynamics Jeffrey fluid and heat transfer over deformable surfaces. The oblique stagnation point flow of a viscoelastic fluid above a stretching surface was evaluated by Labropulu et al. [66]. Mahapatra and Gupta. [67] analyzed the stagnation point flow towards a stretching sheet with heat transfer. Recently electrically conducting and viscous fluid with the existance of a uniform magnetic field over a stretching/shrinking surface in the context of a non orthogonal stagnation point flow is explored by Lok et al. [68].

Heat transfer plays a key role in processes like gas turbines, thermal energy storage, nuclear plants etc. The transfer of heat in a stagnation point fluid flow over a horizontally stretching sheet having a linear velocity was studied by Chiam [69]. Further Guo et al. [70] presented a detailed theory for heat transfer enhancement, in which they established the relationship with heat sources between conduction and convection. The heat transfer problem for a general viscous fluid in a shrinking/stretching sheet along with the convective boundary condition at the wall was explored by Yao et al. [71].

Magnetohydrodynamics is the theory of the magnetic properties of fluids which are electrically conducting. Magnetohydrodynamics oblique stagnation point flow was investigated by Grosan et al. [72], in which they reached the conclusion that the magnetic parameter brings a change in the location of the point of zero skin friction with the wall. Furthermore Singh et al. [73] extended the idea of Grosan et al. [72] with the conclusion that the behavior of boundary layer affects the position of the stagnation point. Nadeem et al. [74] examined the joint effects of partial slip and hydromagnetodynamics on obliquely colliding fluid past over a stretching surface. Oblique stagnation-point flow in addition to MHD over a stretching/shrinking surface was figure out by Lok et al. [75].

Fluids together with the nanoparticles are known as nanofluids. In 1995, Choi and Eastman [76] presented the revolutionary idea that the thermal conductivity of fluids can be amplified by saturating the fluid with the nanoparticles. This work gave a new approach to many engineering problems like cancer therapy, coolants of nuclear reactors, safety problems emerging in nuclear reactors and safer surgeries. According to Wang and Mujumdar [77], the enhancement of heat transfer depends on the quantity of nanoparticles, particle-shape and material type. Buongiorno [78] presented a model, explaining the phenomenon of heat transfer within nanofluids. The study of nanoparticles along with the natural convection phenomenon in a porous medium past over a vertical flat plate in addition to the Brownian motion and thermophoresis effects was scrutinized by Nield and Kuznestov [79]. The dilemma of the boundary layer nanofluid which arises due to the stretching of a surface was studied by Khan and Pop [80]. Thermal radiation and slip effects on stagnation point flow of hydromagnetodynamics for a nanofluid over a stretching sheet was studied by Haq et al. [81]. Moreover Nadeem et al. [82] examined the oblique stagnation point flow of a Casson nanofluid model in addition to the convective boundary conditions.

1.3 Thesis outline

The thesis is comprised of seven chapters. The basic governing laws and numerical technique to deal with the system of differential equations are dicussed in **Chapter 2**.

In **Chapter 3**, MHD stagnation point flow and heat transfer in viscoelastic fluid with Cattaneo-Christov heat flux model is discussed. This chapter is accepted in an international journal , "*Neural Computing & Applications*" ($http://doi.org/10.1007/s00521-017-2902-2$) in 2017.

Chapter 4 is focused on the study of the effects of chemical reaction on stagnation point flow with mass and heat transfer in magneto UCM fluid employed with Cattaneo-Christov heat flux model. This chapter is submitted for possible

publication in "*Romanian Journal of Mathematics and Computer Science*".

Chapter 5 consists of an investigation on MHD stagnation point flow of Williamson fluid over a stretching cylinder with variable thermal conductivity and homogeneous/heterogeneous reaction. This chapter is published in "*Communications in Theoratical Physics*", volume 67, pages 688-696, 2017.

Chapter 6 examines the MHD oblique stagnation point flow of nanofluid over a convective stretching surface. This chapter is published in "*Journal of Computational and Theoretical Nanoscience*", volume 14, pages 1724-1734(11), 2017.

The conclusion of the thesis has been made in **Chapter 7**.

Chapter 2

Basic Governing Laws and Solution Methodology

2.1 Fundamental Laws

2.1.1 Law of Conservation of Mass

The continuity equation or law of conservation of mass is written as

$$\frac{\partial \rho}{\partial t} + \nabla \cdot (\rho \mathbf{V}) = 0. \tag{2.1}$$

For incompressible fluids, the above equation can be expressed in the following way

$$\nabla \cdot \mathbf{V} = 0. \tag{2.2}$$

2.1.2 Law of Conservation of Momentum

The mathematical expression for the law of momentum is

$$\rho \frac{D\mathbf{V}}{Dt} = \nabla \cdot \tau + \rho \mathbf{b}. \tag{2.3}$$

The Cauchy stress tensor for an incompressible flow is $\tau = -p\mathbf{I} + \mathbf{S}$ in which $\frac{D}{Dt}$ is the material time derivative, $\mathbf{S}$ the extra stress tensor, $\mathbf{I}$ the identity tensor and $\mathbf{b}$

the body force. The Cauchy stress tensor and the velocity field are

$$\tau = \begin{bmatrix} \sigma_{xx} & \tau_{xy} & \tau_{xz} \\ \tau_{yx} & \sigma_{yy} & \tau_{yz} \\ \tau_{zx} & \tau_{zy} & \sigma_{zz} \end{bmatrix} \tag{2.4}$$

$$\text{and} \quad \mathbf{V} = [u(x,y,z),\ v(x,y,z),\ w(x,y,z)] \ , \tag{2.5}$$

where σ_{xx}, σ_{yy} and σ_{zz} are the normal stresses, τ_{xy}, τ_{xz}, τ_{yx}, τ_{yz}, τ_{zx} and τ_{zy} stand for the shear stresses and the velocity components along the x, y and z-directions are u, v and w respectively. Eq. (2.3) in the scalar form gets the following shape

$$\rho \left(\frac{\partial\, u}{\partial\, t} + u \frac{\partial u}{\partial x} + v \frac{\partial u}{\partial y} + w \frac{\partial u}{\partial z} \right) = \frac{\partial(\sigma_{xx})}{\partial x} + \frac{\partial(\tau_{xy})}{\partial y} + \frac{\partial(\tau_{xz})}{\partial z} + \rho b_x, \tag{2.6}$$

$$\rho \left(\frac{\partial v}{\partial t} + u \frac{\partial v}{\partial x} + v \frac{\partial v}{\partial y} + w \frac{\partial v}{\partial z} \right) = \frac{\partial(\tau_{yx})}{\partial x} + \frac{\partial(\sigma_{yy})}{\partial y} + \frac{\partial(\tau_{yz})}{\partial z} + \rho b_y, \tag{2.7}$$

$$\rho \left(\frac{\partial w}{\partial t} + u \frac{\partial w}{\partial x} + v \frac{\partial w}{\partial y} + w \frac{\partial w}{\partial z} \right) = \frac{\partial(\tau_{zx})}{\partial x} + \frac{\partial(\tau_{zy})}{\partial y} + \frac{\partial(\sigma_{zz})}{\partial z} + \rho b_z, \tag{2.8}$$

where b_x, b_y and b_z show the components of body force along the x, y and z-axes, respectively. The above equations for the two-dimensional flow become

$$\rho \left(\frac{\partial u}{\partial t} + u \frac{\partial u}{\partial x} + v \frac{\partial u}{\partial y} \right) = \frac{\partial(\sigma_{xx})}{\partial x} + \frac{\partial(\tau_{xy})}{\partial y} + \rho b_x, \tag{2.9}$$

$$\rho \left(\frac{\partial v}{\partial t} + u \frac{\partial v}{\partial x} + v \frac{\partial v}{\partial y} \right) = \frac{\partial(\tau_{yx})}{\partial x} + \frac{\partial(\sigma_{yy})}{\partial y} + \rho b_y. \tag{2.10}$$

2.1.3 Equation of Heat Transfer

By employing the first law of thermodynamics, the heat transfer equation is

$$\rho \frac{d\varepsilon}{dt} = \tau : \mathbf{L} - \nabla \cdot \mathbf{q} + \rho r_h, \tag{2.11}$$

where $\varepsilon = c_p \mathbf{T}$ is the internal energy, $\mathbf{T}$ the temperature, $\mathbf{q} = -k\nabla\mathbf{T}$ denotes the heat flux, $\mathbf{L} = \nabla\mathbf{V}$ the velocity gradient, $\tau : \mathbf{L} = trace(\tau\mathbf{L}) = \sum_{i,j} \tau_{ij}\mathbf{L}_{ij}$ and r_h the radiative heating. The above equation in the absence of radiative heating is

$$\rho c_p \frac{d\mathbf{T}}{dt} = \tau : \nabla\mathbf{V} + k\nabla^2\mathbf{T}. \tag{2.12}$$

2.1.4 Mass Transfer with Chemical Reaction

" According to [83], the general equation of mass transfer when accompanied by a chemical reaction is an unsteady-state mass transport equation, that incorporates not only diffusion but also the convective mass transport and chemical reaction contributions. In the two dimensional form, the equation for mass transfer can be written as follows:

$$\frac{\partial C}{\partial t} + u\frac{\partial C}{\partial x} + v\frac{\partial C}{\partial y} = D\left(\frac{\partial^2 C}{\partial x^2} + \frac{\partial^2 C}{\partial y^2}\right) + R_i, \tag{2.13}$$

where

$$u\frac{\partial C}{\partial x} + v\frac{\partial C}{\partial y}, \tag{2.14}$$

is the convective mass transport contribution and

$$D\left(\frac{\partial^2 C}{\partial x^2} + \frac{\partial^2 C}{\partial y^2}\right), \tag{2.15}$$

is the molecular diffusion contribution, R_i is the chemical reaction contribution, and D is the diffusion coefficient of the liquid."

2.1.5 Boundary Layer Equation of Upper-convected Maxwell Fluid

It is a non-Newtonian fluid model and a simple subclass of the rate type fluids which elaborates the features of linear viscoelastic fluids having only the relaxation time. Example includes polymer solutions of low molecular weight. The extra stress tensor $\mathbf{S}$ for a Maxwell fluid is

$$\left(1 + \lambda_1 \frac{D}{Dt}\right)\mathbf{S} = \mu A_1, \tag{2.16}$$

in which λ_1 is the relaxation time, $\frac{D}{Dt}$ the covariant differentiation, μ denotes the kinematic viscosity and A_1 the first Rivlin - Erickson tensor. The first Rivlin - Erickson tensor can be defined as

$$A_1 = \nabla\mathbf{V} + (\nabla\mathbf{V})', \tag{2.17}$$

where $'$ (prime) denotes the matrix transpose. Here

$$A_1 = \begin{bmatrix} 2\frac{\partial u}{\partial x} & \frac{\partial u}{\partial y}+\frac{\partial v}{\partial x} & \frac{\partial u}{\partial z}+\frac{\partial w}{\partial x} \\ \frac{\partial u}{\partial y}+\frac{\partial v}{\partial x} & 2\frac{\partial v}{\partial y} & \frac{\partial v}{\partial z}+\frac{\partial w}{\partial y} \\ \frac{\partial u}{\partial z}+\frac{\partial w}{\partial x} & \frac{\partial v}{\partial z}+\frac{\partial w}{\partial y} & 2\frac{\partial w}{\partial z} \end{bmatrix}. \tag{2.18}$$

The covariant derivative for a tensor $\mathbf{S}$ of rank two, a vector $\mathbf{a_2}$ and a scalar b_2 are expressed by

$$\frac{D\mathbf{S}}{Dt} = \frac{\partial \mathbf{S}}{\partial t} + (\mathbf{V}\cdot\nabla)\,\mathbf{S} - \mathbf{S}\,(\nabla\mathbf{V})' - (\nabla\mathbf{V})\,\mathbf{S}, \tag{2.19}$$

$$\frac{D\mathbf{a_2}}{Dt} = \frac{\partial \mathbf{a_2}}{\partial t} + (\mathbf{V}\cdot\nabla)\,\mathbf{a_2} - (\nabla\mathbf{V})\,\mathbf{a_2}, \tag{2.20}$$

$$\frac{Db_2}{Dt} = \frac{\partial b_2}{\partial t} + (\mathbf{V}\cdot\nabla)\,b_2. \tag{2.21}$$

Multiplying equation of motion for Maxwell fluid by $\left(1+\lambda_1\frac{D}{Dt}\right)$, we have

$$\rho\,\left(1+\ \lambda_1\frac{D}{Dt}\right)\ \frac{D\mathbf{V}}{Dt} = \ -\ \left(1+\ \lambda_1\frac{D}{Dt}\right)\ \nabla p + \ \left(1+\ \lambda_1\ \frac{D}{Dt}\right)\ (\nabla\cdot\mathbf{S})\,. \tag{2.22}$$

Applying

$$\frac{D}{Dt}\,(\nabla\cdot) = \nabla\cdot\frac{D}{Dt}, \tag{2.23}$$

and invoking the expression for $\mathbf{S}$, we have

$$\rho\,\left(1+\ \lambda_1\frac{D}{Dt}\right)\ \frac{DV}{Dt} = \ -\ \left(1+\ \lambda_1\frac{D}{Dt}\right)\ \nabla p + \nabla\cdot\ \left(1+\ \lambda_1\ \frac{D}{Dt}\right)\mathbf{S}. \tag{2.24}$$

By utilizing the Eq. (2.16) and ignoring the pressure gradient, the above equation takes the following form:

$$\rho\,\left(1+\ \lambda_1\frac{D}{Dt}\right)\ \frac{D\mathbf{V}}{Dt} = \mu\nabla\cdot A_1. \tag{2.25}$$

The component form of the two-dimensional steady flow of Maxwell fluid can be represented by the following expressions:

$$u\frac{\partial u}{\partial x}+v\frac{\partial u}{\partial y}+\lambda_1\left(u^2\frac{\partial^2 u}{\partial x^2}+v^2\frac{\partial^2 u}{\partial y^2}+2uv\frac{\partial^2 u}{\partial x\partial y}\right) = \nu\left(\frac{\partial^2 u}{\partial x^2}+\frac{\partial^2 u}{\partial y^2}\right), \tag{2.26}$$

$$u\frac{\partial v}{\partial x}+v\frac{\partial v}{\partial y}+\lambda_1\left(u^2\frac{\partial^2 v}{\partial x^2}+v^2\frac{\partial^2 v}{\partial y^2}+2uv\frac{\partial^2 v}{\partial x\partial y}\right) = \nu\left(\frac{\partial^2 v}{\partial x^2}+\frac{\partial^2 v}{\partial y^2}\right). \tag{2.27}$$

2.1.6 Boundary Layer Equation of Williamson Fluid

The momentum equation for Williamson fluid is described as follows:

$$\rho\frac{D\mathbf{V}}{Dt} = \nabla\cdot\mathbf{T_0} + \rho\mathbf{b}. \tag{2.28}$$

The Cauchy stress tensor $\mathbf{T_0}$ for an incompressible flow is $-p\mathbf{I}+\mathbf{S}$ in which $\mathbf{I}$ is the identity tensor, τ the extra stress tensor and $\frac{D}{Dt}$ the material time derivative. The extra stress tensor is

$$\tau = \left[\mu_\infty + \frac{\mu_0-\mu_\infty}{1-\Gamma\dot{r}}\right]A_1. \tag{2.29}$$

Here $\mu_\infty, \mu_0, \Gamma, A_1, \dot{r}$ correspond to the viscosity at infinity, viscosity at zero, positive time constant, first Rivlin-Erickson tensor and shear rate. The shear rate is defined as:

$$\dot{r} = \sqrt{\frac{\chi}{2}}, \tag{2.30}$$

where

$$\chi = \frac{trace(A_1^2)}{2}. \tag{2.31}$$

By considering $\mu_\infty = 0$ *and* $\Gamma\dot{r} < 1$, we get the form

$$\tau = \left[\frac{\mu_0}{1-\Gamma\dot{r}}\right]A_1. \tag{2.32}$$

Apply the binomial expansion upto first order.

$$\tau = \mu_0\left[1+\Gamma\dot{r}\right]A_1, \tag{2.33}$$

where

$$\dot{r} = \sqrt{\left[\left(\frac{\partial v}{\partial r}\right)^2 + \frac{v^2}{r^2} + \frac{1}{2}\left(\frac{\partial v}{\partial x}+\frac{\partial u}{\partial r}\right)\right]}, \tag{2.34}$$

$$\tau_{rr} = 2\mu_0\left[1+\Gamma\dot{r}\right]\left(\frac{\partial v}{\partial r}\right), \tag{2.35}$$

$$\tau_{rx} = \mu_0\left[1+\Gamma\dot{r}\right]\left(\frac{\partial v}{\partial x}+\frac{\partial u}{\partial r}\right), \tag{2.36}$$

$$\tau_{\theta\theta} = 2\mu_0\left[1+\Gamma\dot{r}\right]\left(\frac{v}{r}\right), \tag{2.37}$$

$$\tau_{xr} = \mu_0\left[1+\Gamma\dot{r}\right]\left(\frac{\partial v}{\partial x}+\frac{\partial u}{\partial r}\right). \tag{2.38}$$

The component form becomes:

$$\frac{\partial(rv)}{\partial r} + \frac{\partial(ru)}{\partial x} = 0, \tag{2.39}$$

$$u\frac{\partial u}{\partial x} + v\frac{\partial u}{\partial r} = \frac{1}{r}\frac{\partial}{\partial r}\left(r\tau_{rr}\right) + \frac{1}{r}\frac{\partial}{\partial \theta}\left(\tau_{r\theta}\right) + \frac{\partial}{\partial x}\left(\tau_{rx}\right), \tag{2.40}$$

$$u\frac{\partial u}{\partial x} + v\frac{\partial u}{\partial r} = \frac{1}{r}\frac{\partial}{\partial r}\left(r\tau_{rx}\right) + \frac{1}{r}\frac{\partial}{\partial \theta}\left(\tau_{\theta x}\right) + \frac{\partial}{\partial x}\left(\tau_{xx}\right), \tag{2.41}$$

where *u(r, x)* and *v(r, x)* represent the velocity components along and normal to the flow direction. In the absence of the pressure gradiant, boundary layer approximation becomes:

$$\frac{\partial(rv)}{\partial r} + \frac{\partial(ru)}{\partial x} = 0, \tag{2.42}$$

$$u\,\frac{\partial u}{\partial x} + \,v\frac{\partial u}{\partial r} = \nu\left[\frac{1}{r}\frac{\partial u}{\partial r} + \frac{\partial^2 u}{\partial r^2} + \frac{\Gamma}{\sqrt{2}r}\left(\frac{\partial u}{\partial r}\right)^2 + \sqrt{2}\Gamma\frac{\partial u}{\partial r}\frac{\partial^2 u}{\partial r^2}\right]. \tag{2.43}$$

2.1.7 Fourier's Law

The Fourier's law for heat transfer is stated as follows:

$$\mathbf{q} = -k\frac{d\mathbf{T}}{dx}, \tag{2.44}$$

where $\mathbf{q}$ denotes the heat flux and $\frac{d\mathbf{T}}{dx}$ the temperature gradient. The negative sign is used due to the flow of heat in the direction of motion of the negative gradient temperature.

2.1.8 Cattaneo-Christov Law

According to Christov [10], material invariant form of the balance law for the internal energy is:

$$\rho c_p\left(\frac{\partial \mathbf{T}}{\partial t} + \mathbf{V}\cdot\nabla\mathbf{T}\right) = -\nabla\cdot\mathbf{q}. \tag{2.45}$$

The heat flux $\mathbf{q}$ satisfies the following relation:

$$\mathbf{q} + \,\lambda_2\,\left[\frac{\partial \mathbf{q}}{\partial t} + \mathbf{V}\cdot\,\nabla\mathbf{q} - \mathbf{q}\cdot\,\nabla\mathbf{V} + (\nabla\cdot\,\mathbf{V})\mathbf{q}\right] = \,-\,k\,\nabla\mathbf{T}. \tag{2.46}$$

The continuity equation for the incompressible fluid implies $\nabla \cdot \mathbf{V} = 0$, which when used in Eq. (2.46) yields the following:

$$\mathbf{q} + \lambda_2 \left[\frac{\partial \mathbf{q}}{\partial t} + \mathbf{V} \cdot \nabla \mathbf{q} - \mathbf{q} \cdot \nabla \mathbf{V} \right] = - k \nabla \mathbf{T}. \tag{2.47}$$

Eliminating $\mathbf{q}$ from Eqs. (2.47) and (2.45), we get:

$$u \frac{\partial \mathbf{T}}{\partial x} + v \frac{\partial \mathbf{T}}{\partial y} + \lambda_2 \begin{pmatrix} (u \frac{\partial u}{\partial x} + v \frac{\partial u}{\partial y}) \frac{\partial \mathbf{T}}{\partial x} + (u \frac{\partial v}{\partial x} + v \frac{\partial v}{\partial y}) \frac{\partial \mathbf{T}}{\partial y} \\ + u^2 \frac{\partial^2 \mathbf{T}}{\partial x^2} + v^2 \frac{\partial^2 \mathbf{T}}{\partial y^2} + 2uv \frac{\partial^2 \mathbf{T}}{\partial x \partial y} \end{pmatrix} = \alpha \frac{\partial^2 \mathbf{T}}{\partial y^2}. \tag{2.48}$$

2.2 Solution Methodology

We have used two different techniques to deal with the nonlinear ordinary differential equations. The shooting method and a built-in MATLAB function bvp4c.

2.2.1 Shooting Method with RK Scheme

Amongst many numerical schemes to solve the boundary value problems, the shooting method [84] is an appropriate method in which the initial point is shot by retrieving a profile set which assures the trajectory of a profile by changing the initial slope. The targetted value, i.e., the terminal value is achieved by considering different initial guesses because guess is essential for all unknown values as there are not enough initial conditions for the initial value problem. "To learn the mechanism of the method [85], consider the following second order non-linear boundary value problem

$$y''(x) = f(x, y, y'(x)) \tag{2.49}$$

subject to the boundary conditions

$$y(0) = 0, \quad y(L) = A. \tag{2.50}$$

By denoting y by y_1 and y_1' by y_2, Eq. (2.49) can be written as the following system of first order equations.

$$\left.\begin{aligned} y_1' &= y_2, & y_1(0) &= 0, \\ y_2' &= f(x, y_1, y_2), & y_1(L) &= A. \end{aligned}\right\} \tag{2.51}$$

Denote the missing initial condition $y_2(0)$ by s, to have

$$\left.\begin{aligned} y_1' &= y_2, & y_1(0) &= 0, \\ y_2' &= f(x, y_1, y_2), & y_2(0) &= s. \end{aligned}\right\} \tag{2.52}$$

Now the problem is to find s such that the solution of the IVP (2.52) satisfies the boundary condition $y(L) = A$. In other words, if the solutions of the initial value problem (2.52) are denoted by $y_1(x, s)$ and $y_2(x, s)$, one should search for that value of s which is an approximate root of the equation.

$$y_1(L, s) - A = \phi(s) = 0. \tag{2.53}$$

To find an approximate root of the Eq. (2.53) by the Newton's method, the iteration formula is given by

$$s_{n+1} = s_n - \frac{\phi(s_n)}{d(\phi(s_n))/ds}, \tag{2.54}$$

or

$$s_{n+1} = s_n - \frac{y_1(L, s_n) - A}{dy_1(L, s_n)/ds}. \tag{2.55}$$

To find the derivative of y_1 with respect of s, differentiate (2.52) with respect to s. For simplification, use the following notations,

$$\frac{dy_1}{ds} = y_3, \quad \frac{dy_2}{ds} = y_4. \tag{2.56}$$

This process results in the following IVP.

$$\left.\begin{aligned} y_3' &= y_4, & y_3(0) &= 0, \\ y_4' &= \frac{\partial f}{\partial y_1} y_3 + \frac{\partial f}{\partial y_2} y_4, & y_4(0) &= 1. \end{aligned}\right\} \tag{2.57}$$

Now, solving the IVP Eq. (2.57), the value of y_3 at L can be computed. This value is actually the derivative of y_1 with respect of s computed at L. Setting the

value of $y_3(L, s)$ in Eq. (2.55), the modified value of s can be achieved. This new value of s is used to solve the Eq. (2.52) and the process is repeated until the value of s is within a described degree of accuracy."

Example

Let us consider the boundary value problem having order four.

$$y'''' - 2yy'' = 0, \tag{2.58}$$

with boundary condition

$$y(0) = 1, \quad y'(0) = 0, \quad y(1) = 0, \quad y'(1) = 0. \tag{2.59}$$

To convert Eq. (2.58) into a system of first order equations, the following notations have been introduced.

$$y = y_1, \quad y' = y_2, \quad y'' = y_3, \quad y''' = y_4. \tag{2.60}$$

The given BVP, is then converted to the following form.

$$\left.\begin{aligned} y_1' &= y_2, & y_1(0) &= 1, \\ y_2' &= y_3, & y_2(0) &= 0, \\ y_3' &= y_4, & y_1(1) &= 0, \\ y_4' &= 2y_1y_3, & y_2(1) &= 0. \end{aligned}\right\} \tag{2.61}$$

Denote the missing initial conditions $y_3(0)$ and $y_4(0)$ by s and t respectively, to have the following IVP

$$\left.\begin{aligned} y_1' &= y_2, & y_1(0) &= 1, \\ y_2' &= y_3, & y_2(0) &= 0, \\ y_3' &= y_4, & y_3(0) &= s, \\ y_4' &= 2y_1y_3, & y_4(0) &= t. \end{aligned}\right\} \tag{2.62}$$

Now, solving the above IVP by using the RK-4 method over the interval [0,1]. The solution obtained by the RK-4 is then analyzed for $y(1)$ and $y'(1)$. If these solutions meet the boundary condition given in Eq. (2.59), then the problem is solved. However, usually this does not happen in the first go. So we have to refine the initial guesses iteratively. For this purpose we use the Newton's method to

solve the following system of nonlinear algebraic equations,

$$\left.\begin{aligned} y_1(x,s,t) &= 0, \\ y_2(x,s,t) &= 0, \end{aligned}\right\}. \tag{2.63}$$

The iterative scheme for the Newton's method for the system of non-linear equations (2.62), is given by

$$\begin{bmatrix} s_{n+1} \\ t_{n+1} \end{bmatrix} = \begin{bmatrix} s_n \\ t_n \end{bmatrix} - \begin{bmatrix} \frac{\partial}{\partial s} y_1(1,s_n,t_n) & \frac{\partial}{\partial t} y_1(1,s_n,t_n) \\ \frac{\partial}{\partial s} y_2(1,s_n,t_n) & \frac{\partial}{\partial t} y_2(1,s_n,t_n) \end{bmatrix}^{-1} \begin{bmatrix} y_1(1,s_n,t_n) \\ y_2(1,s_n,t_n) \end{bmatrix} \tag{2.64}$$

For simplification, use the following notations,

$$\left.\begin{aligned} \frac{\partial y_1}{\partial s} \equiv y_5, \quad \frac{\partial y_2}{\partial s} \equiv y_6, \quad \frac{\partial y_3}{\partial s} \equiv y_7, \quad \frac{\partial y_4}{\partial s} \equiv y_8, \\ \frac{\partial y_1}{\partial t} \equiv y_9, \quad \frac{\partial y_2}{\partial t} \equiv y_{10}, \quad \frac{\partial y_3}{\partial t} \equiv y_{11}, \quad \frac{\partial y_4}{\partial t} \equiv y_{12}, \end{aligned}\right\}. \tag{2.65}$$

To find the Jacobian matrix, differentiating the system of Eqs. (2.62) first with respect to s and then with respect to t and using the new notations, we get

$$\left.\begin{aligned} y_5' &= y_6, & y_5(0) &= 0, \\ y_6' &= y_7, & y_6(0) &= 0, \\ y_7' &= y_8, & y_7(0) &= 1, \\ y_8' &= 2(y_1 y_7 + y_3 y_5), & y_8(0) &= 0, \\ y_9' &= y_{10}, & y_9(0) &= 0, \\ y_{10}' &= y_{11}, & y_{10}(0) &= 0, \\ y_{11}' &= y_{12}, & y_{11}(0) &= 0, \\ y_{12}' &= 2(y_1 y_{11} + y_3 y_9), & y_1(0) &= 1. \end{aligned}\right\} \tag{2.66}$$

Solve the above system of equations (2.66) by the RK-4 method and put the computed values of y_5, y_9, y_6 and y_{10} in (2.64). This gives new modified initial guesses. This procedure is repeated until we achieved the solutions with required accuracy. The result obtained by the shooting method, can be graphed as follows.

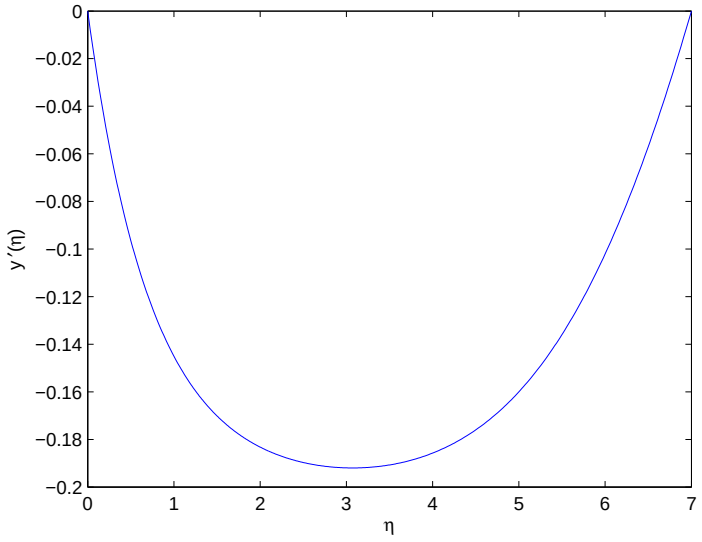

FIGURE 2.1: Solution of example

2.2.2 bvp4c

It is a MATLAB built-in function [86], which can be used to solve the system of nonlinear boundary value problems. Three-stage Lobatto IIIa formula embedded with a finite difference scheme plays a key role in the construction of the built-in coding process of bvp4c. Basically it is a collocation formula, C-1 continuous solution is provided by the collocation polynomial and it is a fourth order accurate in [a,b]. The residual of the continuous solution depends on the error control and the mesh selection. The following Matlab syntax is used for it: sol = bvp4c(@odefun, @bcfun, solinit, options)

Chapter 3

MHD Stagnation Point Flow and Heat Transfer in Viscoelastic Fluid with Cattaneo-Christov Heat Flux Model

3.1 Introduction

This chapter presents an energy transfer analysis of the stagnation point coupled flow of an UCM fluid over a stretching sheet along with the magnetic effects and slip condition along the boundary. The recently proposed Cattaneo-Christov model [10] is employed in the energy equation to investigate the effects of thermal relaxation time. Similarity transformations play a pivotal role for obtaining the ordinary differential equations from the mathematically modeled partial differential equations. Numerical solution of the system of ODEs is achieved by the classical shooting method embeded with Runge-Kutta method of order four. The dominant effects of stretching ratio parameter, elasticity number, heat flux relaxation time, Magnetic parameter, slip coefficient and Prandtl number on the velocity and temperature profiles are examined graphically and numerically. It is perceived that temperature boosts up with an increment in the thermal relaxation time.

3.2 Mathematical Model

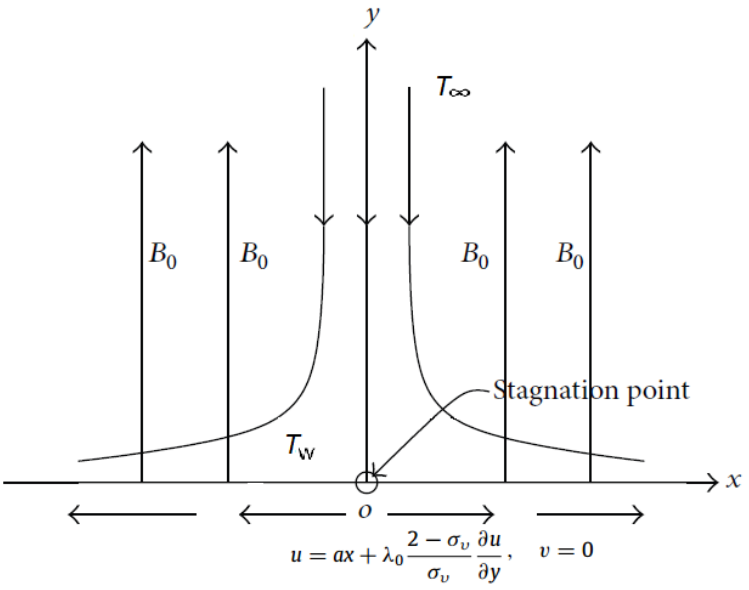

FIGURE 3.1: Geometry of the model.

Consider steady, two-dimensional, incompressible and laminar stagnation point flow of a viscoelastic fluid over a semi infinite plate. A fixed temperature T_w which is sustained at the plate and the ambient fluid temperature T_∞ are shown in Fig. 3.1. Magnetic field having a strength of B_0 is exerted normally to the direction of flow. As we considered limited magnetic Reynolds number thats why the electric field is vanished and also an induced magnetic field is overlooked. Further first order velocity slip condition is assumed at the wall. The heat flux model introduced by Cattaneo-Christov is taken into consideration. By using standard boundary layer approximations, the partial differential equations for the continuity, momentum and temperature flow [5], [13] and [21] are:

$$\frac{\partial u}{\partial x} + \frac{\partial v}{\partial y} = 0, \tag{3.1}$$

$$u\,\frac{\partial u}{\partial x} + v\,\frac{\partial u}{\partial y} + \lambda_1\left(u^2\,\frac{\partial^2 u}{\partial x^2} + v^2\frac{\partial^2 u}{\partial y^2} + 2uv\,\frac{\partial^2 u}{\partial x \partial y}\right) = \nu\frac{\partial^2 u}{\partial y^2} + u_e\frac{du_e}{dx} + \frac{\sigma B_0^2}{\rho}\left(u_e - u - \lambda_1 v\frac{\partial u}{\partial y}\right), \tag{3.2}$$

$$\rho c_p \mathbf{V}\cdot\nabla\mathbf{T} = -\nabla\cdot\mathbf{q}. \tag{3.3}$$

The corresponding velocity slip boundary conditions [27] are:

$$\left.\begin{aligned} &u = ax + \lambda_0 \frac{2-\sigma_v}{\sigma_v}\frac{\partial u}{\partial y},\ v = 0,\ T = T_w \text{ at} \quad y = 0, \\ &u_e(x) = cx, \quad T \to T_\infty \quad \text{as} \quad y \to \infty. \end{aligned}\right\} \tag{3.4}$$

The heat flux $\mathbf{q}$ satisfies the following relation [10]:

$$\mathbf{q} + \lambda_2 \left[\frac{\partial \mathbf{q}}{\partial t} + \mathbf{V}\cdot \nabla \mathbf{q} - \mathbf{q}\cdot \nabla \mathbf{V} + (\nabla \cdot \mathbf{V})\,\mathbf{q}\right] = -k\,\nabla \mathbf{T}, \tag{3.5}$$

where $\mathbf{V} = (u, v)$ is the velocity vector of the Maxwell fluid. If we choose $\lambda_2 = 0$, Eq. (3.5) corresponds to Fourier's law. Continuity equation for the incompressible fluid implies $\nabla \cdot \mathbf{V} = 0$, which when used in Eq. (3.5) yields the following:

$$\mathbf{q} + \lambda_2 \left[\frac{\partial \mathbf{q}}{\partial t} + \mathbf{V}\cdot \nabla \mathbf{q} - \mathbf{q}\cdot \nabla \mathbf{V}\right] = -k\,\nabla \mathbf{T}\cdot \tag{3.6}$$

Eliminating $\mathbf{q}$ from Eqs. (3.3) and (3.6), we get:

$$u\frac{\partial \mathbf{T}}{\partial x} + v\frac{\partial \mathbf{T}}{\partial y} + \lambda_2 \begin{pmatrix} (u\frac{\partial u}{\partial x} + v\frac{\partial u}{\partial y})\frac{\partial T}{\partial x} + (u\frac{\partial v}{\partial x} + v\frac{\partial v}{\partial y})\frac{\partial \mathbf{T}}{\partial y} \\ +u^2\frac{\partial^2 \mathbf{T}}{\partial x^2} + v^2\frac{\partial^2 \mathbf{T}}{\partial y^2} + 2uv\frac{\partial^2 \mathbf{T}}{\partial x \partial y} \end{pmatrix} = \alpha\frac{\partial^2 \mathbf{T}}{\partial y^2}. \tag{3.7}$$

Introducing the following dimensionless variables:

$$\eta = \sqrt{\frac{a}{\nu}}\,y, \quad \psi = \sqrt{a\nu}\ xf(\eta), \quad \theta(\eta) = \frac{T - T_\infty}{T_w - T_\infty}. \tag{3.8}$$

After simplification we come forth with the following ordinary differential equations:

$$f''' + ff'' - f'^2 + \beta\left(2ff'f'' - f^2 f'''\right) + M(e - f' + \beta ff'') + e^2 = 0, \tag{3.9}$$

$$\frac{1}{Pr}\,\theta'' + f\theta' - \gamma\left(ff'\theta' + f^2\theta''\right) = 0. \tag{3.10}$$

The reconstructed boundary conditions of Eq. (3.4) are:

$$\begin{aligned} &f'(0) = 1 + bf''(0), \quad f(0) = 0, \quad \theta(0) = 1, \\ &f'(\infty) = e, \quad \theta(\infty) = 0. \end{aligned} \tag{3.11}$$

Different dimensionless parameters appearing in Eqs. (3.9)-(3.11) are defined as:

$$\beta = \lambda_1 a, \quad \gamma = \lambda_2 a, \quad e = \frac{c}{a}, \quad M = \frac{\sigma B_0^2}{a\rho}, \quad Pr = \frac{\nu}{\alpha} = \frac{\mu c_p}{k}, \quad b = \lambda_0 \frac{2-\sigma_v}{\sigma_v}\sqrt{\frac{a}{\nu}}. \tag{3.12}$$

The skin friction coefficient C_f and Nusselt number Nu are described as:

$$C_f = \frac{\tau_w}{\rho(ax)^2}, \qquad Nu = \frac{xq_w}{\alpha(T_w - T_\infty)}. \tag{3.13}$$

Here the wall shear stress τ_w and the heat flux q_w are defined as:

$$\tau_w = \mu(1+\beta)\left(\frac{\partial u}{\partial y}\right)_{y=0}, \qquad q_w = -\alpha\left(\frac{\partial T}{\partial y}\right)_{y=0}. \tag{3.14}$$

The dimensionless form of drag coefficient and rate of heat transfer is:

$$Re_x^{1/2} C_f = (1+\beta) f''(0), \qquad Re_x^{-1/2} Nu_x = -\theta'(0). \tag{3.15}$$

3.3 Numerical Solution

The resulting nonlinear system of ordinary differential Eqs. (3.9) and (3.10) subject to the conditions (3.11) have been explored numerically with the aid of shooting method [85] for various values of the concerned parameters. On account of number of computational experiments, as there is no significant difference in the results after $\eta = 7$ so we are taking [0, 7] for the domain of the problem rather than [0, ∞). We have chosen the following nomenclature to remodel the boundary value problem into the initial value problem comprising of five single order ordinary differential equations.

$$f = y_1, \; f' = y_2, \; f'' = y_3, \; \theta = y_4, \; \theta' = y_5. \tag{3.16}$$

The coupled nonlinear momentum and heat equations are transformed into the following pattern along with initial conditions.

$$\left.\begin{aligned} y_1' &= y_2, & y_1(0) &= 0 \\ y_2' &= y_3, & y_2(0) &= 1 + by_3(0) \\ y_3' &= \frac{[-y_1y_3(1+2\beta y_2) + y_2^2 - M(e - y_2 + \beta y_1 y_3) - e^2]}{1 - \beta y_1^2}, & y_3(0) &= s \\ y_4' &= y_5, & y_4(0) &= 1 \\ y_5' &= \frac{Pry_1y_5(\gamma y_2 - 1)}{1 - \gamma Pry_1^2}. & y_5(0) &= t \end{aligned}\right\} \tag{3.17}$$

We apply the Runge-Kutta method having order four to solve the above initial value problem. We adopted Newton's method for the refining of the missing values of s and t so that we come across the following yardstick.

$$\max\ \{|y_2(7) - e|,\ |y_4(7) - 0|\} <\ \varepsilon,$$

where $\varepsilon > 0$ is a tiny positive real constant. A threshold $\varepsilon = 10^{-5}$ is adopted for computation of all the numerical results.

3.4 Results and Discussions

In this chapter we utilized the UCM fluid with Cattaneo-Christov heat flux model to explore the boundary layer flow and heat transfer above a stretching plate along with the velocity slip boundary condition. Although we have achieved almost the same numerical results for different quantities of interest by two different techniques, nevertheless for more gratification, a limiting case comparison is made with the some published work of same kind to validate our MATLAB code. To handle it, a reproduction of the numerical results of the skin friction for the models investigated by Sadeghy et al. [20] and Abel et al. [87]. An impressively credible agreement of our obtained numerical results is observed for the Sadeghy et al. and Abel et al. can be seen in Table 3.1. Table 3.2 presents the values of skin friction and Nusselt number for different emerging parameters. Temperature gradient at the sheet shows increasing behavior for the stretching ratio parameter, Prandtl number and thermal relaxation time, while it depicts inverse behavior for elasticity number, slip coefficient and magnetic parameter. Similarly skin friction seems to have an increasing trend for elasticity number and magnetic parameter

and decreasing for slip coefficient and stretching ratio parameter.

A relation between upper-convected Maxwell and Newtonian fluid models is set up by an elastic term. Heat transfer and fluid flow are influenced by elastic force. Figs. 3.2 and 3.3 depict the impact of elasticity number β on velocity and temperature profile. Viscoelastic fluid turns into Newtonian fluid by ignoring the effects of elastic force β. With an increment in the value of β, the elastic forces strengthen up. By enhancement in β, velocity profile shows decreasing and temperature distribution possesses an increasing flow patterns in the viscous fluid. It is because of the fact that a raise in the elasticity number leads to the powerful viscous force that opposes the mobility of the fluid and as a consequence the velocity displays decreasing pattern. Figs. 3.4 and 3.5 illustrate the impact of the magnetic parameter M over velocity and energy boundary layer flow. Magnetic field is adjusted along normal to the fluid flow direction. It is realized that magnetic field prevents the motion of the fluid and enhances the temperature distribution. Figs. 3.6 and 3.7 present the slip effects on velocity and temperature profile. Velocity exhibits the decreasing phenomenon for increment in the value of b and converse for the temperature profile. Figs. 3.8 and 3.9 show the effect of stretching ratio e over velocity and temperature distribution. With an increment in the stretching ratio, we experienced an enhancement in velocity profile and decrement in the thermal boundary layer. When $e < 1$, the stretching sheet velocity ax is larger than the velocity of the far stream cx. Fig. 3.10 portrays the aftermath of thermal relaxation time γ on energy profile. The energy pattern shows decreasing behavior for enhancement in the thermal relaxation time. If we consider $\gamma = 0$ then the current model converts into Fourier's Law. It is noticed that the temperature observed in Fourier's model is comparably higher than the Cattaneo-Christov heat flux model. Fig. 3.11 shows that with the enlargement in Prandtl number Pr, the energy boundary layer comes to be thinner, because Prandtl number is experienced an opposite connection with the thermal diffusivity. All the calculations are performed in hpi5 mechine with 4GB ram, it takes 1.561 seconds to plot a single graph.

TABLE 3.1: Comparison of numerical values of $-f''(0)$ with those of Sadeghy [20] and Abel [87] for $M = e = \gamma = b = 0$ and $Pr = 1$.

	$-f''(0)$		
β	Sadeghy et al. [20]	Abel et al. [87]	Present
0.0	1.0000	0.999962	1.0001725
0.2	1.0549	1.051948	1.0519731
0.4	1.10084	1.101850	1.1019446
0.6	1.0015016	1.150163	1.1501584
0.8	1.19872	1.196692	1.1967224
1.2	-	1.285257	1.2853239
1.6	-	1.368641	1.3673413
2.0	-	1.447617	1.4463152

TABLE 3.2: Numerical values of -$(1+\beta)$ f'' (0) and - θ' (0) for different parameters.

e	Pr	γ	β	b	M	Shooting		bvp4c	
						$-(1+\beta)f''(0)$	$-\theta'(0)$	$-(1+\beta)f''(0)$	$-\theta'(0)$
0.1	1	0.1	0.1	0.1	0.05	0.968554	0.575354	0.968554	0.575354
0.2						0.915324	0.602832	0.915324	0.602832
0.3						0.845289	0.630777	0.845289	0.630777
0.1	0.5					0.968554	0.368480	0.968554	0.368480
	1.5					0.968554	0.744492	0.968554	0.744492
	2.5					0.968554	1.017927	0.968554	1.017927
	1	0.2				0.968554	0.583098	0.968554	0.583098
		0.4				0.968554	0.599482	0.968554	0.599482
		0.5				0.968554	0.608089	0.968554	0.608089
			0.2			1.077807	0.600289	1.077807	0.600288
			0.4			1.305184	0.585631	1.305184	0.585631
			0.8			1.790399	0.561494	1.790399	0.561494
				0.2		1.554512	0.540975	1.554512	0.540975
				0.5		1.134616	0.498868	1.134616	0.498868
				0.9		0.848754	0.463693	0.848754	0.463693
					0.5	0.933687	0.424693	0.933687	0.424693
					1	1.002469	0.395878	1.002469	0.395878
					1.5	1.054939	0.375867	1.054939	0.375867

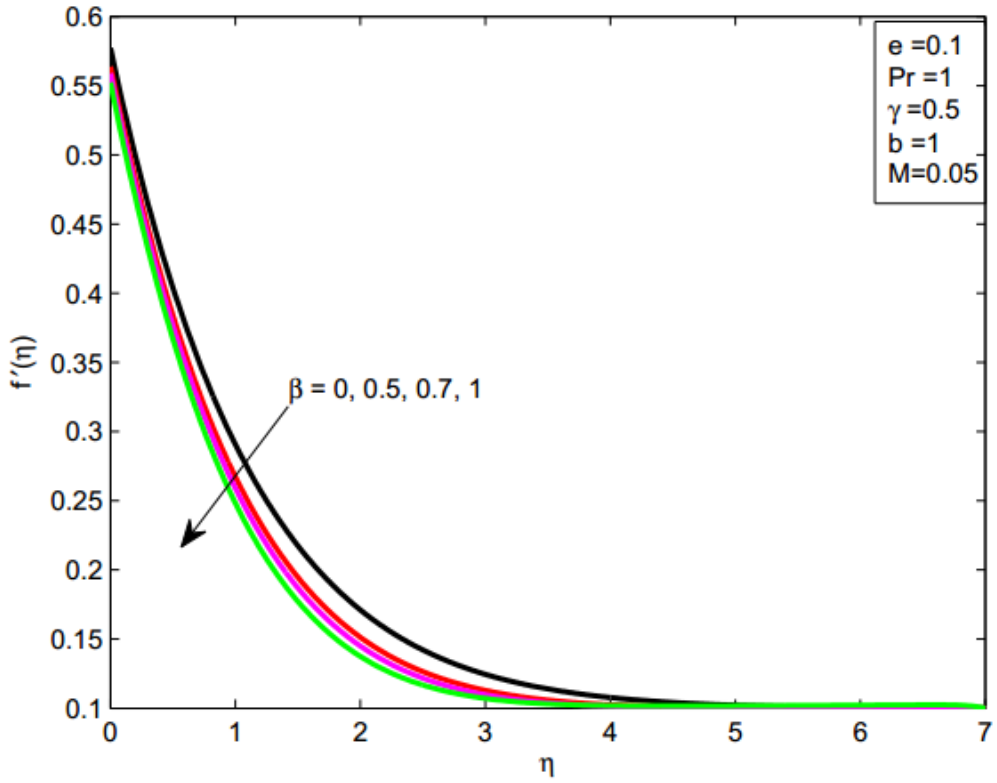

FIGURE 3.2: Influence of β on $f'(\eta)$.

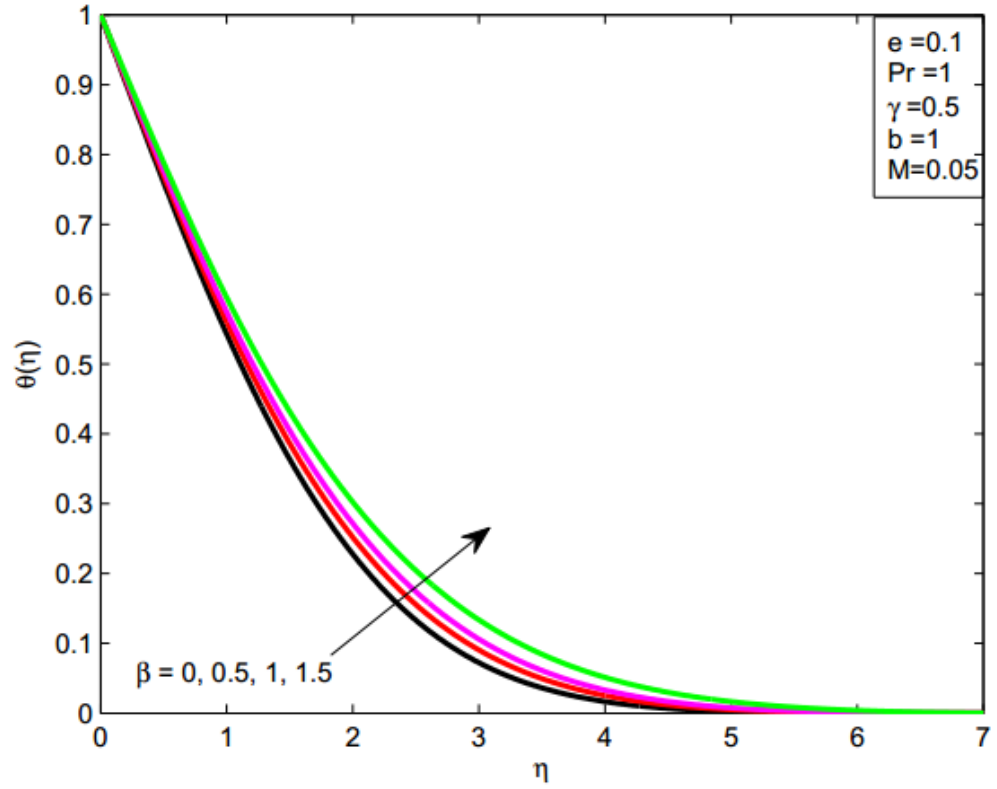

FIGURE 3.3: Influence of β on $\theta(\eta)$.

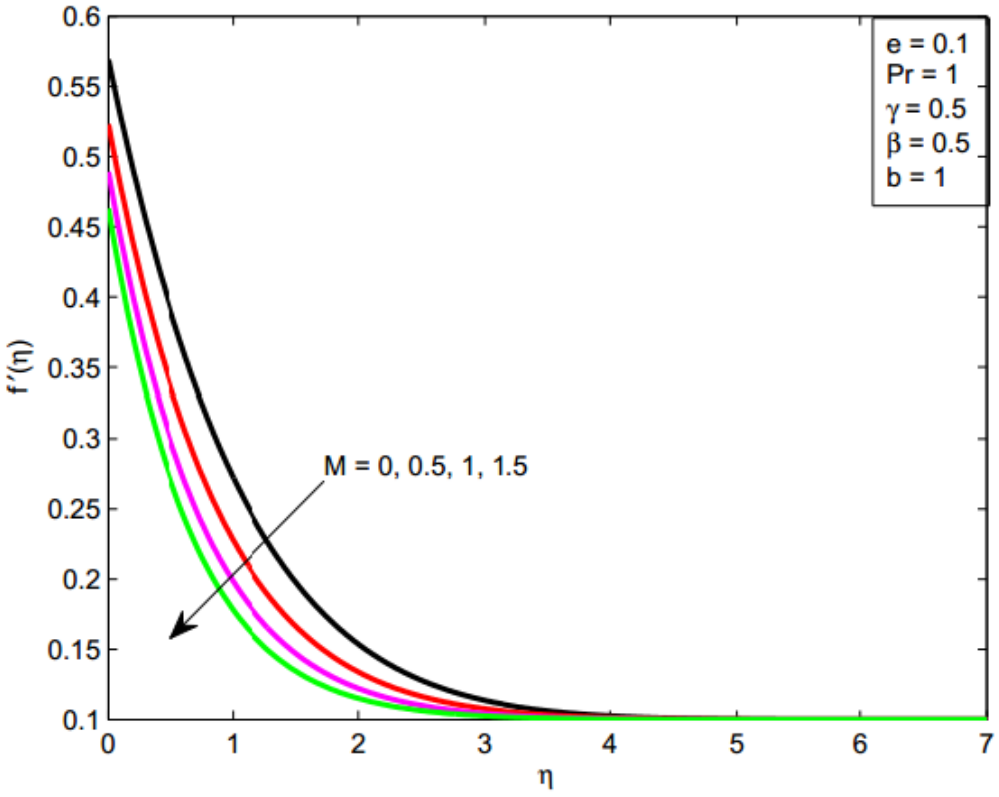

FIGURE 3.4: Impact of M on $f'(\eta)$.

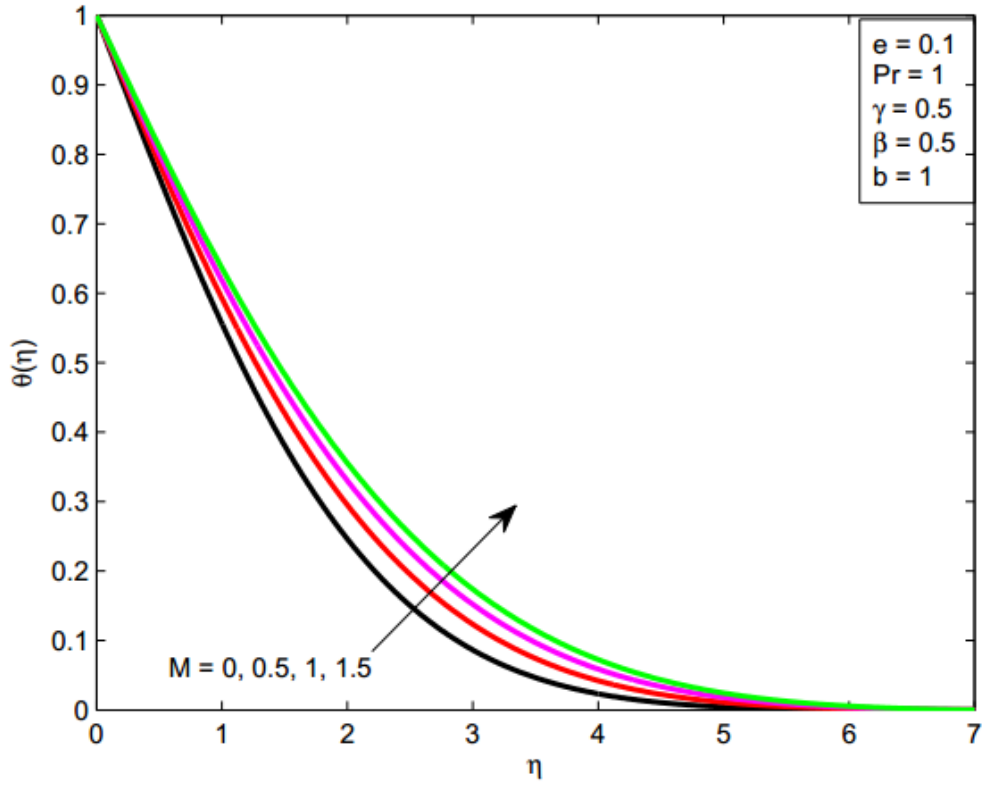

FIGURE 3.5: Influence of M on θ.

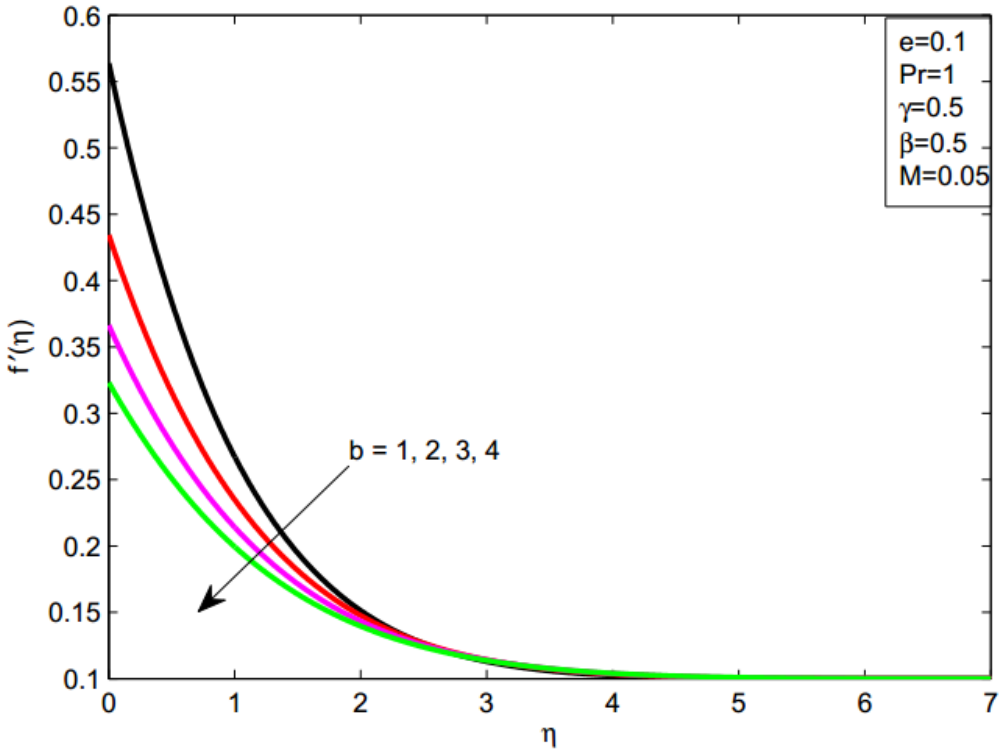

FIGURE 3.6: Impact of b on $f'(\eta)$.

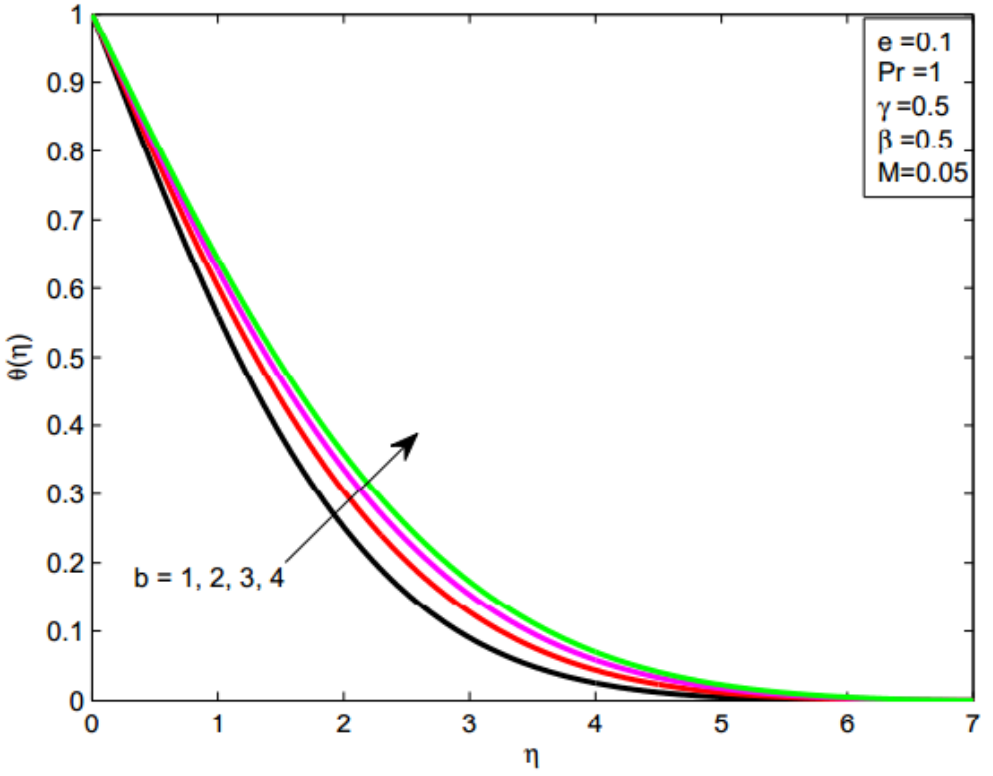

FIGURE 3.7: Influence of b on θ.

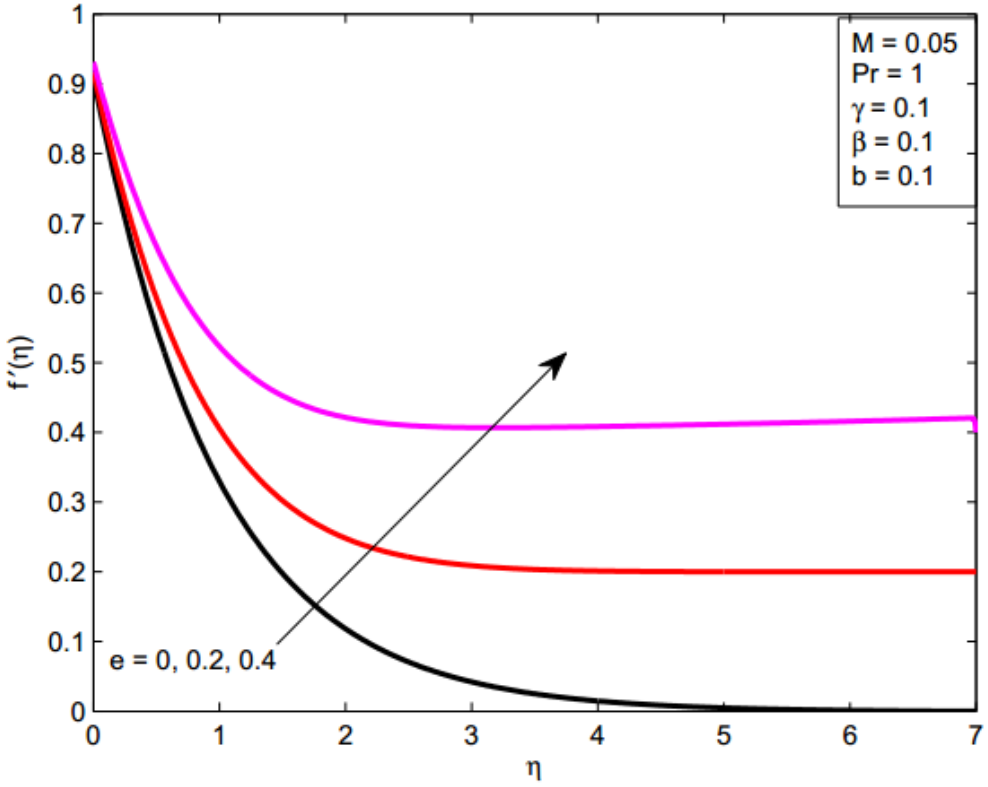

FIGURE 3.8: Effect of e on $f'(\eta)$.

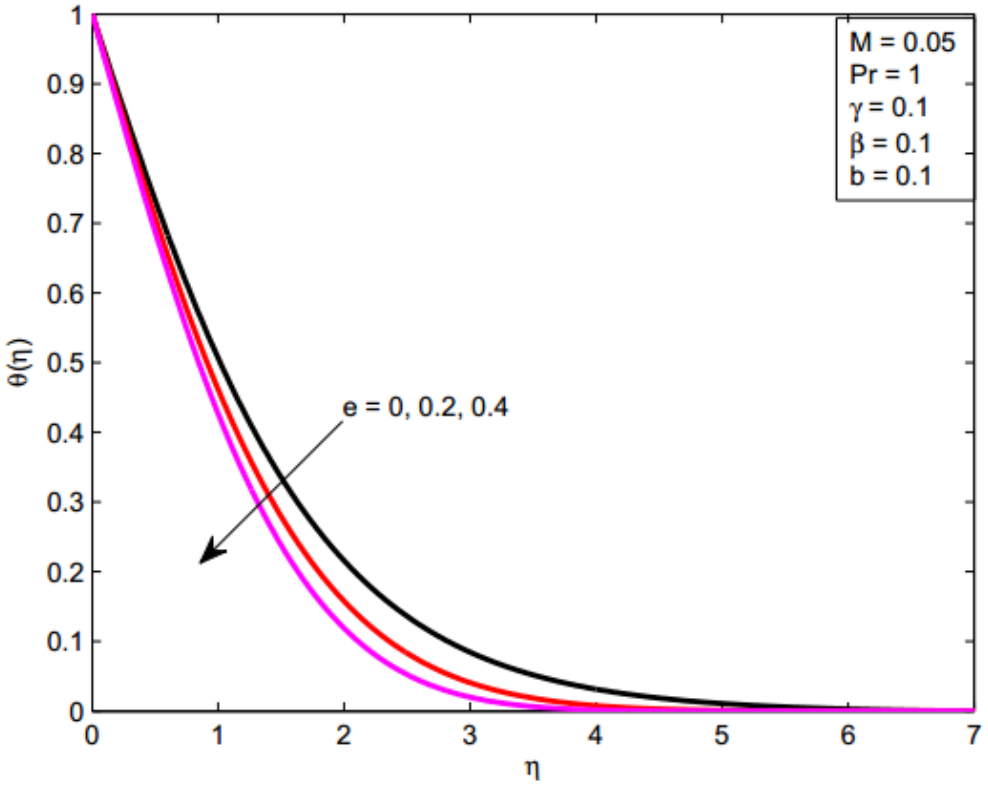

FIGURE 3.9: Effect of e on θ.

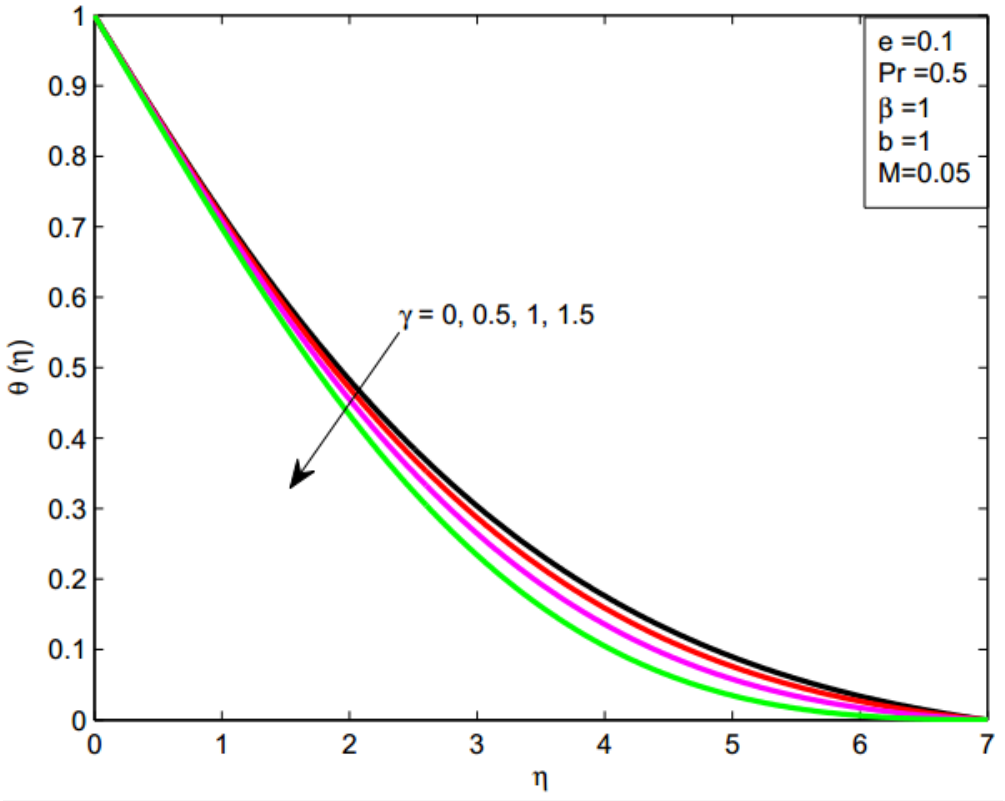

FIGURE 3.10: Effect of γ on θ.

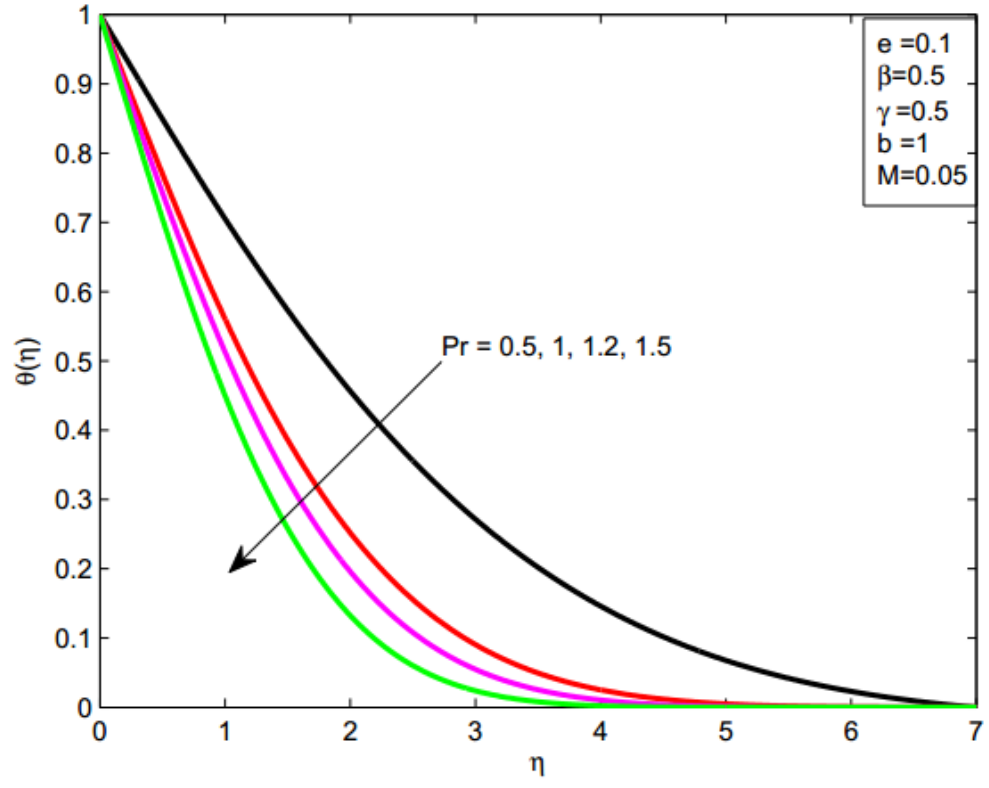

FIGURE 3.11: Effect of Pr on θ.

3.5 Concluding Remarks

The present model addresses the magnetic effects in the stagnation point flow on UCM fluid along with the Cattaneo-Christov heat flux model. To solve the system of coupled ordinary differential equations, we adopted the shooting method. To strengthen the code, we also employed the MATLAB built-in function bvp4c. The main observations are summarised as follows:

- By increasing the magnetic field intensity, velocity profile exhibits a decreasing pattern and an opposite behavior is seen in the energy boundary layer.
- A boost in the elasticity number and slip coefficients causes the decrease in the velocity phenomenon and an reverse expression is observed in the energy profile.
- An intensification in the stretching ratio parameter results a decrease in the wall shear stress and an enrichmentt in the Nusselt number.
- By increasing the thermal relaxation time, temperature raises up.

Chapter 4

Effects of Chemical Reaction on Stagnation Point Flow with Mass and Heat Transfer in Magneto UCM Fluid Employed with Cattaneo-Christov Heat Flux Model

4.1 Introduction

The present chapter addresses the influence of the magnetic field on the Cattaneo-Christov heat flux in the presence of stagnation point flow towards a linear stretching surface and transfer of mass analysis along with the chemical reaction properties. Upper convected Maxwell fluid is taken to confront the analysis and modeling. Similarity transformations play a pivotal role for obtaining the ordinary differential equations from the mathematically modeled partial differential equations. The shooting method involving the Runge-Kutta method embedded with order four plays the main role to capture the numerical solution of the system of ODEs. The effects of stretching ratio parameter, elasticity number, Schmidt number, heat flux relaxation time, chemical reaction, magnetic parameter and Prandtl number

over temperature, velocity and concentration profiles are scrutinized graphically and numerically.

4.2 Mathematical Model

Consider the two-dimensional, incompressible and steady stagnation point flow of an UCM fluid over a semi-infinite plate. The plate is assumed to have a constant temperature T_w at stretching sheet as described in Fig. 4.1. Magnetic force having a strength of B_0 is exerted normally to the direction of flow. As we have considered only the small magnetic Reynolds number, thats why the electric and induced magnetic fields are not under discussion. To study the effects of heat flux, we adopt the model introduced by Cattaneo-Christov [10]. By using standard boundary layer approximations, the equations for the continuity, momentum, temperature and concentration flow are described as:

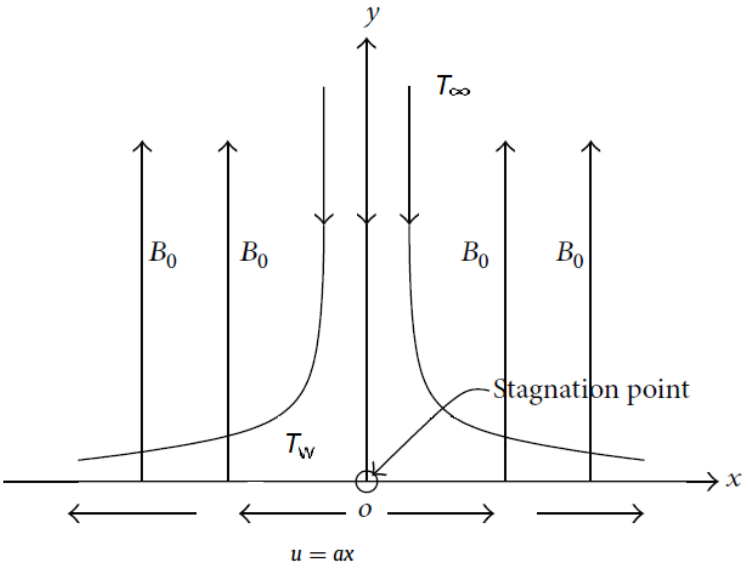

FIGURE 4.1: Geometry of the model.

$$\frac{\partial u}{\partial x}+\frac{\partial v}{\partial y}=0, \tag{4.1}$$

$$u\ \frac{\partial u}{\partial x}+v\ \frac{\partial u}{\partial y}+\ \lambda_1\left(u^2\ \frac{\partial^2 u}{\partial x^2}+\ 2uv\frac{\partial^2 u}{\partial x\partial y}+\ v^2\frac{\partial^2 u}{\partial y^2}\right)=u_e\frac{du_e}{dx}+\nu\frac{\partial^2 u}{\partial y^2} + \frac{\sigma B_0^2}{\rho}\left(u_e-u-\lambda_1 v\frac{\partial u}{\partial y}\right), \tag{4.2}$$

$$\rho c_p\mathbf{V}\cdot\nabla\mathbf{T}=-\nabla\cdot\mathbf{q}, \tag{4.3}$$

$$u\ \frac{\partial C}{\partial x}+\ v\frac{\partial C}{\partial y}=\ D\ \frac{\partial^2 C}{\partial y^2}-K\ (C-C_\infty). \tag{4.4}$$

The boundary conditions are set as follows:

$$\begin{aligned} &u=ax,\quad v=0,\quad T=T_w,\quad C=C_w \quad \text{at} \qquad y=0,\\ &u_e\ (x)=cx,\quad T\to T_\infty,\quad C\to C_\infty \quad \text{as} \qquad y\to\infty. \end{aligned} \tag{4.5}$$

The heat flux $\mathbf{q}$ satisfies the following relationship:

$$\mathbf{q}+\lambda_2\left[\frac{\partial\mathbf{q}}{\partial t}+\ \mathbf{V}\cdot\ \nabla\ \mathbf{q}+\ (\nabla\cdot\ \mathbf{V})\mathbf{q}-\ \mathbf{q}\cdot\ \nabla\ \mathbf{V}\right]=\ -k\ \nabla\mathbf{T}, \tag{4.6}$$

where $\mathbf{V}=(u,v)$ is the velocity vector of the Maxwell fluid. If we choose $\lambda_2=0$, Eq. (4.6) corresponds to Fourier's law. Continuity equation for the incompressible fluid implies $\nabla\cdot\mathbf{V}=0$, which when used in Eq. (4.6) yields the following relation:

$$\mathbf{q}+\lambda_2\left[\frac{\partial\mathbf{q}}{\partial t}-\ \mathbf{q}\cdot\ \nabla\ \mathbf{V}+\ \mathbf{V}\cdot\ \nabla\mathbf{q}\right]=\ -k\ \nabla T. \tag{4.7}$$

Eliminating $\mathbf{q}$ from Eqs. (4.3) and (4.7), we get:

$$u\ \frac{\partial\mathbf{T}}{\partial x}+v\ \frac{\partial\mathbf{T}}{\partial y}+\ \lambda_2\begin{pmatrix}(u\ \frac{\partial u}{\partial x}+v\ \frac{\partial u}{\partial y})\frac{\partial\mathbf{T}}{\partial x}+(u\ \frac{\partial v}{\partial x}+v\ \frac{\partial v}{\partial y})\frac{\partial\mathbf{T}}{\partial y}\\ +u^2\frac{\partial^2\mathbf{T}}{\partial x^2}+v^2\frac{\partial^2\mathbf{T}}{\partial y^2}+2uv\frac{\partial^2\mathbf{T}}{\partial x\partial y}\end{pmatrix}=\ \alpha\ \frac{\partial^2\mathbf{T}}{\partial y^2}. \tag{4.8}$$

To convert the PDEs to ODEs, introducing the following dimensionless variables [13], [64]:

$$\eta=\sqrt{\frac{a}{\nu}}\ y,\quad \psi=\sqrt{a\nu}\ \ xf(\eta),\qquad \theta\,(\eta)=\frac{T-T_\infty}{T_w-T_\infty},\quad \phi\,(\eta)=\frac{C-C_\infty}{C_w-C_\infty}. \tag{4.9}$$

After simplification, we come forth with the following ordinary differential equations:

$$f''' + ff'' - f'^2 + \beta\left(2ff'f'' - f^2f'''\right) + M(e - f' + \beta ff'') + e^2 = 0, \tag{4.10}$$

$$\frac{1}{Pr}\theta'' + f\theta' - \gamma\left(ff'\theta' + f^2\theta''\right) = 0, \tag{4.11}$$

$$\phi'' + Scf\phi' - Sc\gamma_1\phi = 0. \tag{4.12}$$

The transformed boundary conditions (4.5) are:

$$\begin{aligned} &f(0) = 0, \quad \theta(0) = 1, \quad f'(0) = 1, \quad \phi(0) = 1 \\ &f'(\infty) = e, \quad \theta(\infty) = 0, \quad \phi(\infty) = 0 \end{aligned} \tag{4.13}$$

Different dimensionless parameters appearing in Eqs. (4.10)-(4.12) are defined as:

$$\beta = \lambda_1 a, \quad \gamma = \lambda_2 a, \quad e = \frac{c}{a}, \quad M = \frac{\sigma B_0^2}{a\rho}, \quad Pr = \frac{\nu}{\alpha} = \frac{\mu c_p}{k}, \quad Sc = \frac{\nu}{D}, \quad \gamma_1 = \frac{K}{a}. \tag{4.14}$$

The rates of energy transfer Nu and mass transfer Sh are defined as:

$$Nu = \frac{xq_w}{\alpha(T_w - T_\infty)}, \quad Sh = \frac{xj_w}{D(C_w - C_\infty)}. \tag{4.15}$$

Here the the heat flux q_w and mass flux j_w are defined as:

$$q_w = -\alpha\left(\frac{\partial T}{\partial y}\right)_{y=0}, \quad j_w = -D\left(\frac{\partial C}{\partial y}\right)_{y=0}. \tag{4.16}$$

The dimensionless form of Nusselt and Sherwood numbers is:

$$Re_x^{-1/2}Nu_x = -\theta'(0), \quad Re_z^{-1/2}Sh_z = -\phi'(0). \tag{4.17}$$

4.3 Numerical Solution

The nonlinear system of ordinary differential Eqs. (4.10) − (4.12) subject to the condition (4.13) explored numerically with the help of shooting method [85] for different values of the concerned physical parameters. As there is no significant difference in the results after $\eta = \eta_{max}$ because of the analysis of the computational experiments so we are taking into account $[0, \eta_{max}]$ as the boundary of the problem instead of $[0, \infty)$. Here η_{max} is different for different combinations of the physical parameters. We have chosen the following nomenclature to remodel the boundary value problem into the initial value problem consisting of seven first order ordinary

differential equations.

$$f = y_1, \quad f' = y_2, \quad f'' = y_3, \quad \theta = y_4, \quad \theta' = y_5, \quad \phi = y_6, \quad \phi' = y_7. \tag{4.18}$$

The coupled nonlinear momentum, heat and concentration equations are transformed into the subsequent system of seven first order differential equations in conjunction with the initial conditions.

$$\left.\begin{aligned}
y_1' &= y_2, & y_1(0) &= 0,\\
y_2' &= y_3, & y_2(0) &= 1,\\
y_3' &= \frac{[-y_1y_3(1+2\beta y_2) + y_2^2 - M(e - y_2 + \beta y_1 y_3) - e^2]}{1 - \beta y_1^2}, & y_3(0) &= s,\\
y_4' &= y_5, & y_4(0) &= 1,\\
y_5' &= \frac{Pry_1y_5(\gamma y_2 - 1)}{1 - \gamma Pry_1^2}. & y_5(0) &= t,\\
y_6' &= y_7, & y_6(0) &= 1,\\
y_7' &= Sc(-y_1y_7 + \gamma_1 y_6), & y_7(0) &= v.
\end{aligned}\right\} \tag{4.19}$$

We apply the Runge-Kutta method of order four to solve the above initial value problem. We adopted Newton's method for the refining of the missing values of s, t and u so that we meet the following yardstick.

$$\max\{|y_2(\eta_{max}) - e|, |y_4(\eta_{max}) - 0|, |y_6(\eta_{max}) - 0|\} < \varepsilon,$$

where $\varepsilon > 0$ is a small positive real constant. A threshold $\varepsilon = 10^{-5}$ is adopted for computation of all the numerical results.

Although we have achieved almost the same numerical results for different quantities of interest by two different techniques i.e. built-in MATLAB function bvp4c and shooting method, nevertheless for more reliability, a limiting case comparison is made with the some published work of same kind to validate our MATLAB code. To handle it, a reproduction of the numerical results of the Sherwood number for the models investigated by Hayat et al. [21]. An impressively credible agreement of our obtained numerical results is observed for the Hayat et al. [21] can be seen in Table 4.1.

4.4 Results and Discussions

In this chapter, we utilized an UCM fluid along with Cattaneo Christov heat flux model to explore the boundary layer flow and heat transfer above a stretching plate. Table 4.2 presents the values of -$f''(0)$, Nusselt and Sherwood numbers for involved rheological parameters. Temperature gradient at the sheet shows increasing behavior for thermal relaxation time and Prandtl number, while it depicts inverse behavior for Deborah number and magnetic parameter. Similarly Sherwood number seems to have an increasing trend for Schmidt number and chemical reaction parameter and decreasing for Deborah number and magnetic parameter. Sherwood number is more important in mass transfer phenomenon because it is a ratio of the convectived mass transfer and the diffusive mass transportion rate.

A relation between upper-convected Maxwell and Newtonian fluid models is set up by an elastic term. Heat transfer and fluid flow are influenced by elastic force. Figs. 4.2 and 4.3 depict the impact of Deborah number β over velocity and temperature profiles. An UCM fluid turns into Newtonian fluid by ignoring the effects of elastic force β. As while enlargement in the value of β, the elastic forces strengthen up. By enhancement in β, velocity profile shows decreasing and temperature distribution possesses an increasing flow patterns in the viscous fluid. Its reason is because that a boost in the Deborah number leads to the powerful viscous force that opposes the mobility of the fluid, so as a result the velocity displays decreasing pattern. Figs. 4.4 and 4.5 interpret the significance of magnetic parameter M over velocity and temperature boundary layer flow. Magnetic field is considered along perpendicular to the fluid flow. It is noticed that magnetic field counters the fluid motion and enhances the temperature distribution. Figs. 4.6 and 4.7 show the effect of stretching ratio e on velocity and temperature distribution. While enhancement in the stretching ratio, we experienced a growth in the velocity profile and decrement in the thermal boundary layer. When $e < 1$, the stretching sheet velocity ax is larger than the velocity of the far stream cx. Fig. 4.8 portrays the consequence of thermal relaxation time γ over temperature behavior. Thermal profile shows decreasing behavior for enhancement in the thermal relaxation time. If we consider $\gamma = 0$ then the current model converts into Fourier's Law. It is noticed that the temperature observed in Fourier's model is comparably higher than the Cattaneo-Christov heat flux model. Fig. 4.9 shows that with the increment in the Prandtl number Pr, the energy boundary layer becomes thinner, because

the thermal diffusivity has an inverse relationship with the Prandtl number Pr. Figs. 4.10 and 4.11 depict the influence of mass transfer rate Sc and chemical reaction parameter γ_1 over a concentration pattern. Both have a decreasing pattern for mass transfer analysis. Here with the increase in the Schmidt number Sc, we experienced decrement in the the boundary layer thickness and concentration profile. The reason is because the mass diffusion is influenced by Schmidt number Sc and decrease in mass diffusion corresponds to an increase in Schmidt number Sc and hence we experienced reduction in the concentration profile. The case $\gamma_1 = 0$ corresponds to no chemical reaction in the system. As reaction rate parameter increases with the increase in chemical reaction parameter γ_1, so we encounter decrement in concentration phenomenon.

TABLE 4.1: Comparison of numerical values of $-\phi'(0)$ with those of [21] for $\gamma = Pr = 0$ and $Sc = \gamma_1 = 1$.

e	M	β	$-\phi'(0)$	
			Present	[21]
0	1	0.2	1.150920	1.15092
0.2			1.167867	1.16815
0.4			1.186720	1.18727
0.7			1.219928	1.22675
0.2	0		1.181313	1.18142
	0.3		1.179825	1.17980
	0.7		1.173969	1.17385
	1.2		1.163457	1.16351
	1.5	0	1.160593	1.15680
	1	0	1.171696	1.17169
		0.4	1.164136	1.16524
		0.7	1.161626	1.15125
		1	1.153619	1.15505

TABLE 4.2: Numerical values of -$f''(0)$, -$\theta'(0)$ and -$\phi'(0)$ for different parameters by taking $e = 0.2$.

						bvp4c			Shooting		
β	M	γ	Sc	γ_1	Pr	-$f''(0)$	-$\theta'(0)$	-$\phi'(0)$	-$f''(0)$	-$\theta'(0)$	-$\phi'(0)$
0.0	0.5	0.5	0.2	0.2	0.2	1.076823	0.236582	0.307043	1.076823	0.236582	0.307043
0.3						1.156529	0.249362	0.316204	1.156529	0.249362	0.316204
0.8						1.291645	0.239933	0.308038	1.291645	0.239933	0.308038
0.1	0.25					1.026474	0.255240	0.321103	1.026474	0.234653	0.305257
	0.5					1.103648	0.252611	0.318909	1.103648	0.234144	0.305357
	0.75					1.175937	0.231302	0.303291	1.175937	0.231302	0.303291
	0.5	0.1				1.103648	0.232959	0.305358	1.103648	0.232959	0.305358
		0.2				1.103648	0.233084	0.305358	1.103648	0.233084	0.305358
		0.5				1.103648	0.234145	0.305358	1.103648	0.234145	0.305358
			0.5			1.103648	0.234145	0.505602	1.103648	0.234145	0.505602
			0.7			1.103648	0.234145	0.612554	1.103648	0.234145	0.612554
			1.5			1.103648	0.234145	0.944495	1.103648	0.234145	0.944495
			0.2	0.5		1.103648	0.234145	0.392578	1.103648	0.234145	0.392578
				0.7		1.103648	0.234145	0.441754	1.103648	0.234145	0.441754
				1		1.103648	0.234145	0.506724	1.103648	0.234145	0.506724
					0.2	1.103648	0.234145	0.506724	1.103648	0.234145	0.506724
					0.3	1.103648	0.296890	0.506724	1.103648	0.296890	0.506724
					0.5	1.103648	0.411819	0.506724	1.103648	0.411819	0.506724

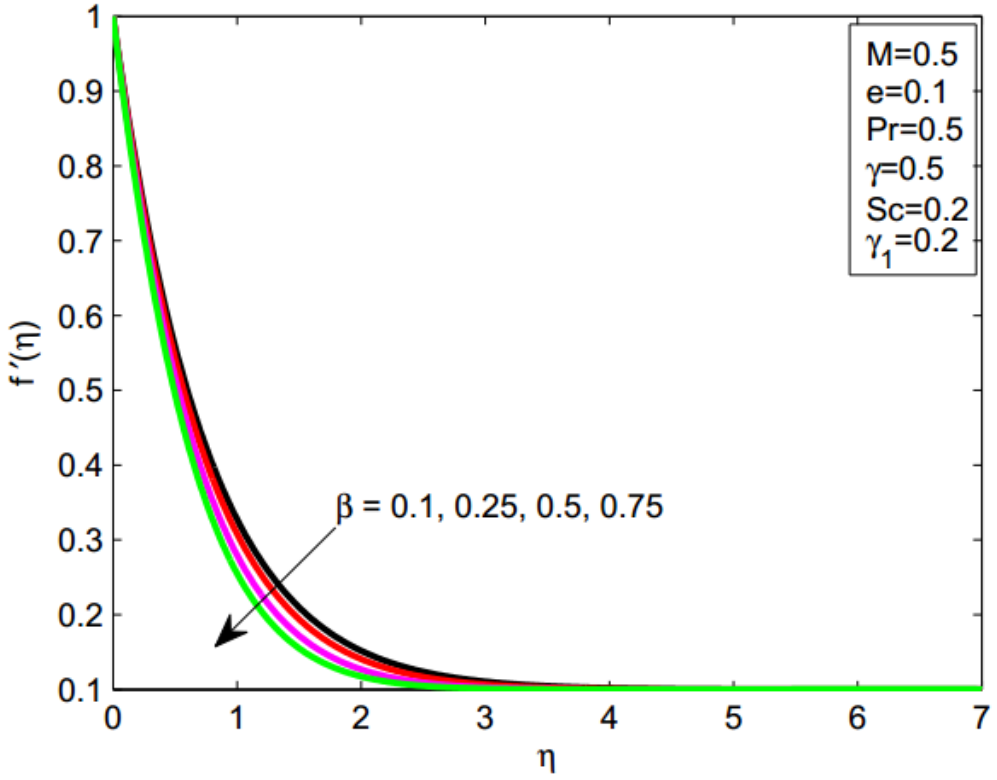

FIGURE 4.2: Impact of β on $f'(\eta)$.

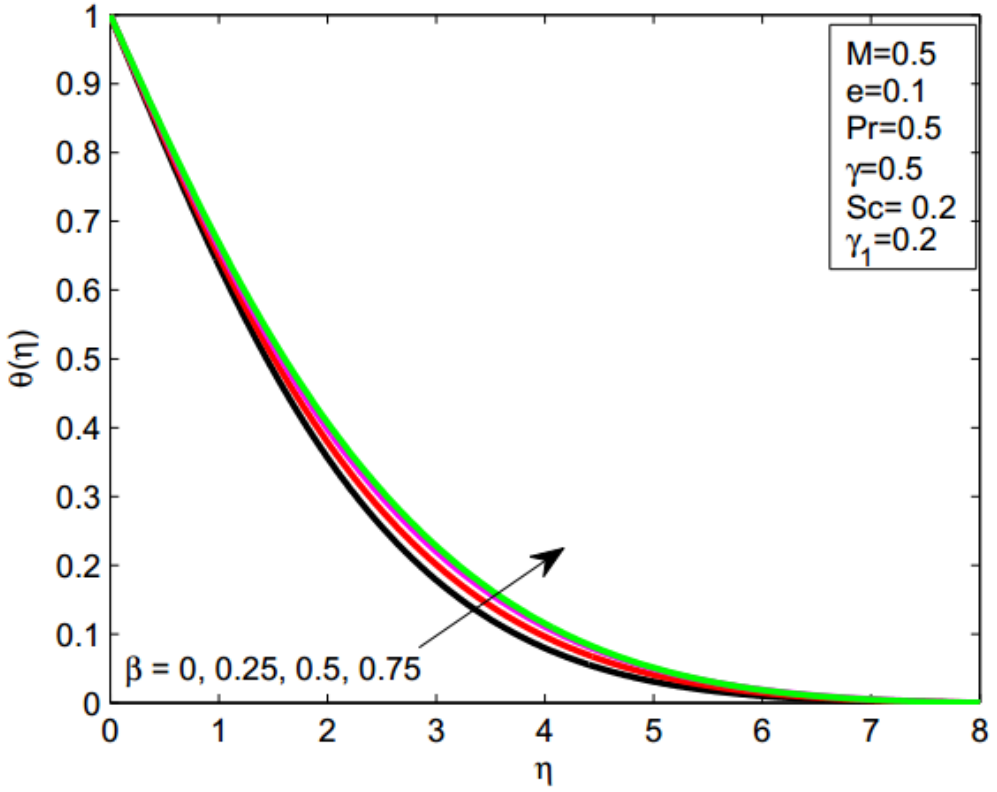

FIGURE 4.3: Impact of β on $\theta(\eta)$.

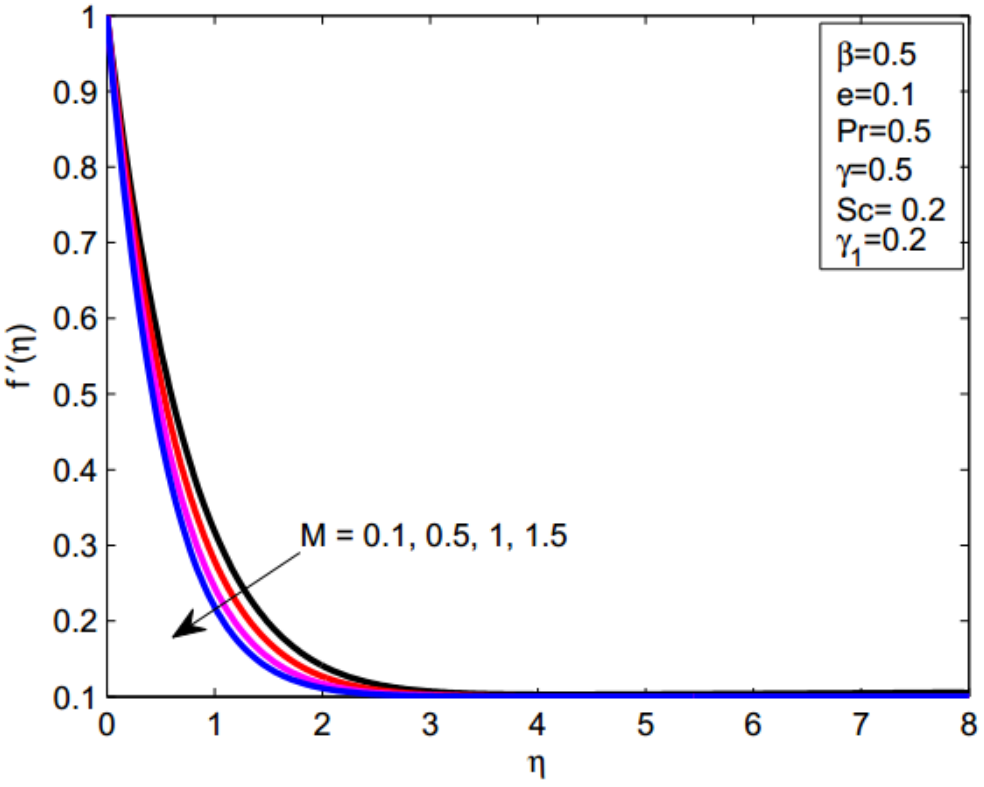

FIGURE 4.4: Impact of M on $f'(\eta)$.

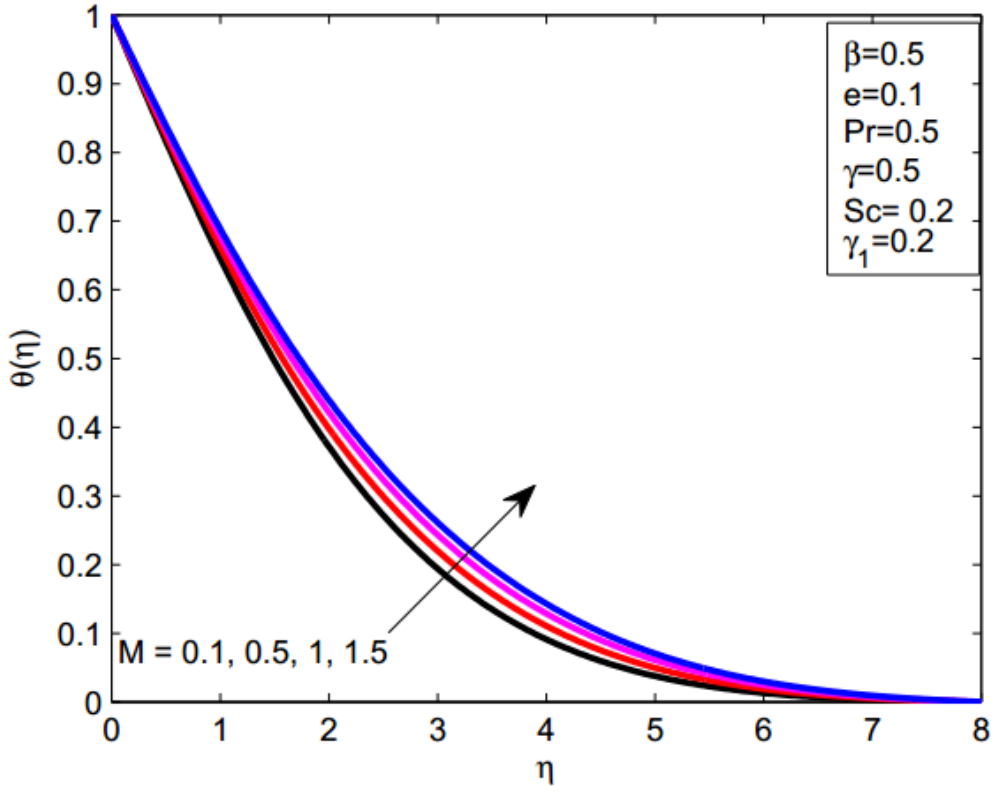

FIGURE 4.5: Impact of M on θ.

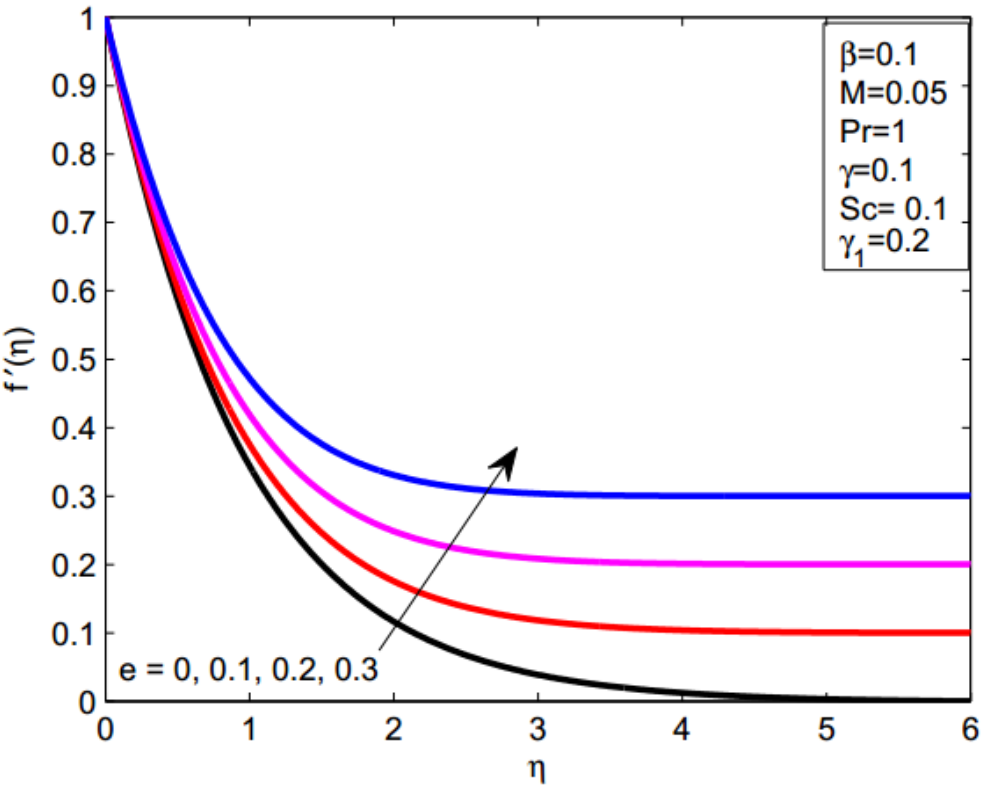

FIGURE 4.6: Effect of e on $f'(\eta)$.

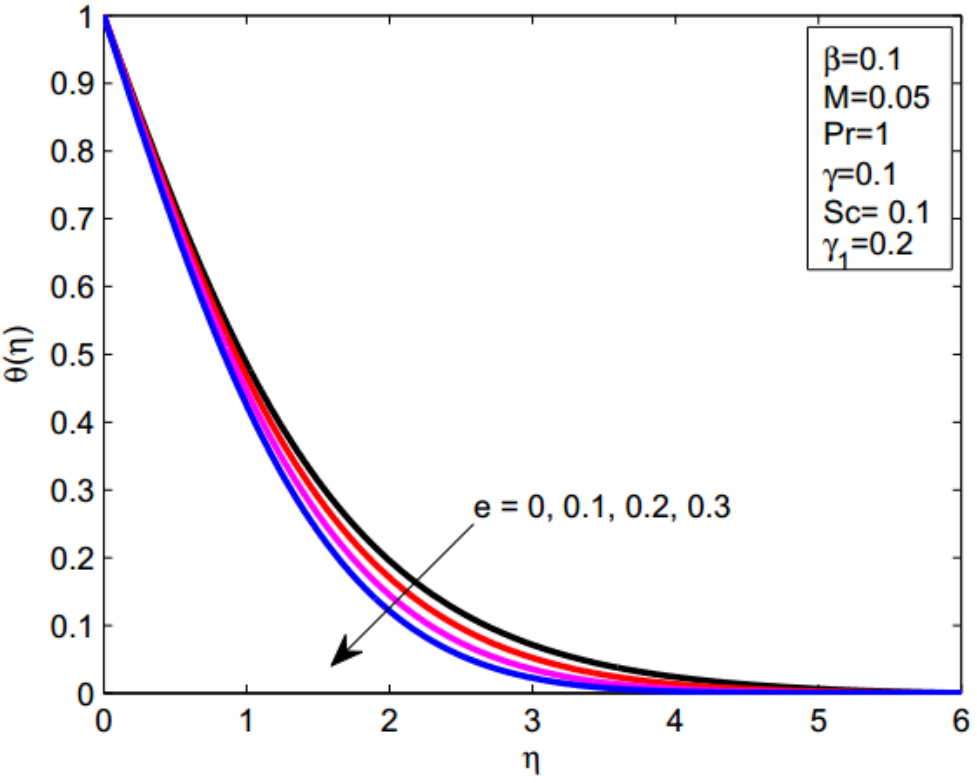

FIGURE 4.7: Effect of e on θ.

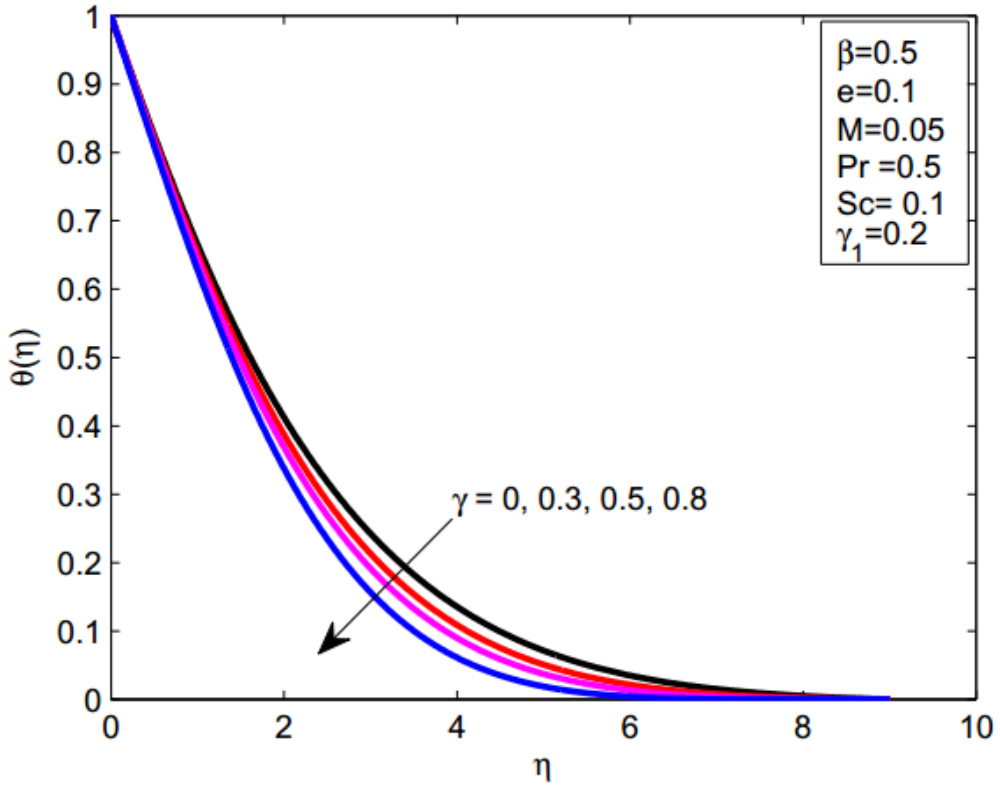

FIGURE 4.8: Effect of γ on θ.

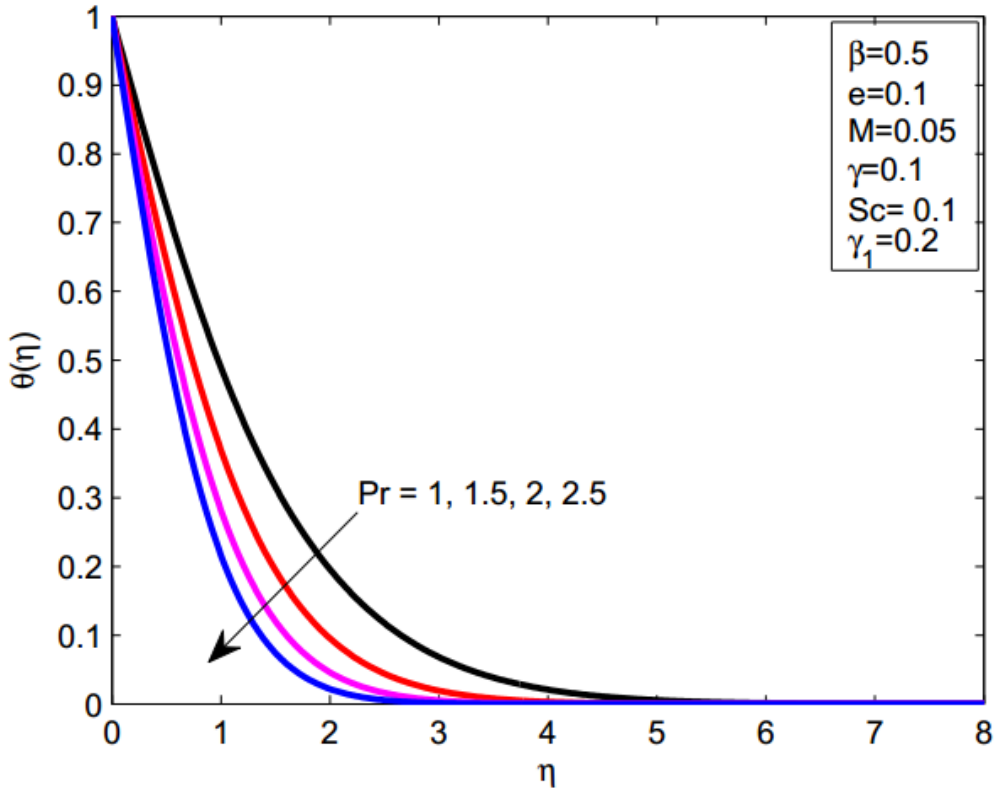

FIGURE 4.9: Effect of Pr on θ.

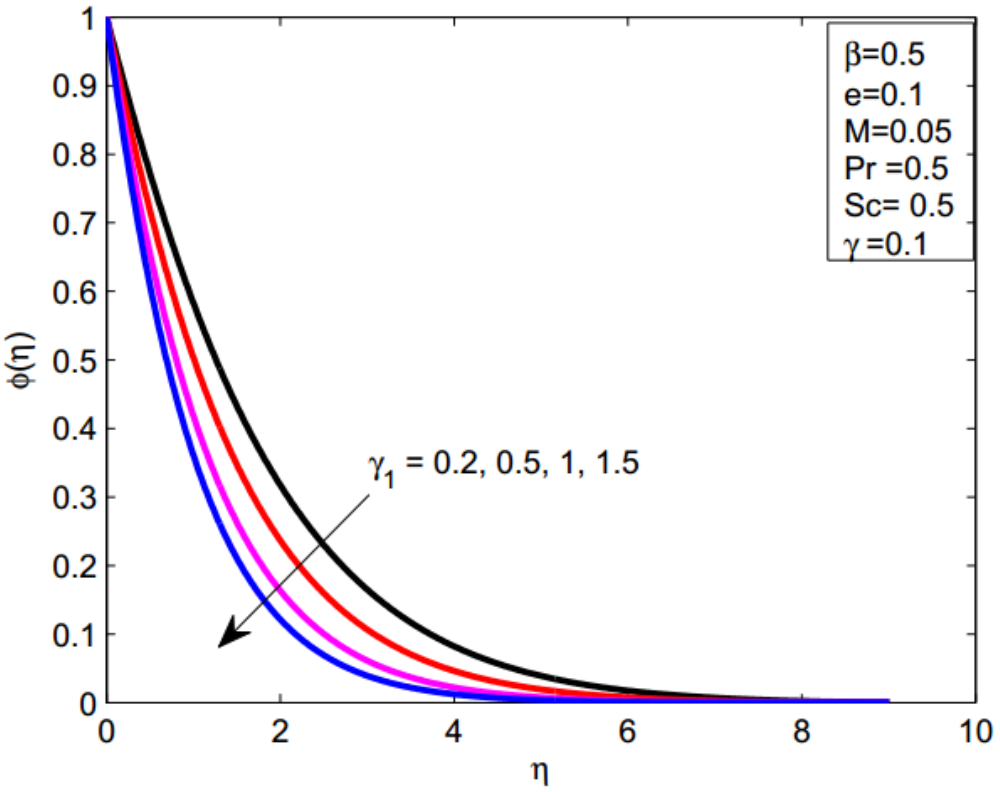

FIGURE 4.10: Impact of γ_1 on $\phi(\eta)$.

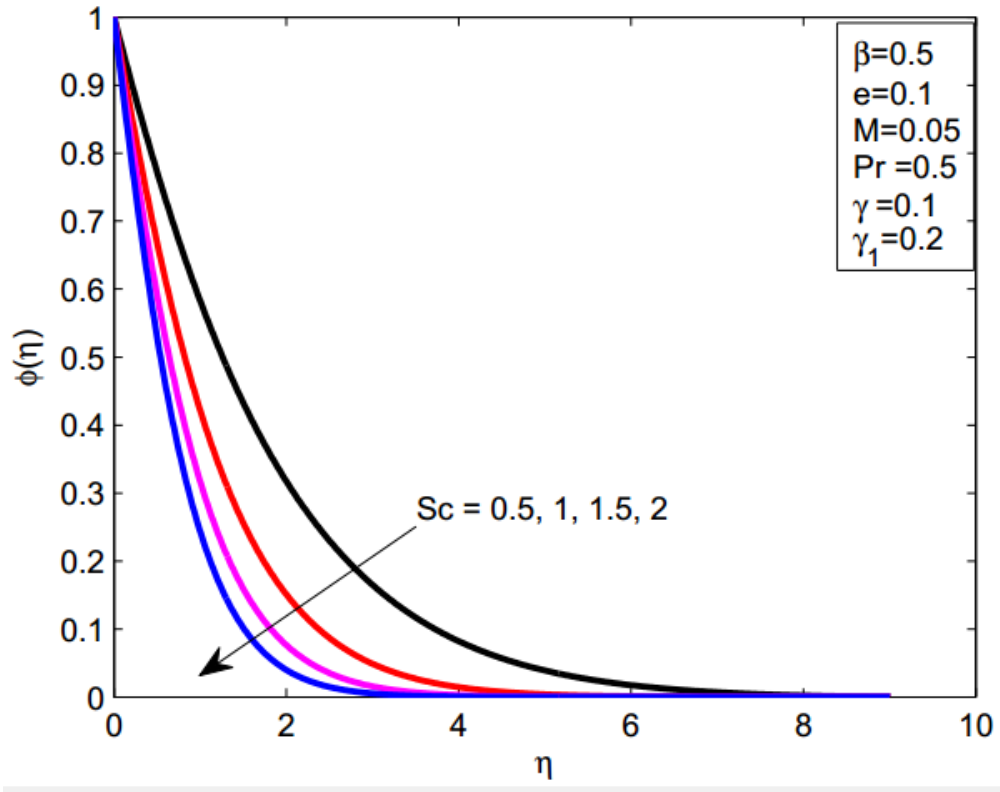

FIGURE 4.11: Impact of Sc on $\phi(\eta)$.

4.5 Concluding Remarks

The present model addresses the magnetic field effects on the stagnation point flow for an UCM fluid along with the Cattaneo-Christov heat flux model. Mass transfer and chemical reaction effects are also considered. As our main concern is to collect a solution of the system of ordinary differential equations, so we adopted a shooting method. To strengthen the results we also employed MATLAB built-in function bvp4c. A comparison is also made with the previous published work. The main observations are summarised as follows:

- By increasing the magnetic field intensity, velocity profile exhibits a decreasing pattern and an opposite behavior is seen in the energy boundary layer.
- A rise of the values of the Deborah number exhibits a decrease in the velocity phenomenon and an opposite response is noticed in the energy pattern.
- Energy profile reduces with an increment in the heat flux relaxation time.
- Concentration profile portrays a decreasing pattern for the chemical reaction parameter and mass transfer rate.

Chapter 5

MHD Stagnation Point Flow of Williamson Fluid Over a Stretching Cylinder with Variable Thermal Conductivity and Homogeneous/Heterogeneous Reaction

5.1 Introduction

The present study reveals the consequence of homogeneous/hetereogeneous reaction on the stagnation point flow of Williamson fluid with the additions of magnetohydrodynamics and heat generation/absorption coefficient over a stretching cylinder. Further the influences of variable thermal conductivity and thermal stratification are also studied. Similarity transformations play a pivotal role for obtaining the ordinary differential equations from the mathematically modeled partial differential equations. The system of non-linear coupled ordinary differential equations is then solved with the aid of shooting technique. The MATLAB shooting code is validated by comparison with the previously published article. Results are further strengthened by comparing with the built-in MATLAB function bvp4c. The effects of leading parameters are deliberated graphically for the

temperature, velocity and concentration profiles. Energy transfer rate and drag coefficient for the various parameters are investigated with the help of tables.

5.2 Model of the Problem

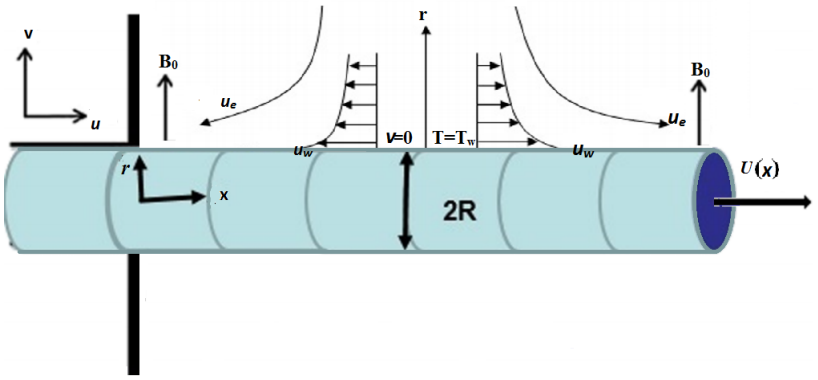

FIGURE 5.1: Geometry of the Problem.

We considered stagnation point hydromagnetodynamics flow of Williamson fluid under the combined effect of heterogeneous/homogeneous reaction and heat generation/absorption over a linearly stretching cylinder along $x-$axis. Mangetic field owning to have a strength B_0 is exerted normally to the direction of flow as shown in Fig. 5.1. As our supposition is small Reynolds number, thats why ignored induced magnetic field in the mathematical modelling. Further a variable thermal conductivity and the effect of thermal stratification at boundary layer flow are also incorporated. In this case, energy far away from the sheet T_∞ is comparably less than the temperature at the sheet T_w. The relationship between homogeneous and heterogeneous reactions is expressed by the following equation.

$$A_1 + 2B_1 \rightarrow 3B_1, rate = l_1 a_1 b_1^2 \ , \tag{5.1}$$

$$A \rightarrow B_1, rate = l_s a_1, \tag{5.2}$$

where l_1, l_s are rate constants and a_1, b_1 denote concentrations of the chemical species A_1, B_1 respectively. Further considered that there occurs negligibe change in temperature for both the reactions. By taking into account all the considerations represented above and employing boundary layer approximations, the equations of the rheological system becomes

$$\frac{\partial (rv)}{\partial r} + \frac{\partial (ru)}{\partial x} = 0, \tag{5.3}$$

$$v\frac{\partial u}{\partial r} + u\frac{\partial u}{\partial x} = u_e\frac{du_e}{dx} + \upsilon\left[\frac{\partial^2 u}{\partial r^2} + \frac{1}{r}\frac{\partial u}{\partial r} + \sqrt{2}\Gamma\frac{\partial u}{\partial r}\frac{\partial^2 u}{\partial r^2} + \frac{\Gamma}{\sqrt{2}r}\left(\frac{\partial u}{\partial r}\right)^2\right] - \frac{\sigma B_0^2}{\rho}(u - u_e), \tag{5.4}$$

$$u\frac{\partial T}{\partial x} + v\frac{\partial T}{\partial r} = \frac{1}{r}\frac{\partial}{\partial r}\left(\alpha r\frac{\partial T}{\partial r}\right) + \frac{Q(T - T_\infty)}{\rho c_p}, \tag{5.5}$$

$$v\frac{\partial a_1}{\partial r} + u\frac{\partial a_1}{\partial x} = D_{A_1}\left(\frac{\partial^2 a_1}{\partial r^2} + \frac{1}{r}\frac{\partial a_1}{\partial r}\right) - l_1 a_1 b_1^2, \tag{5.6}$$

$$v\frac{\partial b_1}{\partial r} + u\frac{\partial b_1}{\partial x} = D_{B_1}\left(\frac{\partial^2 b_1}{\partial r^2} + \frac{1}{r}\frac{\partial b_1}{\partial r}\right) + l_1 a_1 b_1^2, \tag{5.7}$$

subject to the boundary conditions

$$\left.\begin{aligned} &U_w(z) = \frac{U_0 x}{l},\ v = 0,\ T = T_w = T_0 + \frac{sx}{l},\ D_{A_1}\frac{\partial a_1}{\partial r} = l_s a_1, \\ &D_{B_1}\frac{\partial b_1}{\partial r} = -l_s a_1 \text{ at } r = R, \\ &u = u_e \to \frac{V_0 x}{l},\ T \to T_\infty = T_0 + \frac{tx}{l},\ a_1 \to a_{1\infty}, b_1 \to b_{1\infty} \text{ as } r \to \infty. \end{aligned}\right\} \tag{5.8}$$

Using the following transformations

$$\left.\begin{aligned} &\eta = \sqrt{\frac{U_0}{\nu l}}\left(\frac{r^2 - R^2}{2R}\right),\quad \psi = \sqrt{\frac{\nu U_0}{l}}Rxf(\eta),\quad u = \frac{U_0 x}{l}f'(\eta), \\ &v = -\sqrt{\frac{\nu U_0}{l}}\frac{R}{r}f(\eta),\quad \theta(\eta) = \frac{T - T_\infty}{T_w - T_0},\quad m(\eta) = \frac{a_1}{a_{1\ 0}},\quad n(\eta) = \frac{b_1}{a_{1\ 0}}. \end{aligned}\right\} \tag{5.9}$$

In Eq. (5.5), α is variable thermal conductivity that is defined as

$$\alpha = \alpha_\infty(1 + \varepsilon\theta(\eta)). \tag{5.10}$$

Satisfaction of Eq. (5.3) is straightforward, however Eqs. (5.4), (5.5), (5.6) and (5.7) turn into the following non-dimensional form

$$(1+2\eta\gamma_3)\,f'''+ff''-f'^2+2\gamma_3 f''+\frac{3}{2}\,(1+2\eta\gamma_3)^{1/2}\,\gamma_3\lambda f''^2+$$
$$\lambda\,(1+2\eta\gamma_3)^{3/2}\,f''f'''+e^2-M\,(f'-e)=0, \tag{5.11}$$
$$(1+\varepsilon\theta)\,((1+2\eta\gamma_3)\,\theta''+\gamma_3\theta')+Pr\,(f\theta'-f'\,(\theta+\phi_1))+\varepsilon\,(1+2\eta\gamma_3)\,\theta'^2+$$
$$Pr\beta_1\theta=0, \tag{5.12}$$
$$(1+2\eta\gamma_3)\,m''+2\gamma_3 m'+Scfm'-ScL_1mn^2=0, \tag{5.13}$$
$$\delta_1\,(1+2\eta\gamma_3)\,n''+2\gamma_3\delta_1 n'+Scfn'+ScL_1mn^2=0. \tag{5.14}$$

The transformed boundary conditions are:

$$\left.\begin{array}{l} f(0)=0,\quad f'(0)=1,\quad m'\,(0)=L_s m\,(0)\,, \\ \theta'\,(0)\ \ =1-\phi_1,\ \delta_1 n'\,(0)=-L_s n\,(0)\ \text{ at }\quad \eta=\ 0, \\ f'(\infty)\to e,\ m\,(\infty)\to 1,\quad \theta\ \ (\infty)\to 0,\ n\,(\infty)\to 1,\ \text{as }\eta\to\infty. \end{array}\right\} \tag{5.15}$$

Different dimensionless parameters appearing in Eqs. (5.11)-(5.15), are defined as

$$\left.\begin{array}{l} \delta_1=\dfrac{D_{B1}}{D_{A1}},\quad Pr=\dfrac{\nu}{\alpha_\infty},\quad \gamma_3=\sqrt{\dfrac{\nu l}{U_0R^2}}, L_1=\dfrac{la_1^2l_1}{U_0}, L_s=\dfrac{l_s}{D_{A1}}\sqrt{\dfrac{\nu l}{U_0}}, \\ Sc=\dfrac{\nu}{D_{A1}}, \lambda=\dfrac{\Gamma U_0^{3/2}x}{\sqrt{2\nu}l^{3/2}}, M=\dfrac{\sigma B_0^2 l}{U_0\rho}, e=\dfrac{V_0}{U_0}, \phi_1=\dfrac{t}{s}, \beta_1=\dfrac{Ql}{\rho c_p U_0}. \end{array}\right\} \tag{5.16}$$

Assume that diffusion coefficient of chemical species A_1 and B_1 are of analogous magnitude leads us to suppose that D_{A_1} and D_{B_1} are identical provided that $\delta_1=1$. Thus, we have

$$m(\eta)+n(\eta)=1. \tag{5.17}$$

Using Eq. 17, Eqs. (13) and (14) take the form

$$(1+2\eta\gamma_3)\,m''+2\gamma_3 m'+Scfm'-ScL_s m(1-m)^2=0. \tag{5.18}$$

The boundary conditions for Eq. (18) are then converted to the form

$$m'\,(0)=L_s m\,(0)\,,\quad m\,(\infty)\to 1. \tag{5.19}$$

Drag coefficient and energy transfer rate in the dimensional form are

$$C_f=\frac{2\tau_w}{\rho u_w^2}, Nu=\frac{xq_w}{\alpha\,(T_w-T_0)}, \tag{5.20}$$

where τ_w and q_w are the shear stress and surface heat flux given by

$$\tau_w = \mu \left(\frac{\partial u}{\partial r} + \frac{\Gamma}{\sqrt{2}} \left(\frac{\partial u}{\partial r} \right)^2 \right)_{r=R}, \quad q_w = -\alpha \left(\frac{\partial T}{\partial r} \right)_{r=R}. \tag{5.21}$$

The dimensionless form of drag coefficient and energy transfer rate is as follows

$$\frac{C_f \sqrt{Re}}{2} = f''(0) + \frac{\lambda}{2} f''^2(0), Nu Re^{-1/2} = -\theta'(0), \tag{5.22}$$

where $Re = \frac{U_0 x^2}{\nu l}$.

5.3 Solution Methodology

A classical numerical technique i.e. the shooting method [85] is used to get the solution of the system of non-linear ordinary differential equations obtained from the partial differential equations. To solve the system (5.11), (5.12) and (5.18) with the respective boundary conditions, first we have to convert it into a system of first order ordinary differential equations. Afterwards, the missing conditions ι_1, ι_2 and ι_3 are gussed initially and then refined iteratively by Newtons iterative scheme subject to the tolerance of 10^{-6}. For numerical computations, the largest value of η has been taken as $\eta = 8$ instead of $\eta \to \infty$ because for $\eta > 8$, the solutions are found settled asymptotically. The results are further strengthened by using bvp4c, a built-in MATLAB function. For first order initial value problem, we denote f by y_1, θ by y_4 and m by y_6 to have the following equations.

$$\left.\begin{array}{ll}
y_1' = y_2 & y_1(0) = 0, \\
y_2' = y_3 & y_2(0) = 1, \\
y_3' = \frac{(y_2^2 - y_1 y_3 - 2\gamma_3 y_3 - 3/2(1+2\eta\gamma_3)^{1/2}\gamma_3 \lambda y_3^2 - e^2 + M(y_2 - e)}{(1+2\eta\gamma_3) + \lambda(1+2\eta\gamma_3)^{3/2} y_3} & y_3(0) = \iota_1, \\
y_4' = y_5 & y_4(0) = 1 - \phi_1, \\
y_5' = \frac{-\left[Pr(y_1 y_5 - y_2(y_4 + \phi_1)) + (1+\varepsilon y_4)\gamma_3 y_5 + \varepsilon(1+2\eta\gamma_3) y_5^2 + Pr\beta_1 y_4\right]}{(1+\varepsilon y_4)(1+2\eta\gamma_3)} & y_5(0) = \iota_2, \\
y_6' = y_7 & y_6(0) = \iota_3, \\
y_7' = \frac{ScLy_6(1-y_6)^2 - Scy_1 y_7 - 2\gamma_3 y_7}{(1+2\eta\gamma_3)} & y_7(0) = Ly_6(0).
\end{array}\right\} \tag{5.23}$$

The initial value problem (5.23) is solved numerically by Runga-Kutta method of

order four. Newton iterative scheme helps us to refine the missing slopes until the following stoping criteria is met

$$\max\left\{\left|y_2\left(8\right)-e\right|,\left|y_4\left(8\right)-0\right|,\left|y_6\left(8\right)-1\right|\right\}<\epsilon. \tag{5.24}$$

For the sake of verification of the code, a comparison with some published articles is presented in Table 5.1, where a very accurate analogy in the results can be seen.

5.4 Results and Discussions

Numerical solutions of the obtained system of ordinary differential equations along with the affiliated boundary conditions are acquired by applying shooting method. The results are verified by built-in function of MATLAB bvp4c. The numerical results of Nusselt number and drag coefficient for distinct magnitude of various parameters are enumerated in Table 5.2. It is noticeable from the table that friction factor upturns for the augmentation in the magnetic parameter M and curvature parameter γ_3. A reverse behaviour is noticed in case of dimensionless Weissenberg number λ and stretching ratio parameter e as both have decreasing tendency for the skin friction coefficient. A rise in the quantities of curvature parameter γ_3, magnetic parameter M and Weissenberg number λ, depreciates the local Nusselt number while an increment in the stretching ratio parameter e, boosts the rate of heat transfer in fluid.

In Table 5.3, the effect of thermal conductivity parameter ε, Prandtl number Pr, thermal stratification parameter ϕ_1 and heat generation/absorption parameter β_1 on heat transfer rate are presented. It is detected from the table that rise in thermal conductivity reduces the rate of heat transfer and as a consequence the temperature increases. On the other hand Nusselt number enhances for the increasing magnitudes of Prandtl number Pr, thermal stratification parameter ϕ_1 and heat absorption/generation parameter β_1.

The effects of curvature parameter γ_3, dimensionless Weissenberg number λ, magnetic parameter M and stretching ratio parameter e on velocity profile are displayed through Figs. (5.2) – (5.5). In Fig. 5.2, values of velocity function $f'(\eta)$

and the boundary layer thickness surge by enhancing γ_3. The hike in γ_3 implies reduction in radius of cylinder and hence the speed of the fluid gets faster. Fig. 5.3 elucidates the behaviour of Weissenberg number over velocity pattern. Velocity reduces slightly when λ is raised. As Weissenberg number λ is the fraction of relaxation time and specific process time, intensification in relaxation time leads to enhansement the resistance of the fluid and resultantly velocity will reduce. In Fig. 5.4, influence of magnetic parameter M on velocity phenomenon is displayed which shows the reduction in speed together with the boundary layer thickness of the fluid for access in M. It happens due to the retarding force called as Lorentz force which actually is a resistive force. Response of stretching ratio parameter e on velocity distribution is demonstrated in Fig. 5.5. As the values of e increases, the velocity and the boundary layer thickness increase.

Figs. (5.6) – (5.12) show the effect of variation of different parameters on temperature profile. Fig. 5.6 demonstrates the effect of heat generation/absorption coefficient. As expected temperature increases with the increment of heat generation. Same effect is seen for the thermal conductivity parameter ε. It is observed from Fig. 5.7 that energy is enhanced for the increasing value of thermal conductivity parameter. Consequence of curvature parameter γ_3 on thermal profile is depicted in Fig. 5.8. A raise in curvature parameter will reduce the radius of the cylinder which causes low resistance to the fluid flow but due to the smaller diameter, the resistive force between the fluid and wall of the cylinder is enhanced and consequently the temperature increases near the wall as depicted in Fig. 5.8. Further, Fig. 5.9 is portrayed to scrutinize the consequence of magnetic parameter M on dimensionless temperature. Magnetic parameter outturns a resistive force in the fluid motion due to Lorentz force. This frictional force enhances the temperature of the fluid. Variation of velocity stretching ratio parameter e over temperature profile is illustrated in Fig. 5.10. As we know that e is the ratio of far away velocity to the surface velocity and it is also obvious that surface velocity is always greater than ambient velocity, so increase in stretching ratio implies reduction in temperature distribution. Fig. 5.11 is plotted to portray the behaviour of temperature profile due to variation in thermal stratification parameter ϕ_1. Enhancement in thermal stratification yields higher density of the fluid in the lower region and lower in upper region. So the temperature differences between the cylinder and ambient fluid deliberately reduce and this effect is clearly elaborated through Fig. 5.11. Fig. 5.12 indicates that the fluid temperature becomes

TABLE 5.1: Comparison of skin friction coefficient with the previously published work for various values of e when $\gamma_3 = 0$, $\lambda = 0$, $M = 0$, $\theta = 0$, $m = 0$ for $f''(0)$.

e	[88]	[89]	[90]	Present
0.1	-0.9694	-0.9694	-0.9764	-0.96965
0.2	-0.9181	-0.9181	-0.9216	-0.91816
0.5	-0.6673	-0.6673	-0.6677	-0.66726
2.0	2.0175	2.0176	2.0179	2.01750
3.0	4.7293	4.7296	4.7297	4.72928

less for increasing values of Pr. It is contemplated that raising the Prandtl number exhibits a decrement in the thermal diffusivity and consequently the thermal boundary layer which eventually upturns the rate of heat transfer.

Figs. (5.13) – (5.16) are plotted to analyze the behaviour of concentration profile subject to variation of different parameters. Fig. 5.13 shows the increasing effect of curvature parameter on concentration. An increment in curvature certainly reduces the radius of cylinder and hence more fluid is expected to flow which will enhance the mass transfer. Figs. 5.14 and 5.15 portray the impact of strength of homogeneous/heterogeneous reaction over a concentration profile. It is observed that both L_1 and L_S have decreasing behaviour but the boundary layer thickness is increased. Impact of Schmidt number Sc on mass distribution is shown in Fig. 5.16. Accession of mass concentration is noted for raising mass transfer rate. The rate of mass transfer is actually the ratio of momentum diffusivity to mass diffusivity. Increase in Schmidt number will enhance the momentum diffusivity which resultantly raises the mass distribution. Fig. 5.17 is portrayed to see the influence of Weissenberg number λ on temperature distribution. A minor increase in temperature distribution is noticed for an increasing value of Weissenberg number.

TABLE 5.2: Numerical values of Nusselt number and skin friction coefficient for various values of the parameters when $\varepsilon = 0.2$, $Pr = 0.72$, $\beta_1 = 0.1$ and ϕ_1=0.3.

				$\frac{1}{2}C_f\sqrt{Re}$		$NuRe^{-1/2}$	
γ_3	λ	e	M	shooting	bvp4c	shooting	bvp4c
0.3	0.2	0.2	0.6	1.1526747	1.1526747	1.5712269	1.5712269
0.4				1.1823723	1.1823723	1.5510129	1.5510129
0.5				1.2114766	1.2114766	1.5322437	1.5322437
0.6				1.2400468	1.2400468	1.5147575	1.5147575
	0.1			1.1831704	1.1831704	1.5796490	1.5796490
	0.3			1.1184246	1.1184246	1.5610308	1.5610308
	0.4			1.0781184	1.0781184	1.5478376	1.5478376
		0.3		1.0519457	1.0519457	1.6222916	1.6222916
		0.4		0.9381452	0.9381452	1.6677485	1.6677485
		0.5		0.8117330	0.8117330	1.7097891	1.7097891
			0.7	1.1788977	1.1788977	1.5648360	1.5648360
			0.8	1.2043781	1.2043781	1.5586461	1.5586461
			0.9	1.2291690	1.2291690	1.5526430	1.5526430

TABLE 5.3: Numerical values of the Nusselt number for various values of parameters when $\gamma_3 = 0.3$, $\lambda = 0.2$ and $e = 0.2$, $M = 0.6$.

				$NuRe^{-1/2}$	
ϵ	Pr	ϕ_1	β_1	shooting	bvp4c
0.3				1.5019247	1.5019247
0.4				1.4396866	1.4396866
0.5				1.3834405	1.3834405
	1.5			1.0055952	1.0055952
	2.0			1.2148101	1.2148101
	2.5			1.4014374	1.4014374
		0.4		1.5846098	1.5846098
		0.5		1.5986938	1.5986938
		0.6		1.6135129	1.6135129
			0.2	1.5640025	1.5640025
			0.3	1.5777877	1.5777877
			0.4	1.6324602	1.6324608

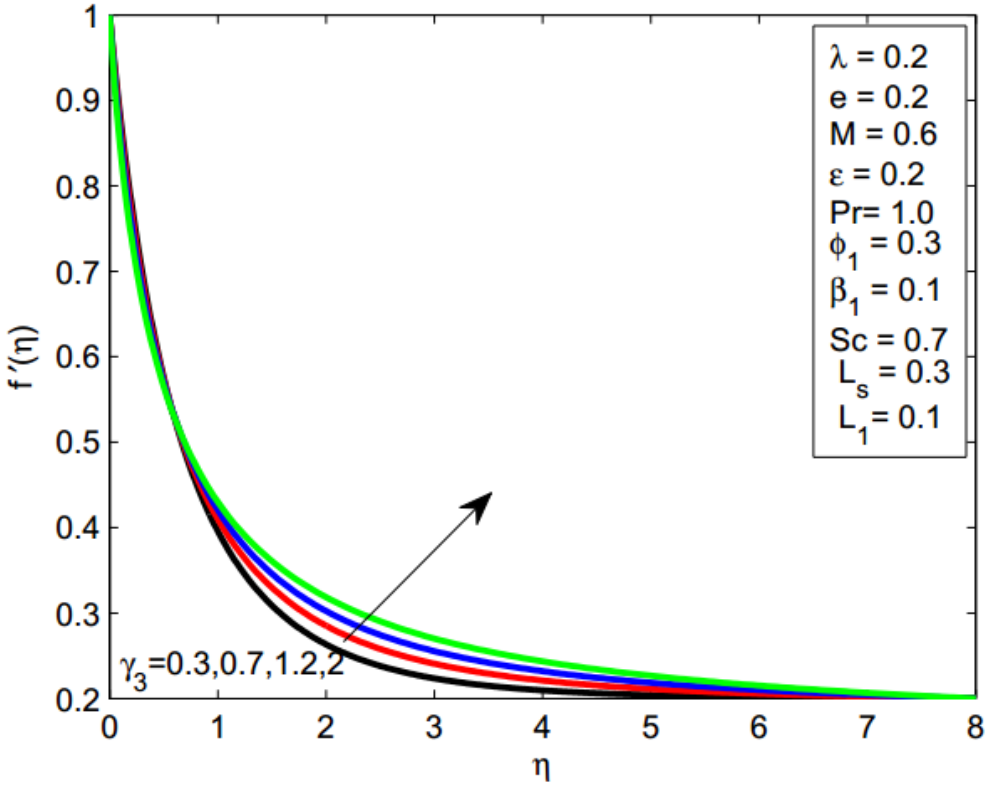

FIGURE 5.2: Impact of γ_3 on f'.

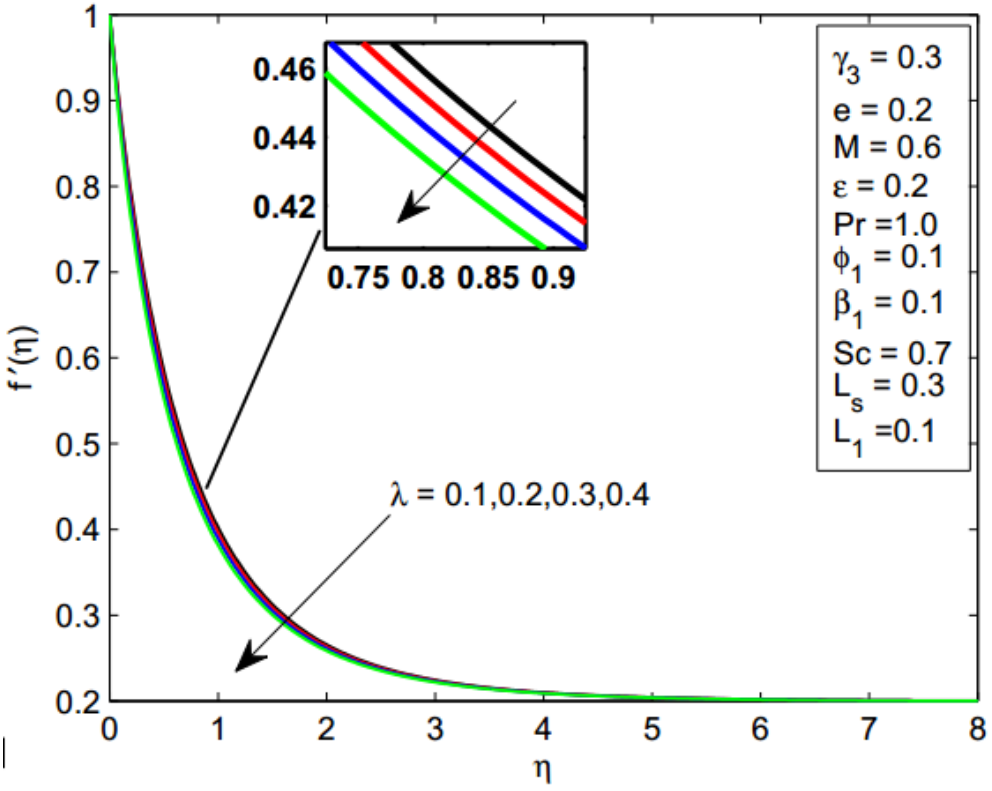

FIGURE 5.3: Impact of λ on f'.

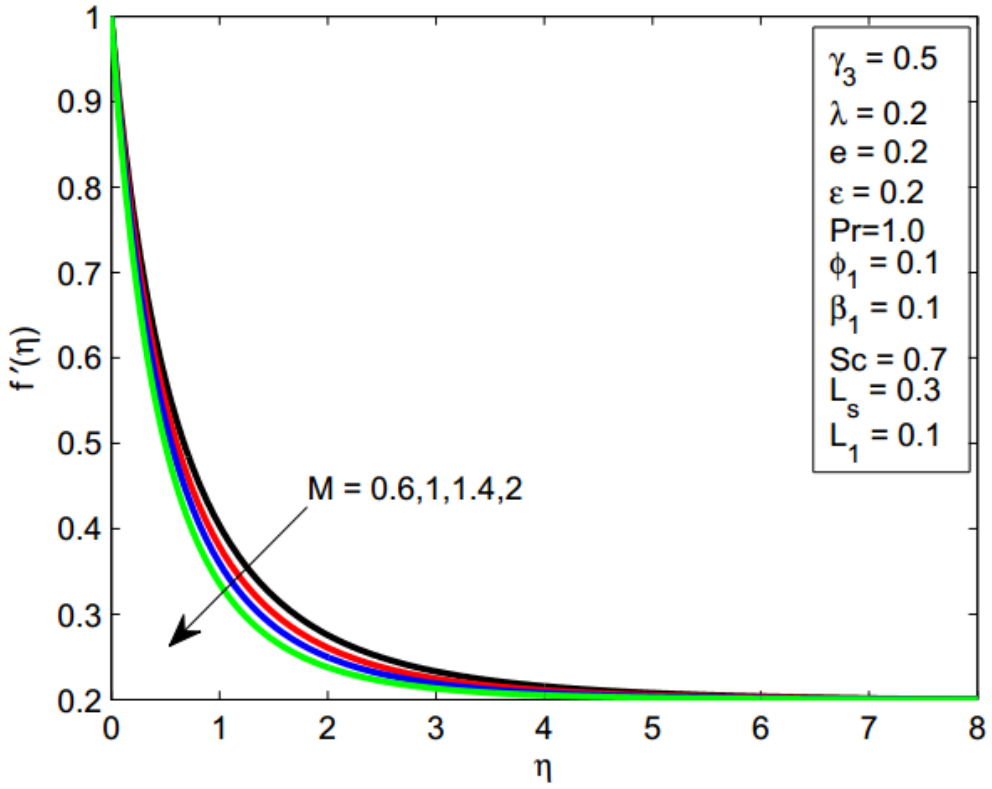

FIGURE 5.4: Impact of M on f'.

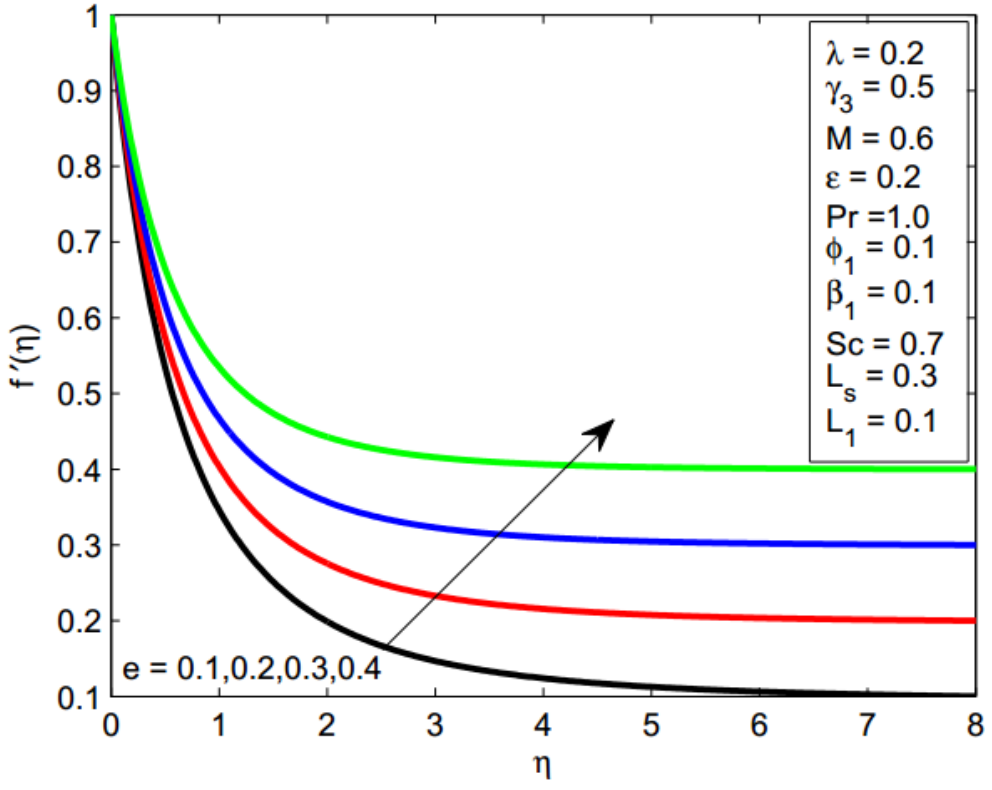

FIGURE 5.5: Impact of e on f'.

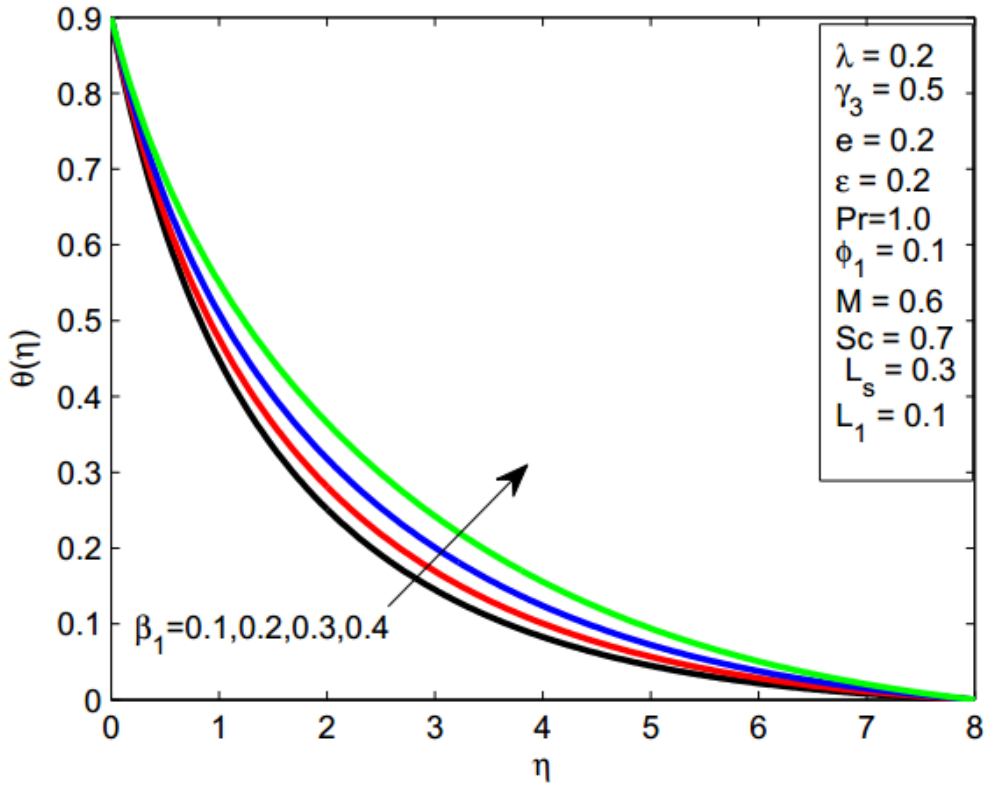

FIGURE 5.6: Impact of β_1 on θ.

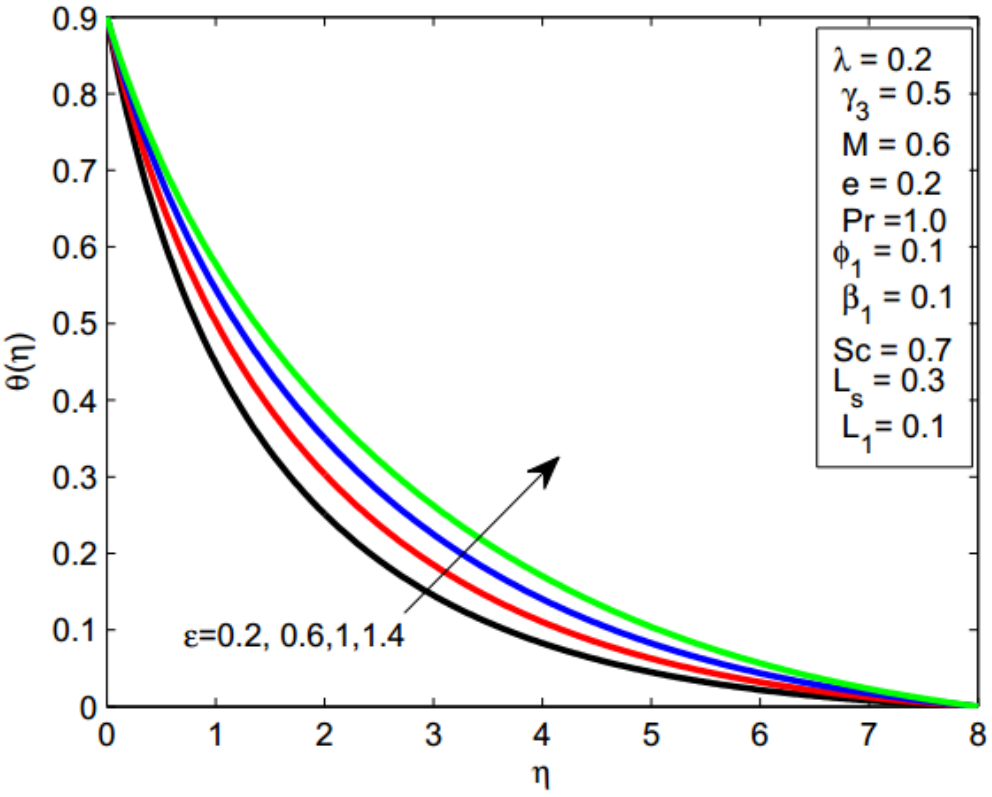

FIGURE 5.7: Impact of ϵ on θ.

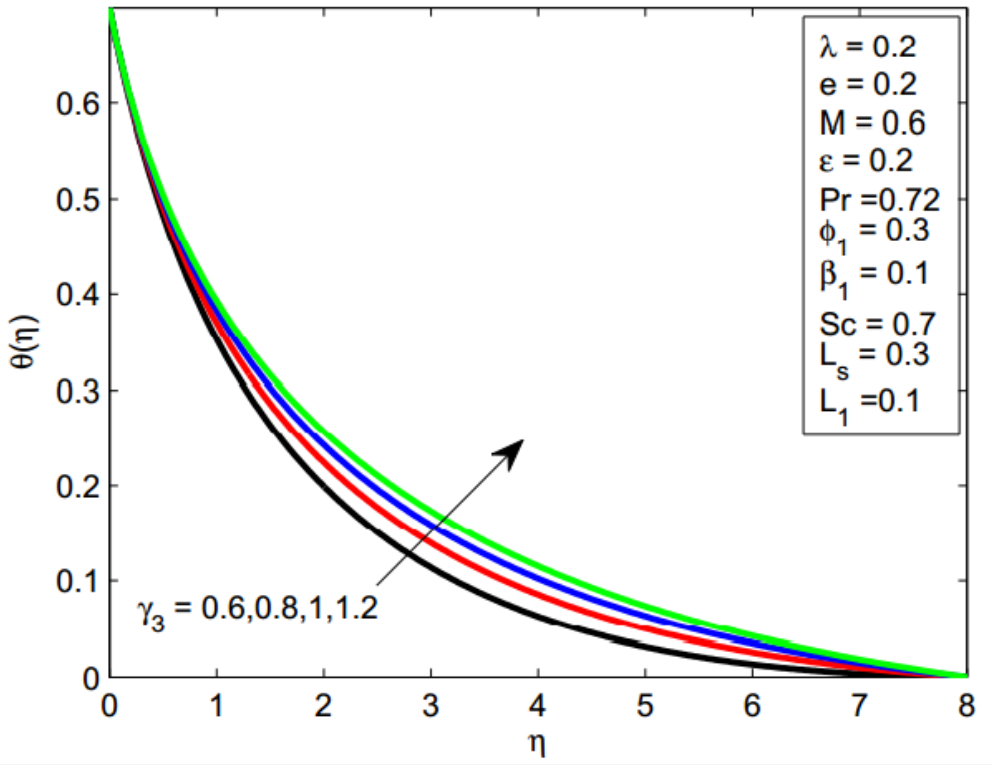

FIGURE 5.8: Impact of γ_3 on θ.

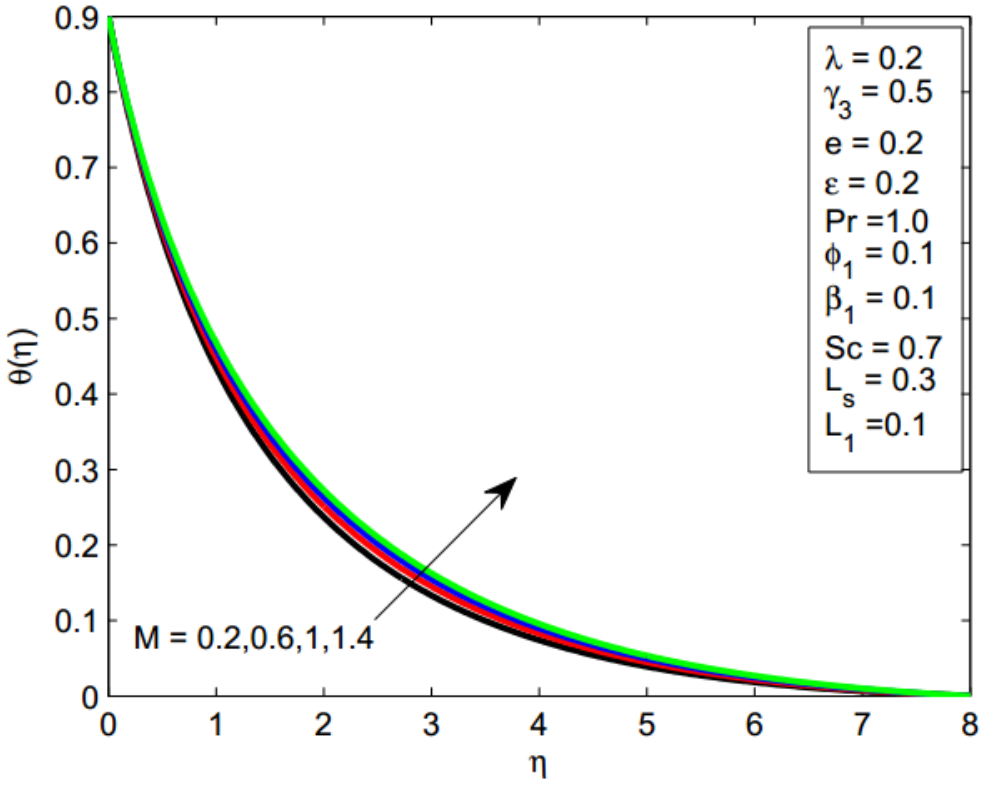

FIGURE 5.9: Impact of M on θ.

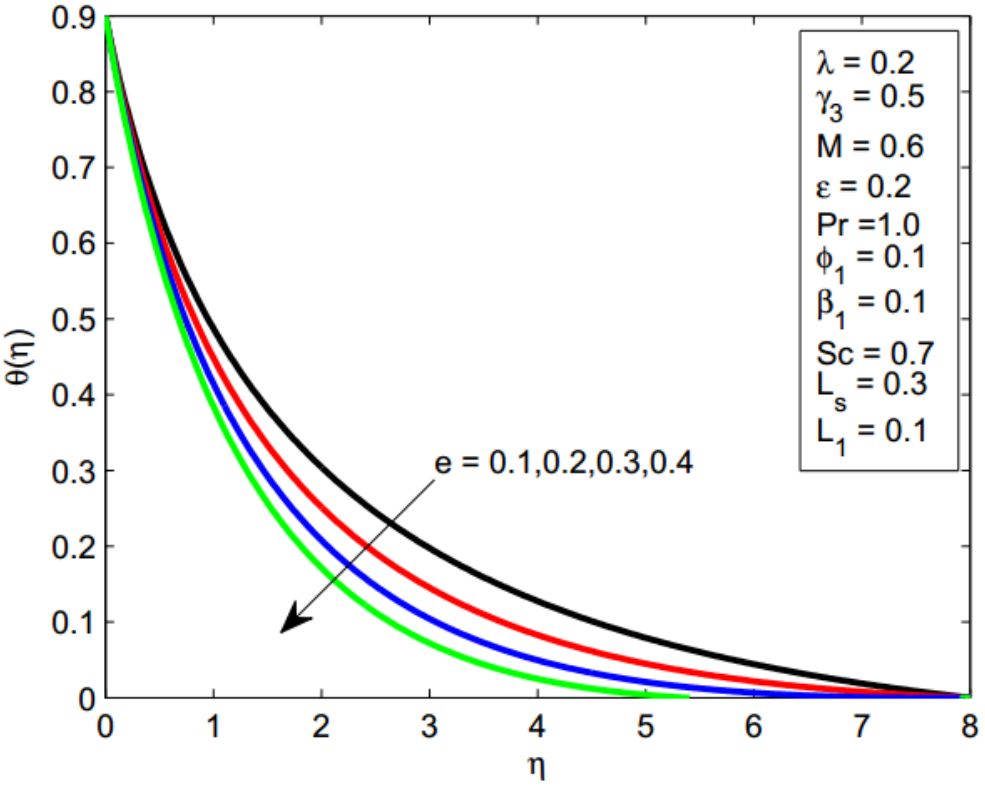

FIGURE 5.10: Impact of e on θ.

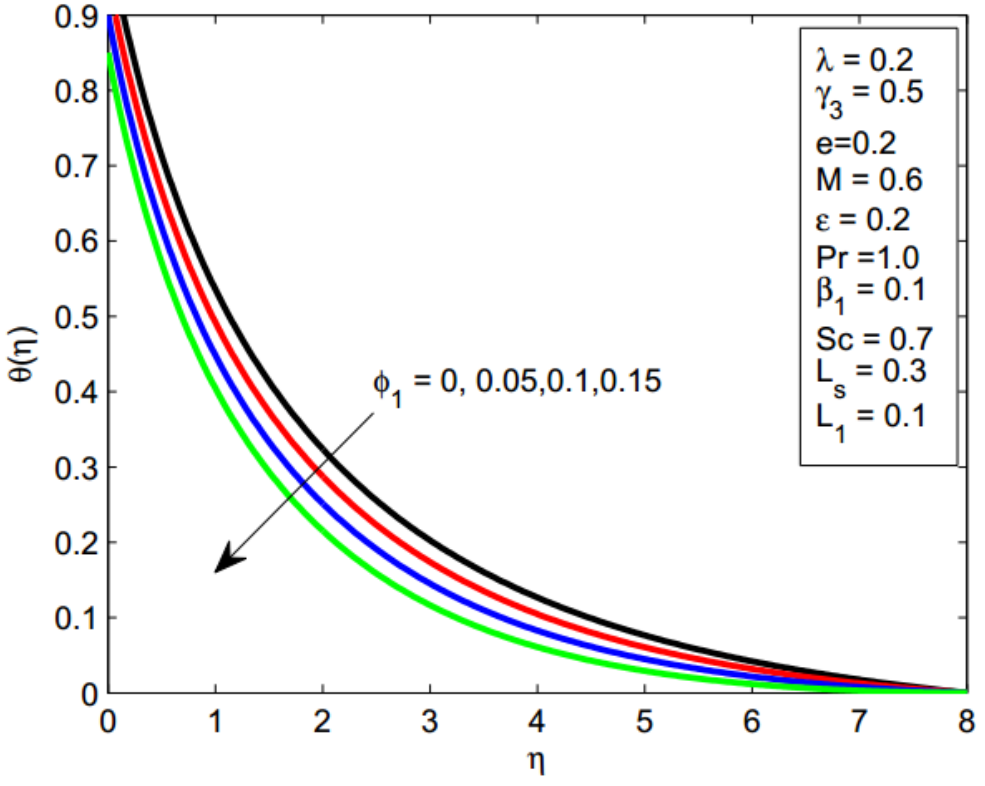

FIGURE 5.11: Impact of ϕ_1 on θ.

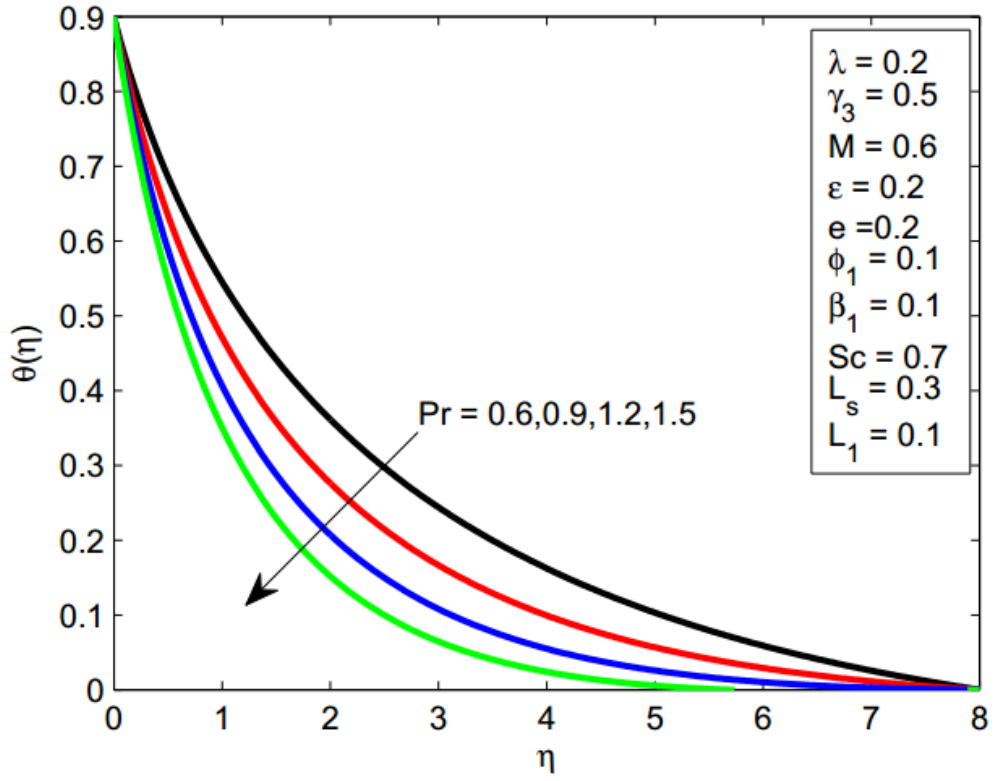

FIGURE 5.12: Impact of Pr on θ.

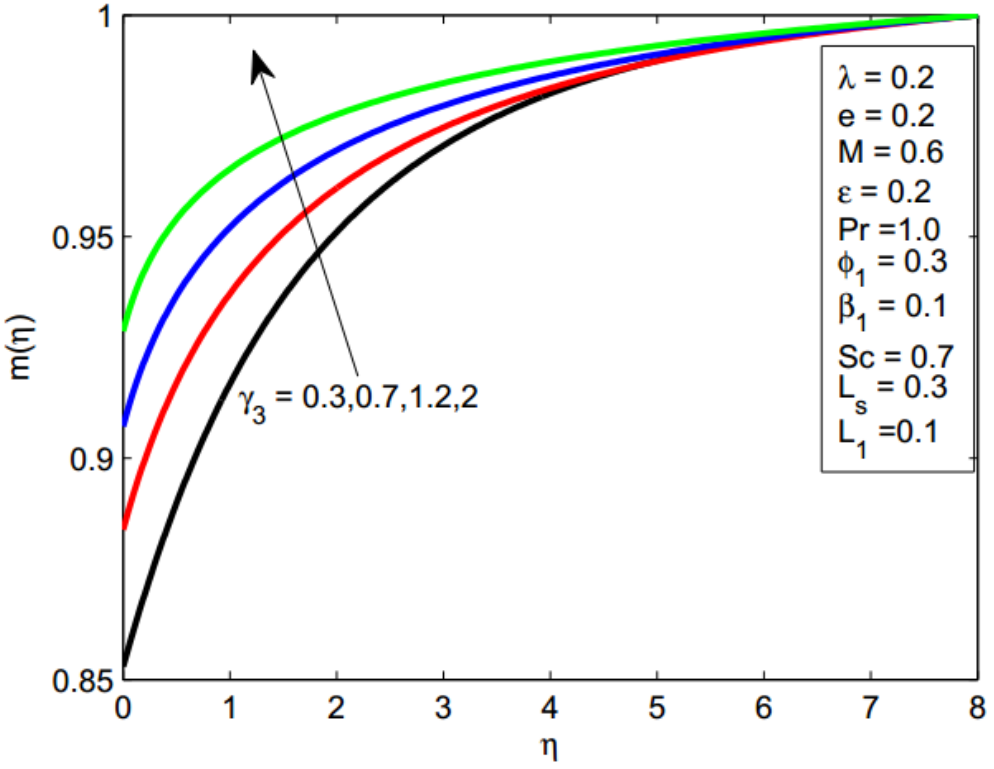

FIGURE 5.13: Impact of γ_3 on $m(\eta)$.

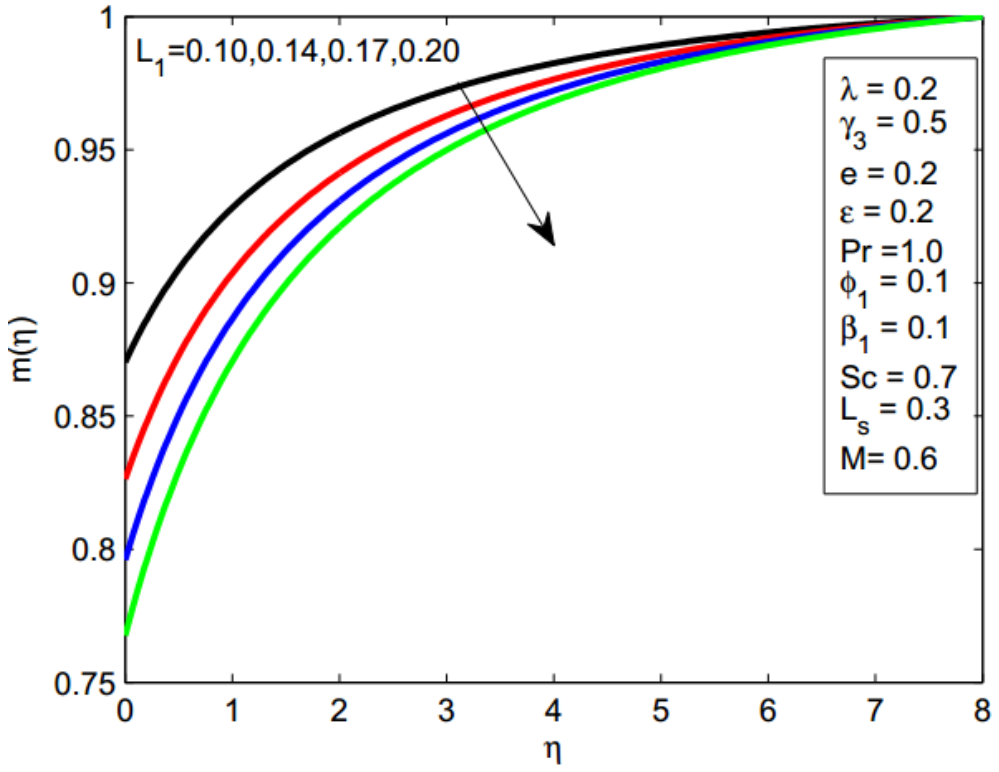

FIGURE 5.14: Impact of L_1 on $m(\eta)$.

5.5 Concluding Remarks

In the present chapter, we have numerically investigated the effect of the stagnation point flow of Williamson fluid over a stretching cylinder along with the response of homogenous/heterogenous reaction, magnetohydrodynamics and variable thermal conductivity. To solve the system of coupled ordinary non linear differential equations, we adopted the shooting method. To strengthen the results we also employed the built-in MATLAB function bvp4c. The main observations are summarised as follows:

- The strength of homogenous and heterogenous reactions shows a decreasing effect on the concentration distribution.
- The temperature field is a growing function of the thermal conductivity and heat generation coefficient.
- Prandtl number and thermal stratification have the tendency to increase to temperature gradient on wall.

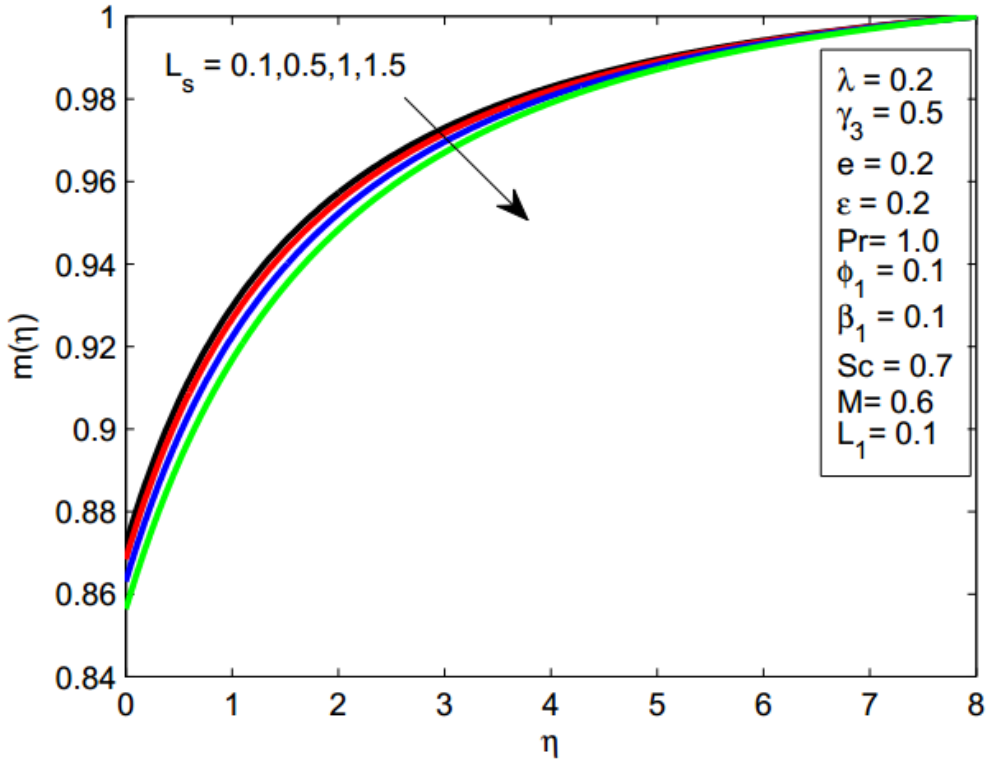

FIGURE 5.15: Reaction of L_s on $m(\eta)$.

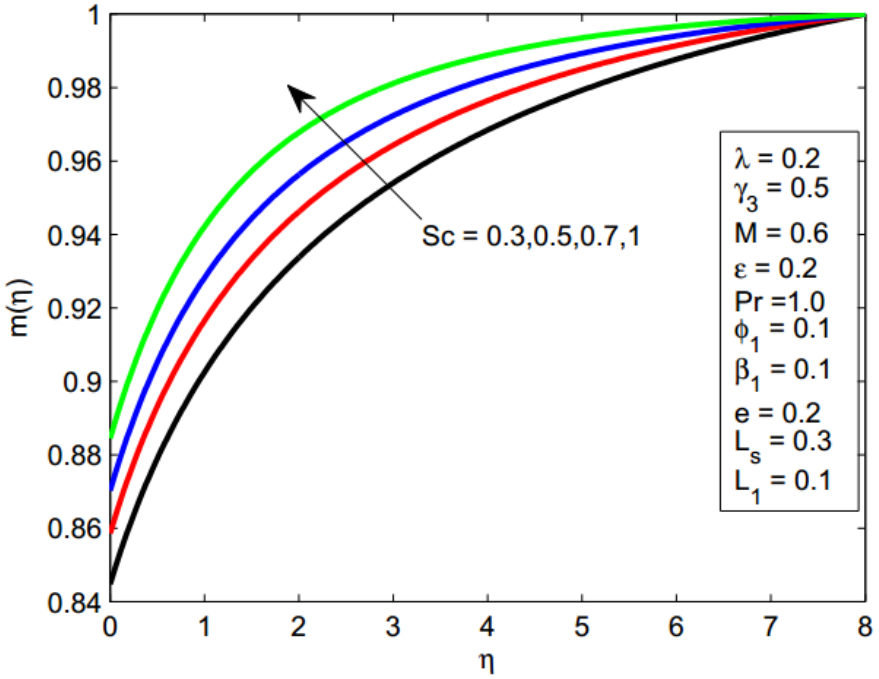

FIGURE 5.16: Reaction of Sc on $m(\eta)$.

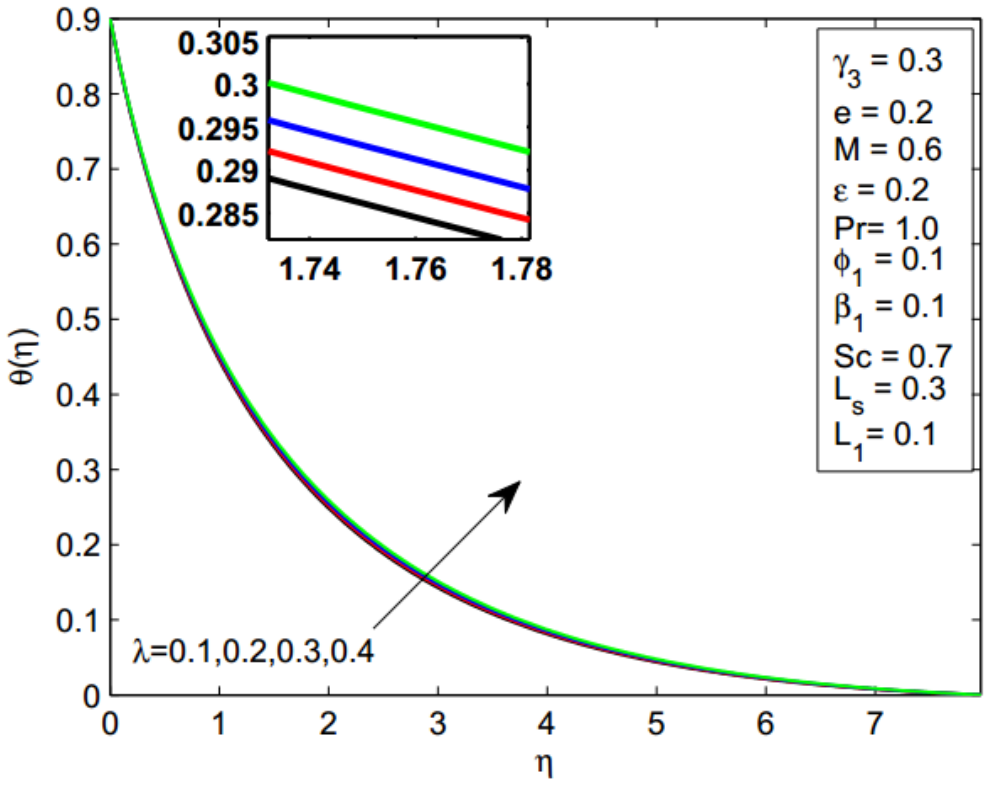

FIGURE 5.17: Reaction of λ on $\theta(\eta)$.

- Enhancing the values of the magnetic parameter boosts the temperature and its boundary layer thickness as well.
- Mass distribution is an intensifying function of Schmidt number Sc.
- A decline in the velocity and rise in the temperature profile is observed via Weissenberg number λ.
- The speed and the skin friction coefficient both rises up for the enhancement in the curvature parameter γ_3.

Chapter 6

MHD Oblique Stagnation Point Flow of Nanofluid Over a Convective Stretching Surface

6.1 Introduction

The present chapter demonstrates the analysis of the non-orthogonal flow of electrically conducting nanofluid past a stretching surface with the existence of uniformly applied magnetic field. To sustain this heat transfer mechanism via hot fluid, we have considered the convective boundary conditions at the lower surface of the stretching sheet. Similarity transformations play a pivotal role for the obtaining the ordinary differential equations from the mathematically modeled partial differential equations. Transformed system is tackled numerically by the shooting method. Moreover, the Matlab built-in routine bvp4c is implemented to validate and strengthen the numerical results which were obtained by the shooting method. The effect of different physical parameters e.g. non-orthogonality parameter, Brownian motion, Hartmann number, thermophoresis parameter, etc. is analyzed through graphs and tables. To analyze the fluid flow behavior, heat and mass transfer at the surface of the sheet, we calculate the numerical values for the Nusselt number, skin friction coefficient and Sherwood number. Flow behavior of nanofluid is analyzed through the stream lines for both the orthogonal and the non-orthogonal cases.

6.2 Mathematical Model

Consider an incompressible, two-dimensional and steady stagnation point flow of

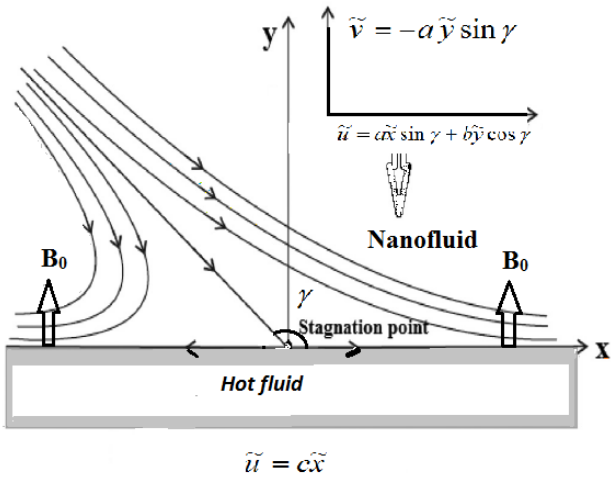

FIGURE 6.1: Physical description of the problem

an electrically conducting MHD nanofluid along a stretching surface. The Cartesian coordinate system (x, y) is adjusted in such a way that sheet is placed along the x-axis and fluid is confined in $y > 0$. To provide heat in the internal system, we have considered the convective boundary conditions with convective heat transfer coefficient h. Since we have considered the non-orthogonal flow, therefore fluid is impinging at the surface with an arbitrary angle of incidence γ_2 and the free stream velocity of the fluid is taken as $\widetilde{u} = a\widetilde{x}\sin\gamma_2 + b\widetilde{y}\cos\gamma_2$. Two forces opposite in direction but equal in magnitude are applied along the x-axis, as shown in Figure 6.1. Further, we assume that the surface has convective fluid temperature T_f and uniform inviscid temperature T_∞ with $T_f > T_\infty$. The rheological equations of the flow are modeled as:

$$\frac{\partial\widetilde{u}}{\partial\widetilde{x}} + \frac{\partial\widetilde{v}}{\partial\widetilde{y}} = 0, \tag{6.1}$$

$$\widetilde{u}\frac{\partial\widetilde{u}}{\partial\widetilde{x}} + \widetilde{v}\frac{\partial\widetilde{u}}{\partial\widetilde{y}} + \frac{1}{\rho}\frac{\partial\widetilde{p}}{\partial\widetilde{x}} = \nu\widetilde{\nabla}^2\widetilde{u} - \frac{\sigma B_o^2}{\rho}\widetilde{u}, \tag{6.2}$$

$$\widetilde{u}\frac{\partial\widetilde{v}}{\partial\widetilde{x}} + \widetilde{v}\frac{\partial\widetilde{v}}{\partial\widetilde{y}} + \frac{1}{\rho}\frac{\partial\widetilde{p}}{\partial\widetilde{y}} = \nu\widetilde{\nabla}^2\widetilde{v}, \tag{6.3}$$

$$\widetilde{u}\frac{\partial\widetilde{T}}{\partial\widetilde{x}} + \widetilde{v}\frac{\partial\widetilde{T}}{\partial\widetilde{y}} = \alpha\widetilde{\nabla}^2\widetilde{T} + \frac{(\rho c)_p}{(\rho c)_f}\left[D_B\widetilde{\nabla}\widetilde{C}.\ \widetilde{\nabla}\widetilde{T} + \frac{D_T}{T_\infty}\widetilde{\nabla}\widetilde{T}.\widetilde{\nabla}\ \widetilde{T}\right], \tag{6.4}$$

$$\widetilde{u}\frac{\partial\widetilde{C}}{\partial\widetilde{x}} + \widetilde{v}\frac{\partial\widetilde{C}}{\partial\widetilde{y}} = D_B\widetilde{\nabla}^2\widetilde{C} + \frac{D_T}{T_\infty}\widetilde{\nabla}^2\widetilde{T}, \tag{6.5}$$

where the boundary conditions

$$\begin{aligned}&\widetilde{u} = \widetilde{u}_w = c\widetilde{x},\ \widetilde{v} = 0, -k\frac{\partial \widetilde{T}}{\partial \widetilde{y}} = h\,(T_f - \widetilde{T}), \widetilde{C} = C_w \quad at\ \widetilde{y} = 0,\\ &\widetilde{u} = a\widetilde{x}\sin\gamma_2 + b\widetilde{y}\cos\gamma_2,\ \widetilde{v} = -a\widetilde{y}\sin\gamma_2,\ \widetilde{T} = T_\infty,\ \widetilde{C} = C_\infty \quad as\ \widetilde{y}\to\infty.\end{aligned} \tag{6.6}$$

In the above discussion, a, b and c are positive constants having dimensions of 1/time.

Now using the non-dimensional variables

$$\begin{aligned}&x = \widetilde{x}\sqrt{\frac{c}{\nu}},\quad y = \widetilde{y}\sqrt{\frac{c}{\nu}},\quad u = \frac{1}{\sqrt{\nu c}}\widetilde{u},\quad v = \frac{1}{\sqrt{\nu c}}\widetilde{v}\\ &p = \frac{1}{\rho\nu c}\widetilde{p},\quad T = \frac{\widetilde{T} - T_\infty}{T_f - T_\infty},\quad C = \frac{\widetilde{C} - C_\infty}{C_w - C_\infty},\end{aligned} \tag{6.7}$$

the flow equations $(1) - (5)$ take the following form,

$$\frac{\partial u}{\partial x} + \frac{\partial v}{\partial y} = 0, \tag{6.8}$$

$$u\frac{\partial u}{\partial x} + v\frac{\partial u}{\partial y} + \frac{1}{\rho}\frac{\partial p}{\partial x} = \nabla^2 u - \frac{\sigma B_o^2}{c\rho}u, \tag{6.9}$$

$$u\frac{\partial v}{\partial x} + v\frac{\partial v}{\partial y} + \frac{1}{\rho}\frac{\partial p}{\partial y} = \nabla^2 v, \tag{6.10}$$

$$Pr\left[u\frac{\partial T}{\partial x} + v\frac{\partial T}{\partial y}\right] = \nabla^2 T + Pr\left[Nb\nabla C.\nabla T + Nt\nabla T.\nabla T\right], \tag{6.11}$$

$$Sc\left[u\frac{\partial C}{\partial x} + v\frac{\partial C}{\partial y}\right] = \nabla^2 C + \frac{Nt}{Nb}\nabla^2 T. \tag{6.12}$$

Different dimensionless parameter appearing in Eqs. $(6.8) - (6.12)$ are defined as

$$\begin{aligned}&e = \frac{a}{c},\ Pr = \frac{\nu}{\alpha},\ Nt = \frac{D_t}{T_\infty}\frac{(\rho c)_p}{(\rho c)_f}\frac{T_f - T_\infty}{\nu}, M^2 = \frac{\sigma B_o^2}{c\rho},\\ &Nb = D_B\frac{(\rho c)_p}{(\rho c)_f}\frac{C_w - C_\infty}{\nu},\ r_2 = \frac{h}{k}\sqrt{\frac{\nu}{c}},\ Sc = \frac{\nu}{D_B}.\end{aligned} \tag{6.13}$$

Stream function ψ is given by

$$u = \frac{\partial \psi}{\partial y},\ v = -\frac{\partial \psi}{\partial x}. \tag{6.14}$$

Substituting Eq. (6.13) into Eqs. $(6.8)-(6.12)$ and cancellation of pressure from the aforementioned equations using $p_{xy}=p_{yx}$ yields

$$\nabla^4\psi+\frac{\partial\psi}{\partial x}\frac{\partial\left(\nabla^2\psi\right)}{\partial y}-\frac{\partial\psi}{\partial y}\left(\frac{\partial\left(\nabla^2\psi\right)}{\partial x}\right)-M^2\frac{\partial^2\psi}{\partial y^2}=0, \tag{6.15}$$

$$Pr\left[\frac{\partial\psi}{\partial y}\frac{\partial T}{\partial x}-\frac{\partial\psi}{\partial\, x}\frac{\partial T}{\partial y}\right]=\nabla^2T+Pr\left[Nb\nabla C.\nabla T+Nt\nabla T.\nabla T\right], \tag{6.16}$$

$$Sc\frac{\partial\psi}{\partial y}\left[\frac{\partial C}{\partial x}-\frac{\partial\psi}{\partial x}\frac{\partial C}{\partial y}\right]=\nabla^2C+\left(\frac{Nt}{Nb}\right)\nabla^2T. \tag{6.17}$$

The associated boundary conditions will take the following form

$$\begin{aligned}&\psi=0,\ \frac{\partial\psi}{\partial y}=x,\ \frac{\partial T}{\partial y}=-\frac{h}{k}\sqrt{\frac{\nu}{c}}\left(1-T\right),\ C=1\text{ at }\ y=0\\&\psi=exysin\gamma_2+\frac{1}{2}y^2r_1\cos\gamma_2,\ T=0,\ C=0\text{ as }y\to\infty,\end{aligned} \tag{6.18}$$

where $r_1=\frac{b}{c}$ represents the secondary stretching parameter in normal direction. Our main motive is to confront the solutions of Eqs. $(6.15)-(6.17)$. For this purpose, consider the following relationship

$$\psi(x,y)=x\ f(y)+\ g(y),\quad T=\ \theta(y),\quad C=\ \phi(y), \tag{6.19}$$

The tangential and normal components of the flow are represented by the functions $f(y)$ and $g(y)$. Substituting Eq. (6.18) in Eqs. $(6.15)-(6.17)$ and simplifying, subsequently we attain the ordinary differential equations in the following form:

$$f'''+f\ f''-f'^2-M^2f'+c_1=0, \tag{6.20}$$

$$g'''\ +f\ g''\ -f'g'-\ M^2g'+c_2=0, \tag{6.21}$$

$$\theta''+Pr\ \left[f\ \theta'+Nb\ \phi'\theta'+Nt\ \left(\theta'\right)^2\right]=0, \tag{6.22}$$

$$\phi''+Sc\ f\phi'+\ \left(\frac{Nt}{Nb}\right)\theta''=0. \tag{6.23}$$

The associated boundary conditions are as follows;

$$\left.\begin{aligned}f(0)=0,\quad f'(0)=1,\quad f'(\infty)=esin\gamma_2,\\g(0)=0,\quad g'(0)=0,\quad g''(\infty)=r_1\cos\gamma_2,\\\theta'(0)=-r_2\left(1-\theta(0)\right),\quad\theta(\infty)=0,\quad\phi(0)=1,\quad\phi(\infty)=0.\end{aligned}\right\} \tag{6.24}$$

In Eqs. $(6.20)-(6.23)$, c_1, c_2 are constants of integration. To evaluate the constants

from Eqs. (6.20) and (6.21), we have taken the limit $y \to \infty$ in Eq. (6.20) and utilizing the boundary condition $f'(\infty) = e\sin\gamma_2$, we get $c_1 = e^2\sin^2\gamma_2$. After solving the boundary layer Eq. (6.20), we get $f(y) = ey\sin\gamma_2 + A$ as $y \to \infty$, where $A = A(\gamma_2, e, M)$ is a constant. Taking the limit $y \to \infty$ in Eq. (6.21) and utilizing the boundary condition at infinity $g'_\infty = r_1\cos\gamma_2$, we get $c_2 = -Ar_1\cos(\gamma_2)$. Thus Eqs. (6.20) – (6.23) become

$$f''' + f\ f'' - f'^2 - M^2 f' + e^2\sin^2\gamma_2 + M^2 e\sin\gamma_2 = 0, \tag{6.25}$$

$$g''' + f\ g'' - f'g' - M^2 g' - Ar_1\cos\gamma_2 = 0, \tag{6.26}$$

$$\theta'' + Pr\ \left[f\theta' + Nb\ \phi'\theta' + Nt\ (\theta')^2\right] = 0, \tag{6.27}$$

$$\phi'' + Scf\phi' + \left(\frac{Nt}{Nb}\right)\theta'' = 0. \tag{6.28}$$

For an obvious simplification, introduce the following substitution

$$g(y) = r_1 h(y)\cos\gamma_2. \tag{6.29}$$

By using Eq. (6.29) in Eq. (6.26), we get

$$h''' + f\ h'' - f'\ h' - Mh' - A = 0, \tag{6.30}$$

with the associated boundary conditions:

$$h(0)\ = 0,\ h'(0) = 0,\ h''(\infty) = 1. \tag{6.31}$$

The concerned physical quantities are the local heat flux, skin friction coefficient and the local mass diffusion flux, which is written in dimensionless form as [82], [91]:

$$\tau_w = \left(\frac{\partial^2\psi}{\partial y^2} - \frac{\partial^2\psi}{\partial x^2}\right), q_w = -\left(\frac{\partial T}{\partial y}\right)_{y=0},\ q_m = -\left(\frac{\partial C}{\partial y}\right)_{y=0}. \tag{6.32}$$

In the present case above quantities take the following arrangement [82], [91]:

$$\tau_w = x\left[f''(0) + r_1 h''(0)\cos\gamma_2\right], q_w = -\theta'(0),\ q_m = -\phi'(0). \tag{6.33}$$

The stream lines and the curve $u = 0$ converge at the stagnation point $\tau_w = 0$. We can get the stagnation point location x_s by using the relationship:

$$x_s = -\frac{r_1 h''(0)\cos\gamma_2}{f''(0)}. \tag{6.34}$$

6.3 Numerical Solution

The resulting nonlinear system of ordinary differential equations (6.25), (6.27), (6.28) and (6.30) subject to the conditions (6.24) and (6.31) have been examined numerically through the shooting method [85] for various values of the parameters. On account of number of computational experiments, as there is no significant difference in the results after $y = 7$ so we are taking $[0, 7]$ for the domain of the problem rather than $[0, \infty)$.

$$\left.\begin{aligned}
f_1' &= f_2, & f_1(0) &= 0\\
f_2' &= f_3, & f_2(0) &= 1\\
f_3' &= f_2^2 - f_1 f_3 + M^2 f_2 - M^2 (e\sin\gamma_2) - (e\sin\gamma_2)^2, & f_3(0) &= s\\
h_1' &= h_2, & h_1(0) &= 0\\
h_2' &= h_3, & h_2(0) &= 0\\
h_3' &= f_2 h_2 - f_1 h_3 + M^2 h_2 + A, & h_3(0) &= t\\
\theta_1' &= \theta_2, & \theta_1(0) &= u\\
\theta_2' &= -Pr\left[f_1\theta_2 + Nb\theta_2\phi_2 + Nt\theta_2^2\right], & \theta_2(0) &= -r_2(1-\theta_1(0))\\
\phi_1' &= \phi_2, & \phi_1(0) &= 1\\
\phi_2' &= \left[-Scf_1\phi_2 + \frac{PrNt}{Nb}\left(f_1\theta_2 + Nb\theta_2\phi_2 + Nt\theta_2^2\right)\right]. & \phi_2(0) &= k
\end{aligned}\right\} \tag{6.35}$$

We apply the Runge-Kutta method of order four to solve the above mentioned system of initial value problem. We adopted Newton's method for the refining of the missing values of s, t, u and k so that we meet the following yardstick.

$$\max\{|f_2(7) - e\sin\gamma_2|, |h_3(7) - 1|, |\theta_1(7)|, |\phi_1(7)|\} < \varepsilon,$$

where $\varepsilon > 0$ is a small positive real constant. A threshold $\varepsilon = 10^{-6}$ is adopted for computation of all the numerical results.

6.4 Results and Discussions

Our main interest is to analyze the influnces of variation of different physical parameters of the current MHD nanofluid model. Tables (6.1) – (6.4) are portrayed for looking into the numerical values of the heat flux, drag coefficient and mass tansfer rate for various concerned physical parameters. It can be observed from Table 6.1 that our obtained numerical results are established a best numeric relation with the accessable previously publish articles. It is noticed from Table 6.2 that the drag coefficient tangential component $h''(0)$ and drag coefficient $f''(0)$ increases with an enhancing values of e. Table 6.3 is presented to investigate the leverages of angle of incidence on drag coefficient, mass and heat flux over the stretching convective surface. It has been observed that when γ_2 is increased, tangential component of the drag coefficient increases and normal component of the drag coefficient decreases but it has not a significant effect on both local heat and mass fluxes. To investigate the effect of $Pr, Nt, r_2, Nb,, Sc$ and M by considering γ_2 and e fixed over local heat flux, Table 6.4 is presented. Greater values of Prandtl number Pr and Biot number r_2 lead to an increment in the values of $-\theta'(0)$, it is due to the fact that heat transfers from the sheet towards fluid because of $(T_f > T_\infty)$. It is also noticed that the surface heat flux downturns for greater values of Nt, Sc and Nb, while Pr and r are kept constant. It is evident that local mass flux shows increasing phenomenon with an enhancement in Nb and Sc because of high concentration from surface to the fluid. At the end, we find out that we experienced a decrement in the local mass flux while increasing the quantities of the parameters like thermophoresis parameter Nt, Prandtl number Pr and Biot number r.

To portray a physical significance of the flow problem, results are plotted in Figs. (6.2) – (6.26) for each velocity profile, temperature distribution, concentration phenomenon and stream lines. Fig. 6.2 illustrates the dimensionless velocity profiles $f'(y)$ for angle of incidence $\gamma_2 = \pi/4$ and diverse values of e. As it is viewed from Fig. 6.2 that with an increase in stretching ratio e, velocity profile shows the increasing behavior. Furthermore for $e > 1/\sin\gamma_2$, a boundary layer pattern of flow is viewed. It means with an hike in e, boundary layer width downturns. This happens for the sake of a locked entries of c with $e > 1/\sin\gamma_2$ act the part of surged acceleration for the external stream becuase of an increment in the straining motion surrounded by the stagnation-point. This prompt to irrigate

of the boundary layer when an enhancement in e is considered. Here also observed from Fig. 6.2 that the flow originates an inverted boundary layer arrangement for $e < 1/\sin\gamma_2$ owing to the stretching velocity of the sheet excels the stagnation velocity at the external stream.

Similarly, Fig. 6.3 depicts the distribution of $f'(y)$ for $e = 0.4$ and varying quantities of γ_2. In Fig. 6.3, by looking into detail that when $e < 1/\sin\gamma_2$, the dimensionless velocity $f'(y)$ enhances by an increment in γ_2. Figs. 6.4 and 6.5 present the effects of changes in e on $h''(y)$ for constant values of e and γ_2. It can be determined from Figs. 6.4 and 6.5 that near the vicinity of the surface, $h''(y)$ provides a slightly increasing behavior while $h''(y)$ switches its behavior after $y = 1$. Fig. 6.6 shows the decreasing behaviour of horizontal velocity profile, while increasing the magnetic parameter M. The effects of variation of emerging physical parameters like e, γ_2, Pr, Sc, Nt, Nb and r_2 over the temperature distribution $\theta(y)$ are considered in Figs. (6.7) – (6.14). It is observed from Figs. 6.7 and 6.8 that the energy at a point downturns for the increasing values of e and γ_2 for constant values of e. From Fig. 6.9, we notice that with an upturns in the Prandtl number Pr, temperature pattern decreases. The surface heat flux increases as with the increasing values of Pr, the thermal boundary layer thickness potrays a decreasing pattern. Figs. (6.10) – (6.14) reflect that the energy profile $\theta(y)$ shows a boosting role for an enhancement in the Schmidt number Sc, Biot number r_2, Brownian motion Nb, thermophoresis parameter Nt and magnetic parameter M . We observe that the Prandtl number enhances with an increment in the kinematic viscosity of the base fluid and decreases for increment in the thermal diffusivity of the nanofluid. Thermophoresis parameter Nt enhances with an boost in the energy profile of the convective fluid at the wall and effective heat capacity of the nanofluid, while it declines for an increment in the kinematic viscosity of the base fluid and ambient temperature.

The concentration profile $\phi(y)$ is influenced by the physical parameters e, γ_2, M, Sc, Nb, Nt and r_2 as shown in Figs. (6.15) – (6.21). After extensive analysis, we find that with the increase in the parameters r, Nt and M, the nanoparticle concentration profile $\phi(y)$ increases, while concentration profile $\phi(y)$ shows decreasing behavior for the various values of each of the physical parameters e, γ_2, Sc and Nb. Brownian motion parameter Nb raises up with enhancement in the concentration of the nanoparticles at the stretching surface and effective heat capacity of the

nanofluid while downturns for an upturn in the kinematic viscosity of the base fluid.

Figs (6.22) – (6.26) depict the stream line patterns of the non-orthogonal stagnation point flows for the parameters e, γ_2, r_1 and M. All calculations of stream lines are made for $\psi = -4, -3, -2, -1, 0, 1, 2, 3, 4$. Stagnation point locations are also expressed in Figs. Stream line patterns due to variations in e are enlisted in Figs (6.22) – (6.24). We notice that with the increase in stretching parameter e, stagnation point location is moved to the right side for the favourable flow confined in the region $0 < \gamma_2 < \pi/2$. We have chosen $Nt = 0.2$, $Nb = 0.5$, $e = 0.1$, $Pr = 1$, $r_2 = 1$, $Sc = 1$, $r_1 = 1$ and $M = 0.1$ for Fig. 25 and $\gamma_2 = \pi/4$ for Fig. 6.26. Fig. 6.25 depicts the influence of the variation in the angle of incidence and corresponding stagnation point. Fig. 6.26 depicts the variations of secondary stretching parameter in normal direction and corresponding stagnation point values. It is noticed in Fig. 6.26 that when r_1 is positive, the fluid is impinging from right side at the wall. Same kind of behavior for stream line is plotted in Fig. 6.26, while for negative values of r_1 it is determined that the fluid is impinging from left side at the wall and for $r_1 = 0$, it is observed that fluid is impinging orthogonally at the wall. It is realized that with the increase in secondary stretching parameter in normal direction, angle of incidence decreases.

TABLE 6.1: Numerical values of $f''(0)$ and $h''(0)$ for $Nt = 0.2$, $Nb = 0.5$, $\gamma_2 = \pi/2$, $Pr = 1$, $r_2 = 0.1$, $Sc = 1$, $M = 0$ and $r_1 = 1$.

	$f''(0)$				$h''(0)$			
e	Present		Ref. [82]	Ref. [61]	Present		Ref. [82]	Ref. [61]
	Shooting	bvp4c			Shooting	bvp4c		
0.1	-0.96939	-0.96939	-0.96938	-0.96938	0.25390	0.25391	0.26341	0.26278
0.3	-0.84942	-0.84901	-0.84937	-0.84937	0.60627	0.59938	0.60631	0.60573
0.8	-0.29938	-0.24509	-0.29937	-0.29937	0.93473	0.75510	0.93472	0.93430
1	0.0	0.0	0.0	0.0	0.99912	1.00533	1	1
2	2.01750	2.01832	2.01750	2.01750	1.16322	1.14289	1.16522	1.16489
3	4.72928	4.85888	4.72928	4.72928	1.23435	1.30427	1.23465	1.23438

TABLE 6.2: Numerical values of $f''(0)$, $h''(0)$, -$\theta'(0)$ and -$\phi'(0)$ for $Nt = 0.2$, $Nb = 0.5$, $\gamma_2 = \pi/4$, $Pr = 1$, $r_2 = 0.5$, $Sc = 1$, $M = 0$ and $r_1 = 1$.

		Shooting				bvp4c			
e	A	$f''(0)$	$h''(0)$	$-\theta'(0)$	$-\phi'(0)$	$f''(0)$	$h''(0)$	$-\theta'(0)$	$-\phi'(0)$
0.1	0.84454	-0.98072	0.15487	0.23527	0.54176	-0.98072	0.15491	0.23527	0.54176
0.3	0.62473	-0.91066	0.48819	0.24155	0.57691	-0.91066	0.48819	0.24155	0.57691
0.7	0.33282	-0.67251	0.77920	0.25372	0.64593	-0.67227	0.77546	0.25374	0.64571
1	0.17431	-0.42431	0.89648	0.26186	0.69422	-0.40759	0.88512	0.26333	0.68384
1.3	0.04443	-0.12572	0.97569	0.26916	0.73972	-0.07033	0.76781	0.27359	0.70605
1.5	-0.03161	0.09854	1.01631	0.27362	0.76868	0.098759	1.02217	0.27366	0.76852
1.9	-0.16426	0.33799	0.13214	0.26896	0.71336	0.60214	1.08374	0.281745	0.82358

TABLE 6.3: Numerical values of -$f''(0)$, $h''(0)$, -$\theta'(0)$ and -$\phi'(0)$ for $Nt = 0.2$, $Nb = 0.5$, $e = 0.1$, $Pr = 1$, $r_2 = 0.5$, $Sc = 1$, $M = 0$, and $r_1 = 1$.

		Shooting				bvp4c			
γ_2	A	$-f''(0)$	$h''(0)$	$-\theta'(0)$	$-\phi'(0)$	$-f''(0)$	$h''(0)$	$-\theta'(0)$	$-\phi'(0)$
$\pi/15$	0.94884	0.99568	-0.23079	0.23324	0.53032	0.99481	-0.25590	0.23351	0.53044
$\pi/12$	0.93715	0.99442	-0.15122	0.23343	0.53143	0.99385	-0.19511	0.23356	0.53199
$\pi/6$	0.88526	0.98762	0.05616	0.23440	0.53688	0.98719	0.03213	0.23449	0.53724
$\pi/4$	0.84453	0.98072	0.15487	0.23527	0.54176	0.98072	0.15491	0.23527	0.54176
$\pi/3$	0.81425	0.97480	0.21244	0.23595	0.54559	0.97480	0.21245	0.23595	0.54559
$\pi/2$	0.79170	0.96940	0.25390	0.23653	0.54886	0.96939	0.253907	0.23653	0.54886

TABLE 6.4: Numerical values of r_2, Nt, Nb, Pr, Sc and M for $r_1 = 1$, $\gamma_2 = \pi/4$, and $e = 0.1$.

						shooting		bvp4c	
r_2	Nt	Nb	Pr	Sc	M	$-\theta'(0)$	$-\phi'(0)$	$-\theta'(0)$	$-\phi'(0)$
0.1	0.2	0.5	1	1	0.5	0.08152	0.55954	0.08152	0.55954
0.3						0.17753	0.53694	0.17753	0.53694
0.5						0.23158	0.52433	0.23158	0.52433
0.1	0.4	0.5	1	1	0.5	0.08134	0.54042	0.08134	0.54042
	0.6					0.08115	0.52156	0.08115	0.52156
0.1	0.2	0.1	1	1	0.5	0.08450	0.47016	0.08450	0.47016
		0.3				0.08309	0.54456	0.08309	0.54456
		0.5				0.08152	0.55954	0.081517	0.55954
0.1	0.2	0.5	2	1	0.5	0.08563	0.55739	0.08563	0.55739
			2.5			0.08658	0.55692	0.08658	0.55692
0.1	0.2	0.5	1	2	0.5	0.08044	0.88630	0.08044	0.88630
				2.5		0.08013	1.01974	0.08013	1.01974
0.1	0.2	0.5	1	1	1	0.08040	0.51915	0.080402	0.51915
					2	0.04631	0.52432	0.07757	0.43636

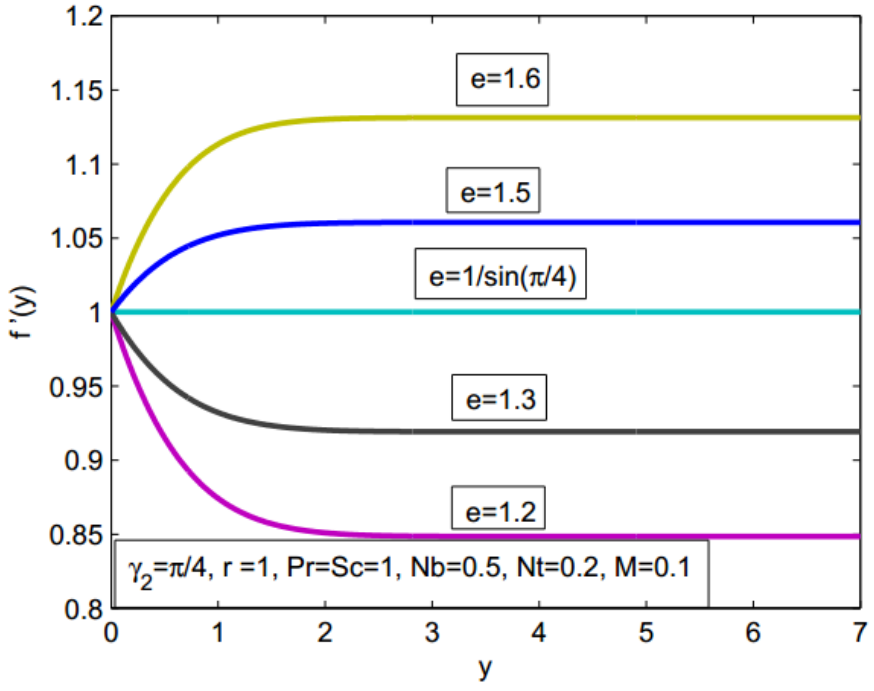

FIGURE 6.2: Consequence of e on $f'(y)$.

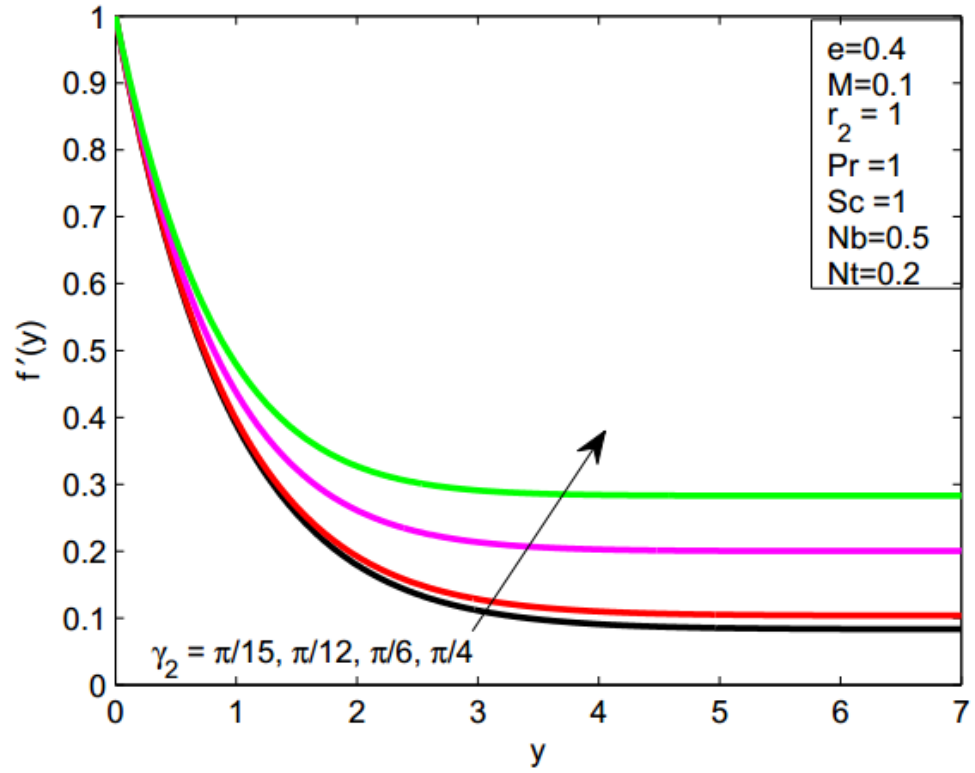

FIGURE 6.3: Consequence of γ_2 on $f'(y)$.

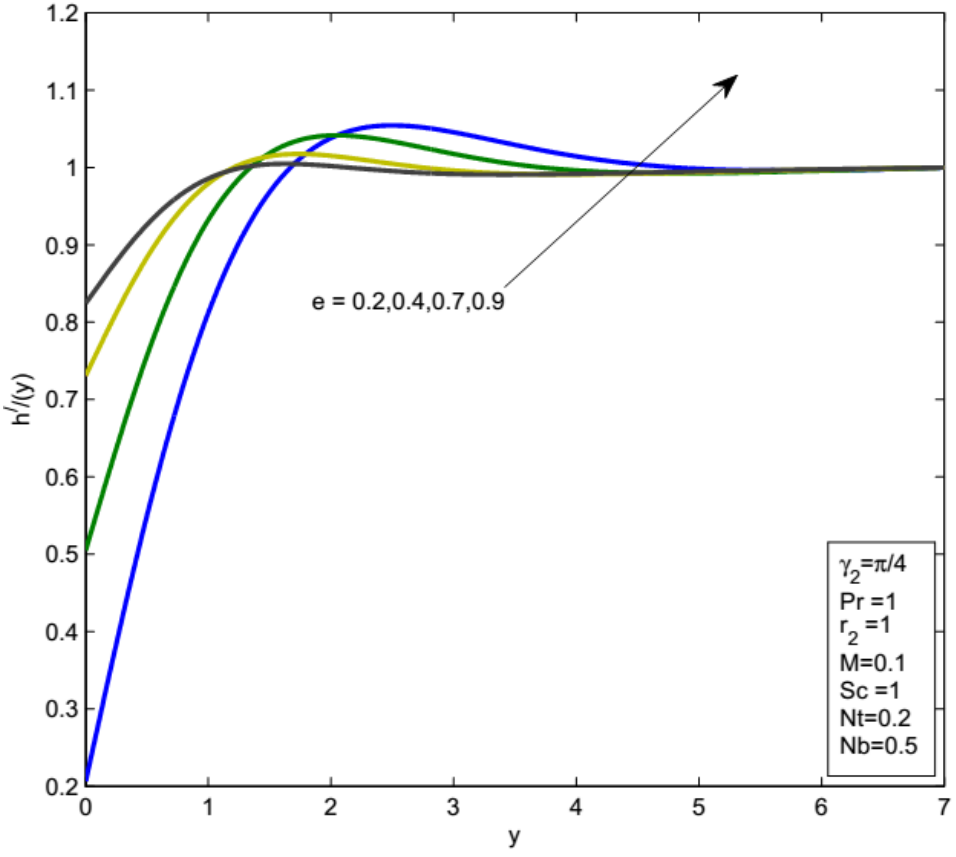

FIGURE 6.4: Consequence of e on $h''(y)$.

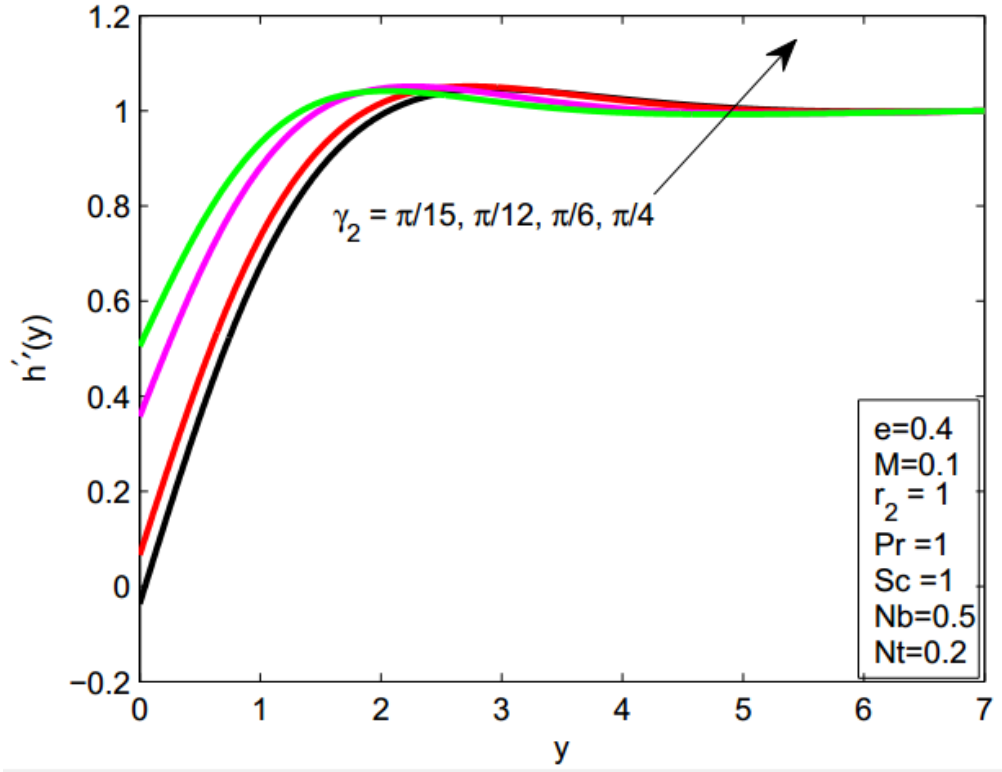

FIGURE 6.5: Consequence of γ_2 on $h''(y)$.

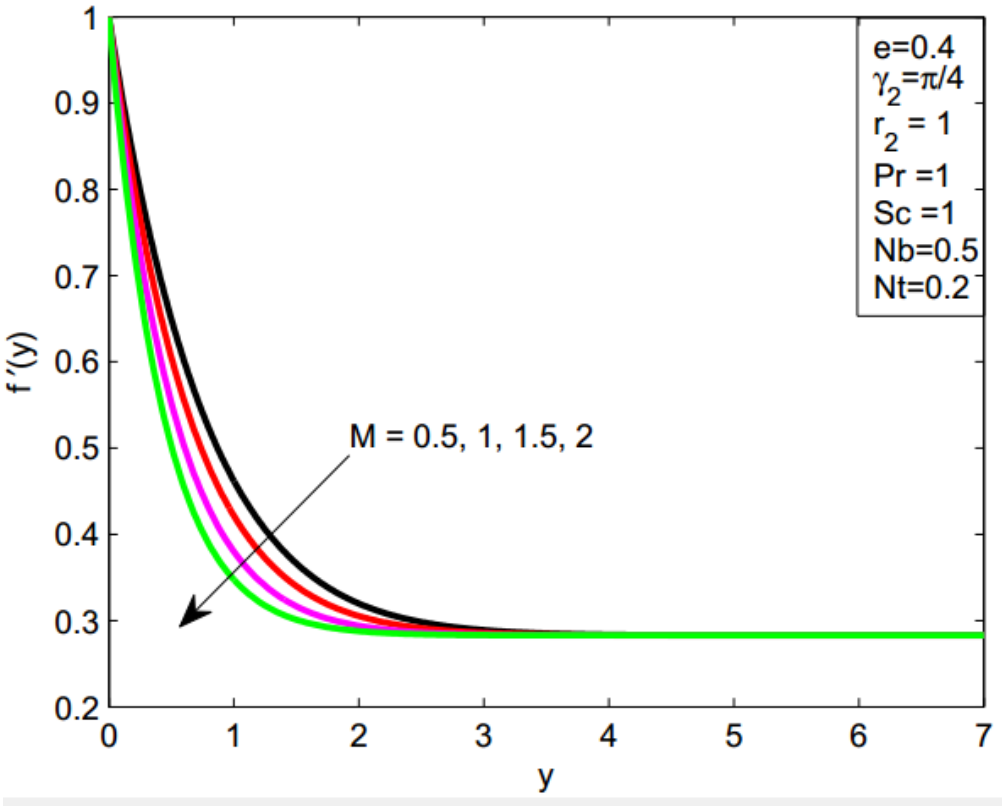

FIGURE 6.6: Consequence of M on f'.

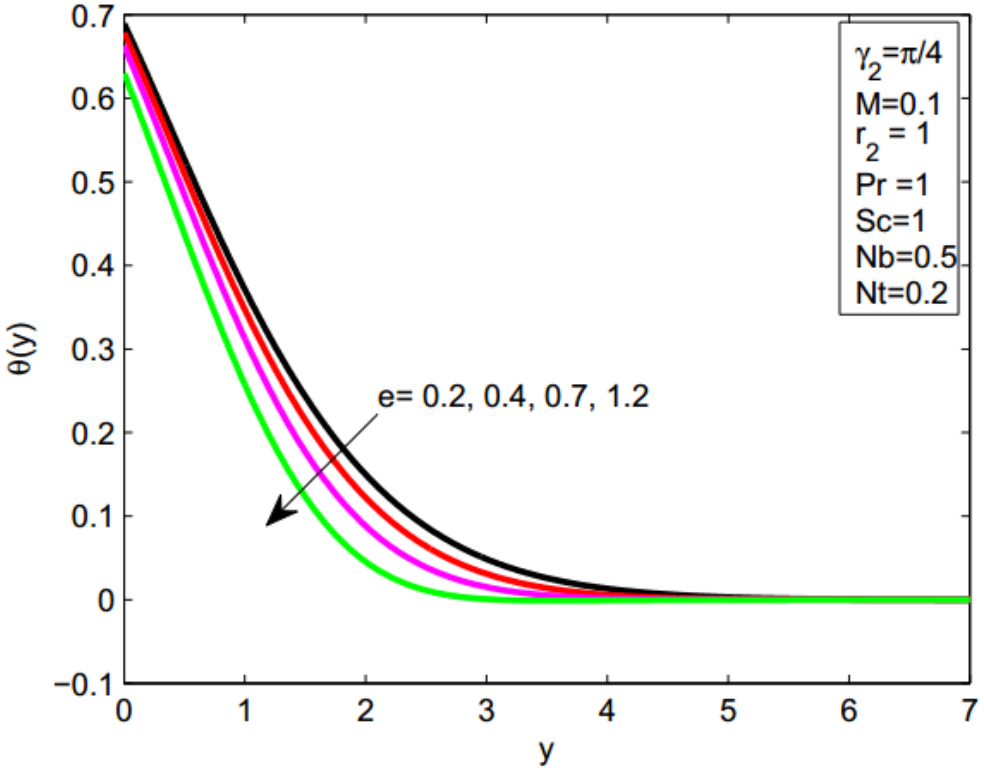

FIGURE 6.7: Consequence of e on θ.

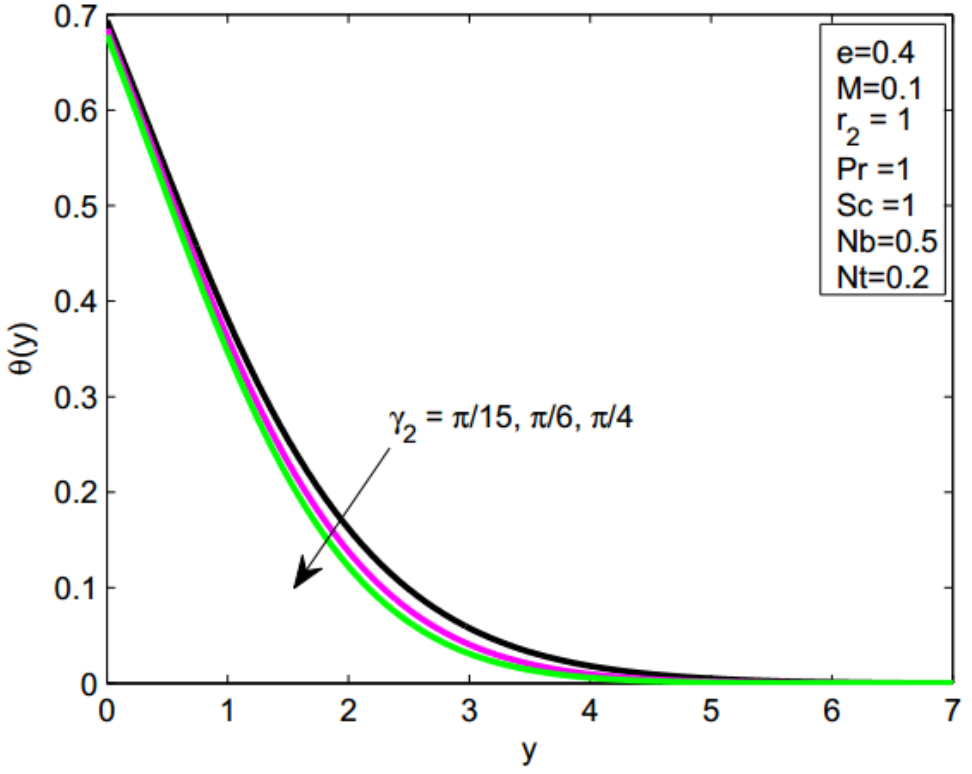

FIGURE 6.8: Consequence of γ_2 on θ.

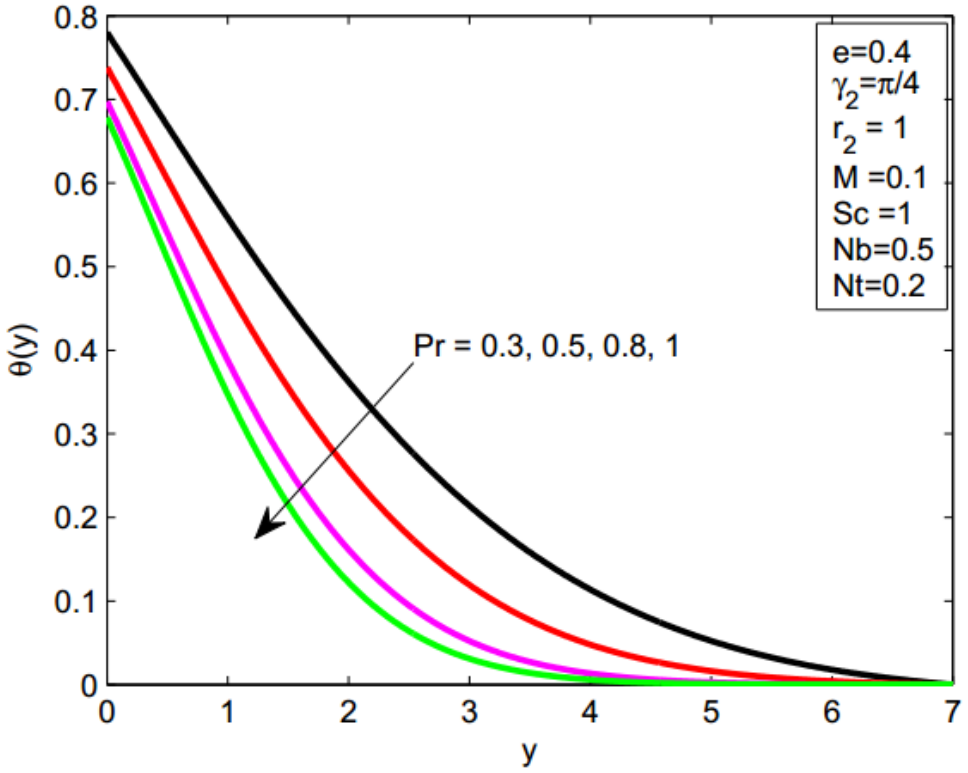

FIGURE 6.9: Consequence of Pr on θ.

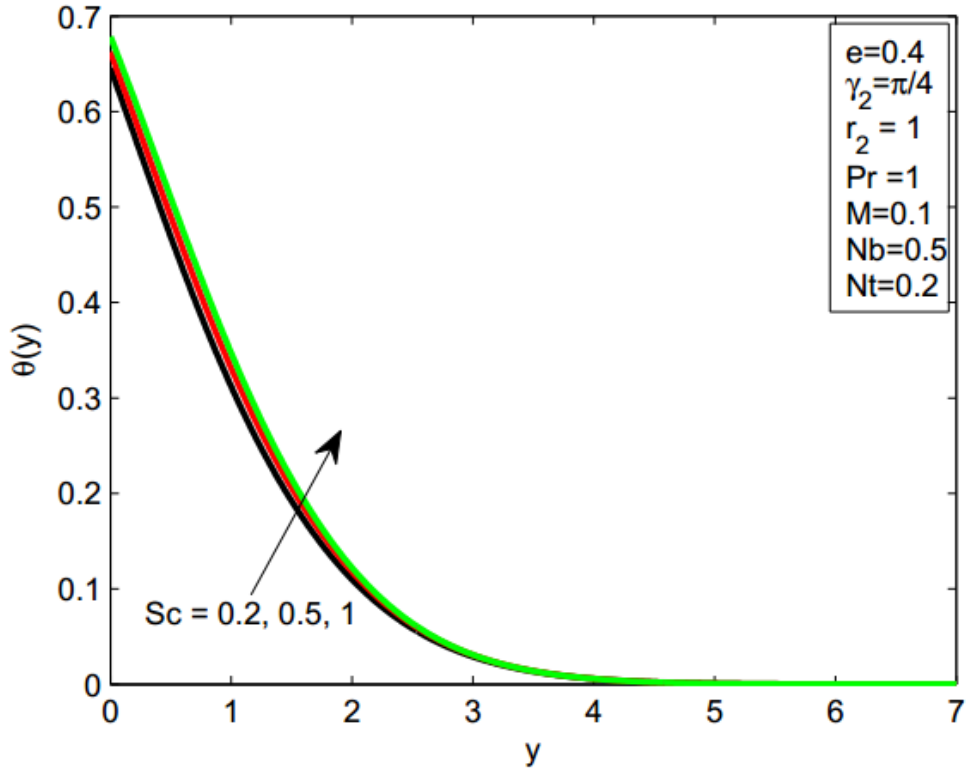

FIGURE 6.10: Consequence of Sc on θ.

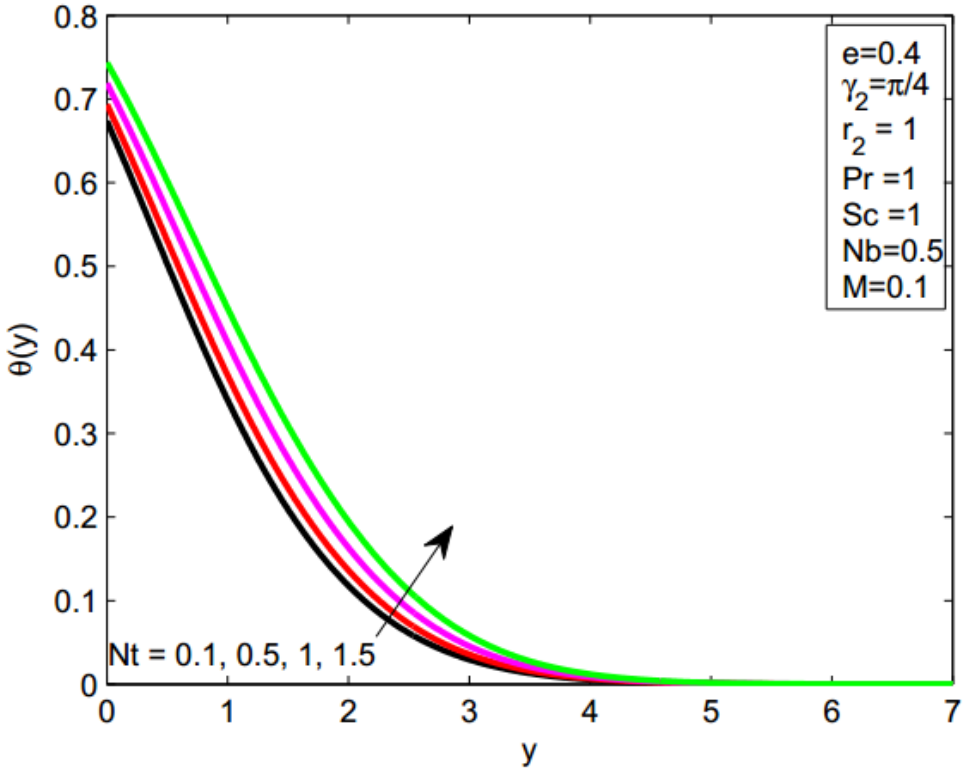

FIGURE 6.11: Consequence of Nt on θ.

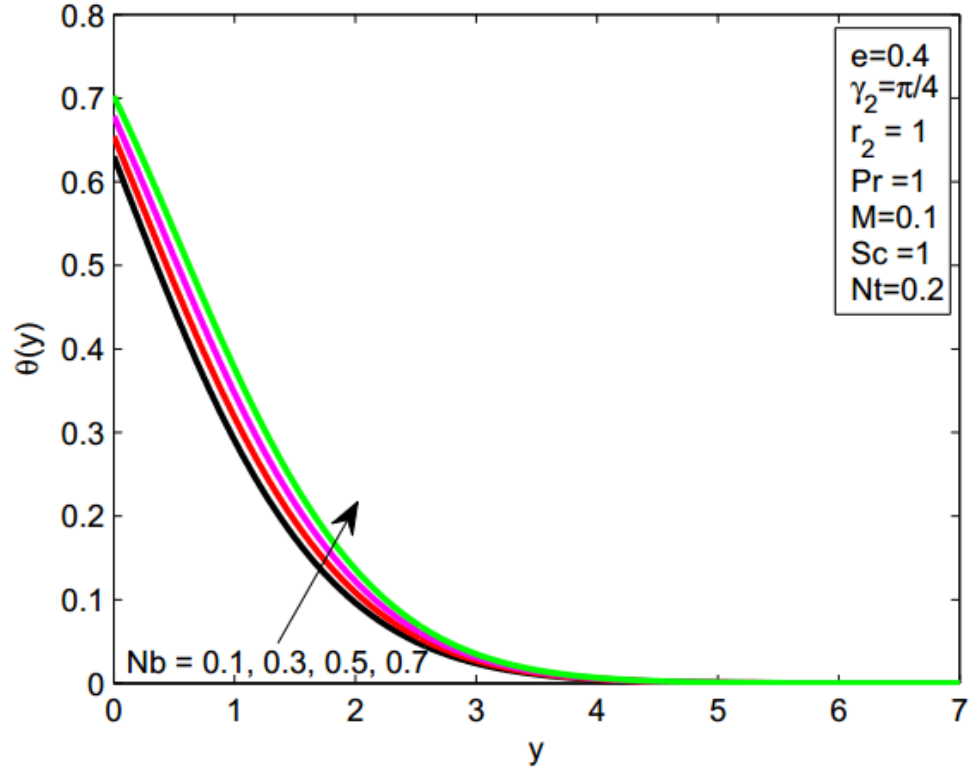

FIGURE 6.12: Consequence of Nb on θ.

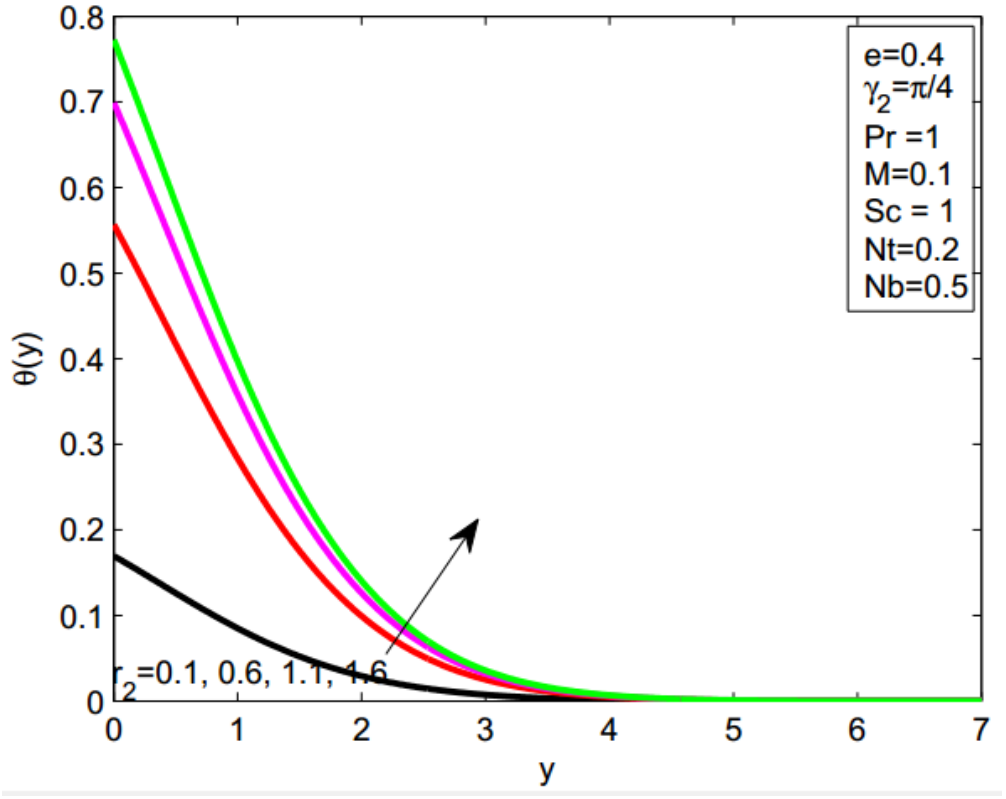

FIGURE 6.13: Consequence of r_2 on θ.

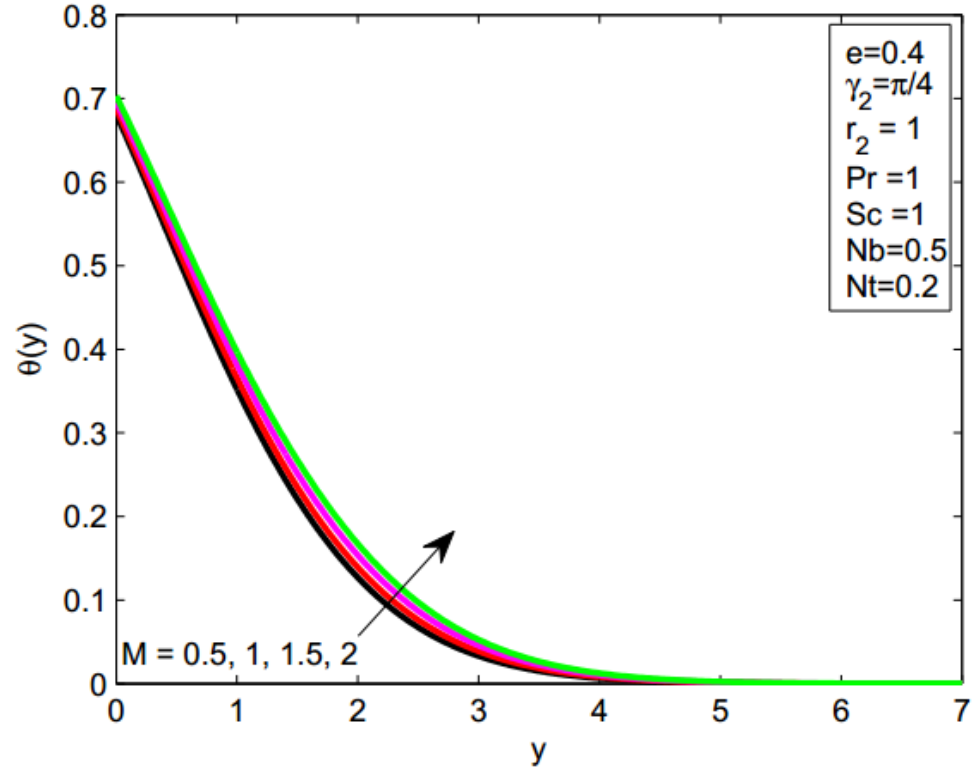

FIGURE 6.14: Consequence of M on θ.

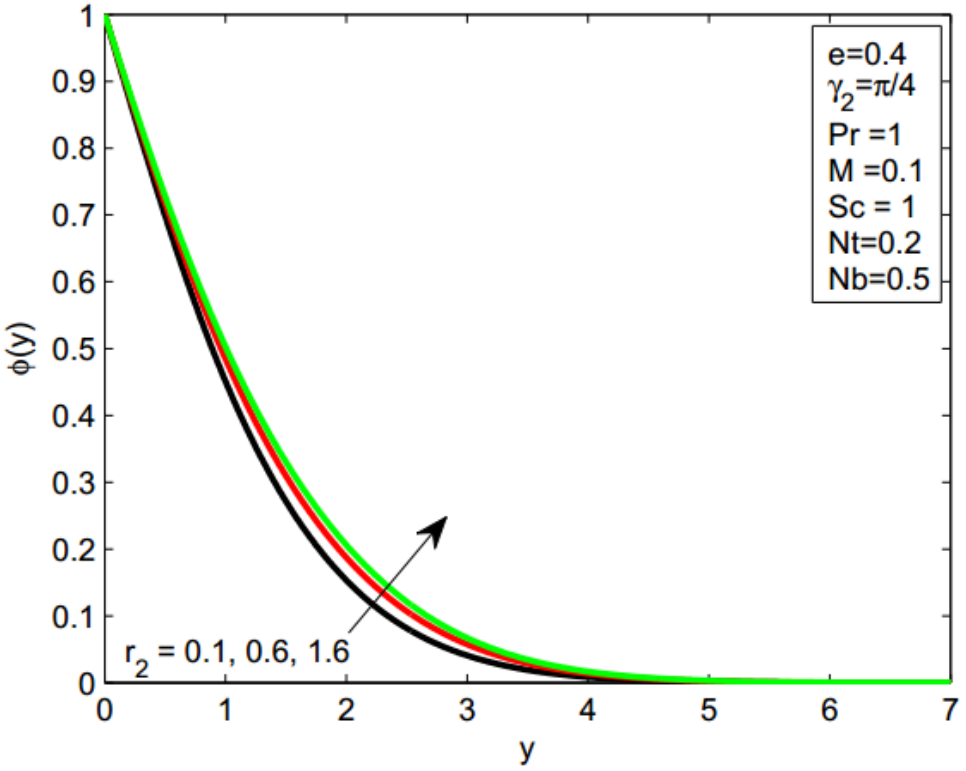

FIGURE 6.15: Impact of r_2 on ϕ.

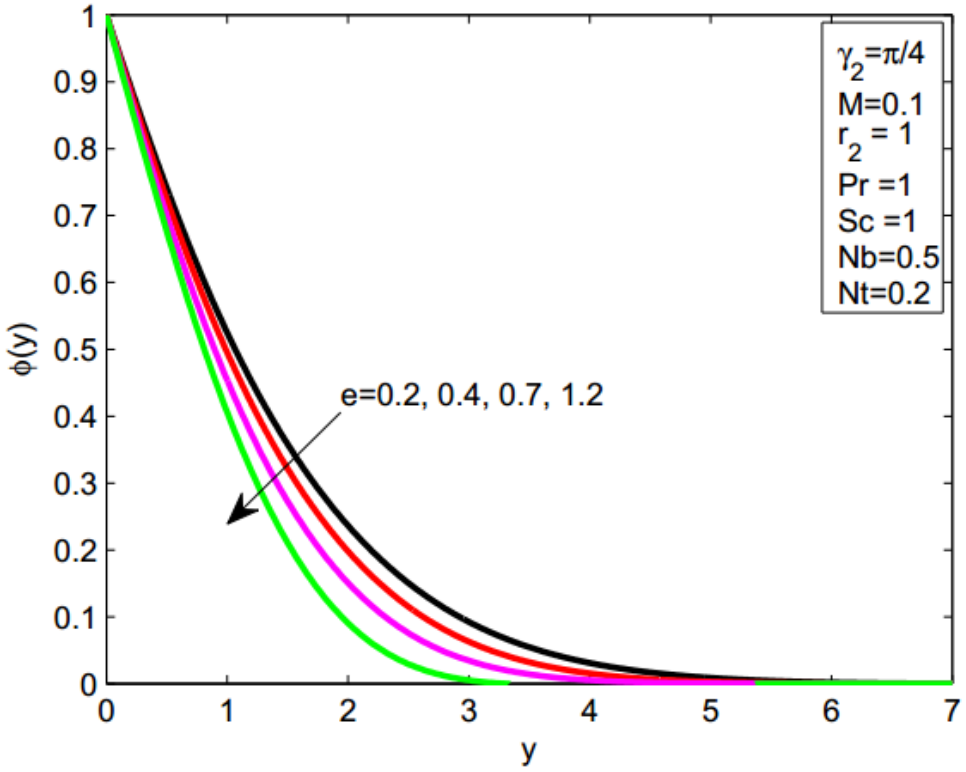

FIGURE 6.16: Impact of e on ϕ.

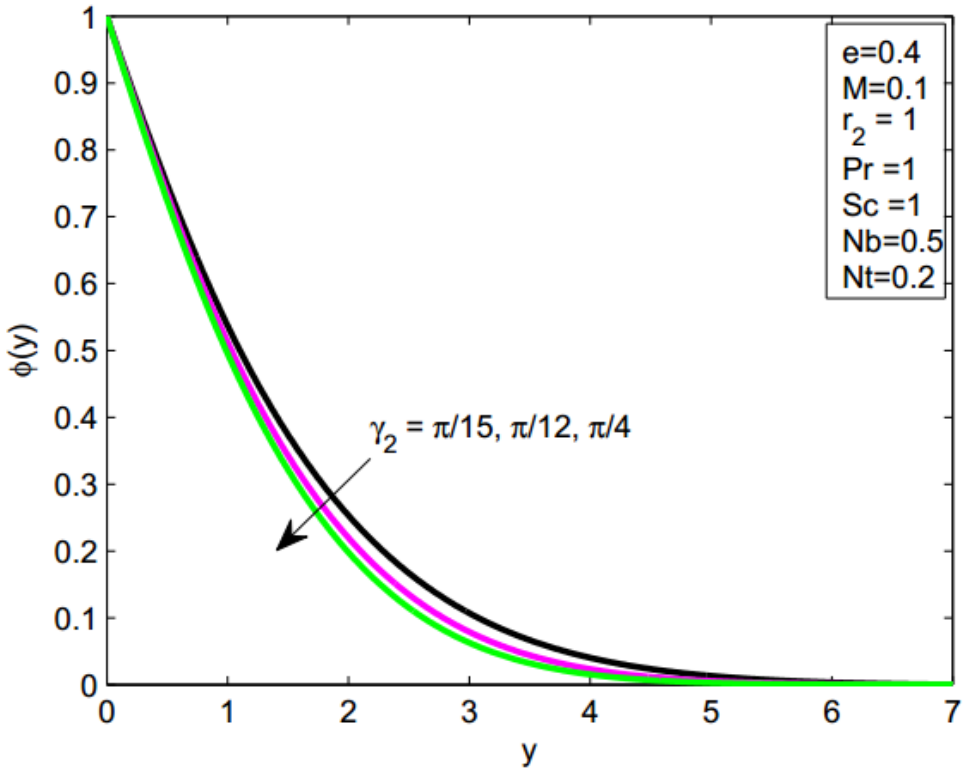

FIGURE 6.17: Impact of γ_2 on ϕ.

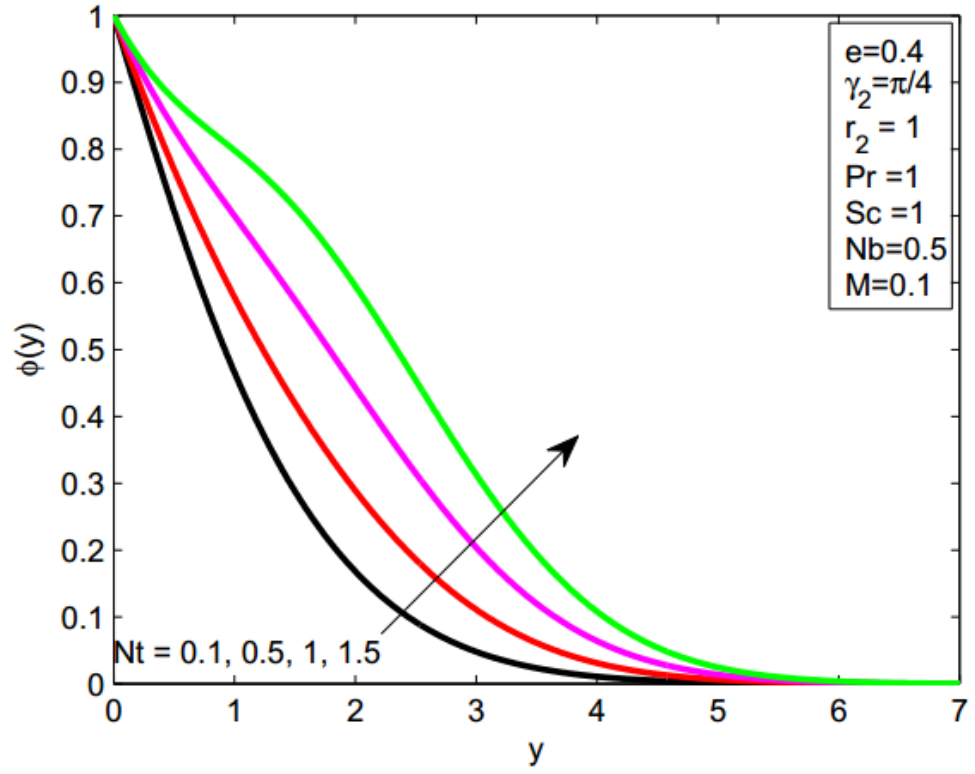

FIGURE 6.18: Consequence of Nt on ϕ.

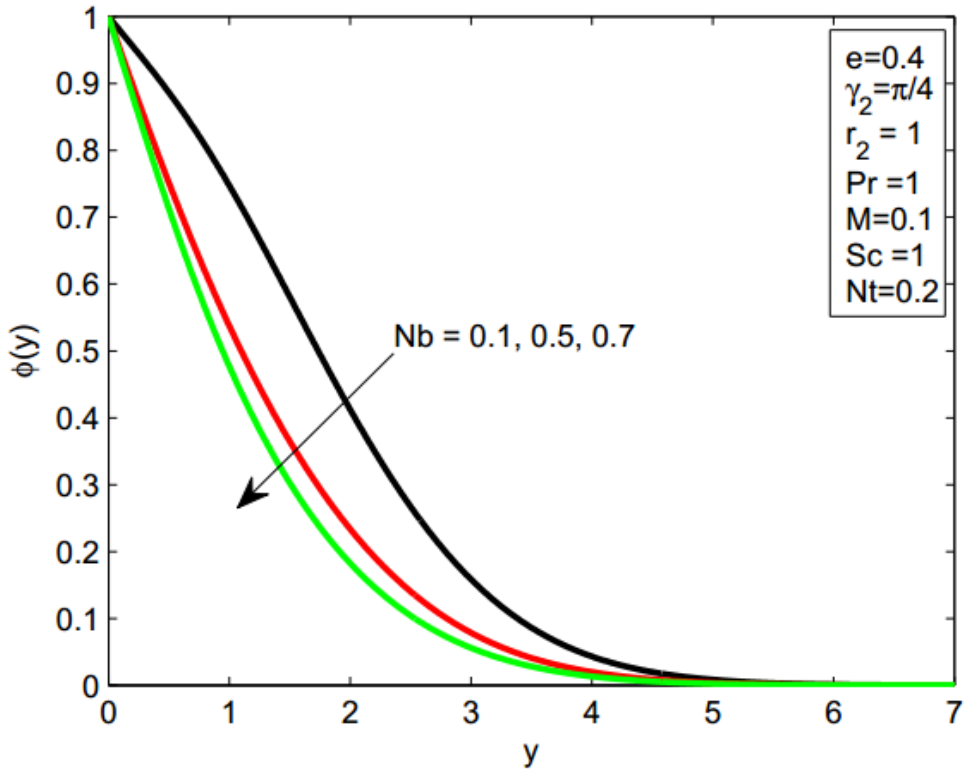

FIGURE 6.19: Consequence of Nb on ϕ.

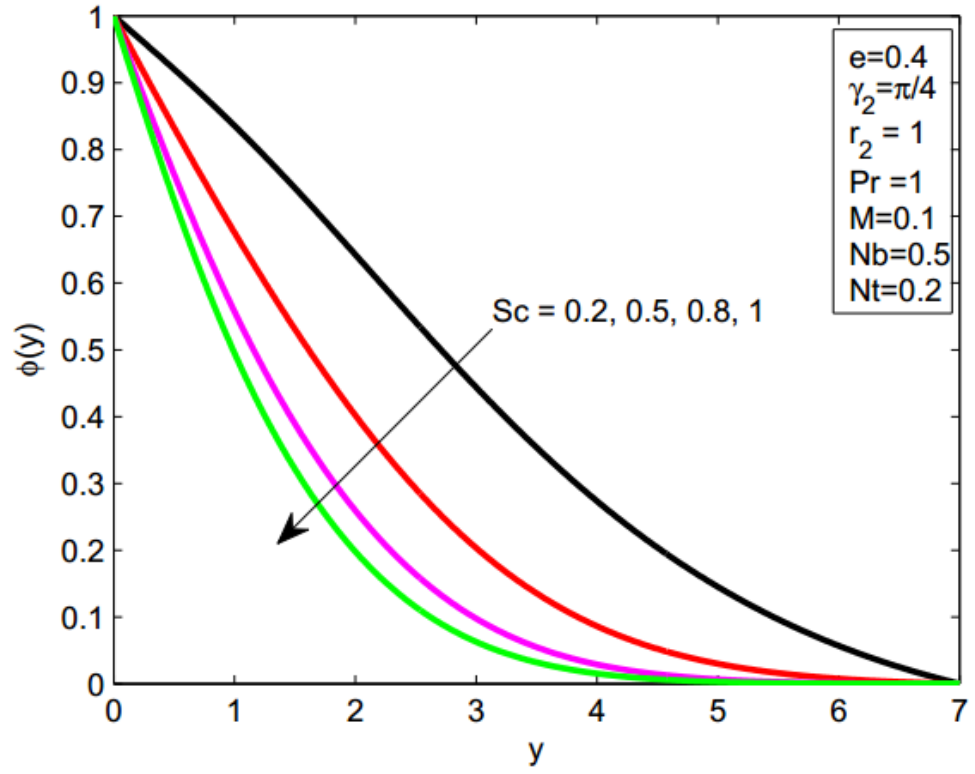

FIGURE 6.20: Impact of Sc on ϕ.

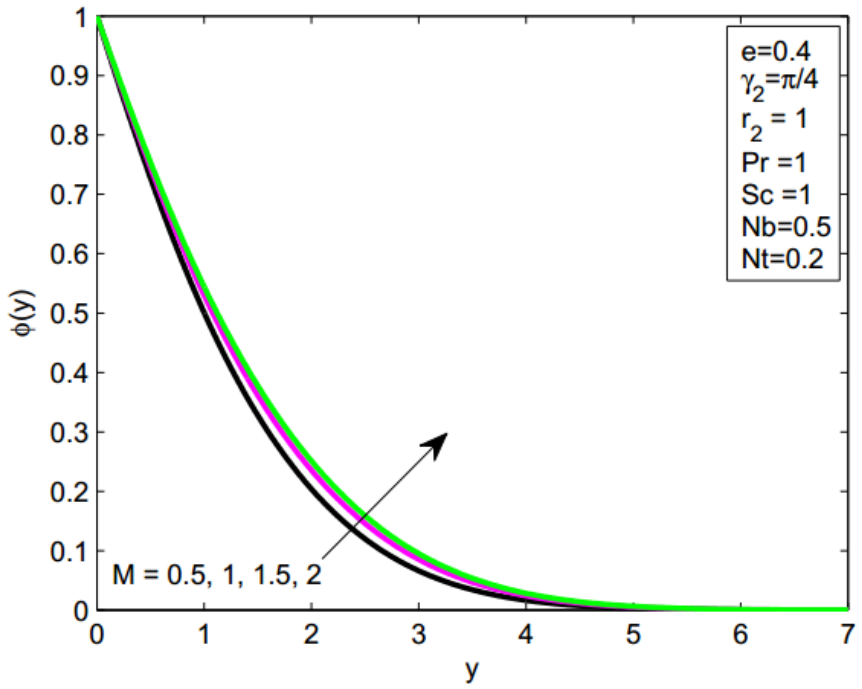

FIGURE 6.21: Impact of M on ϕ.

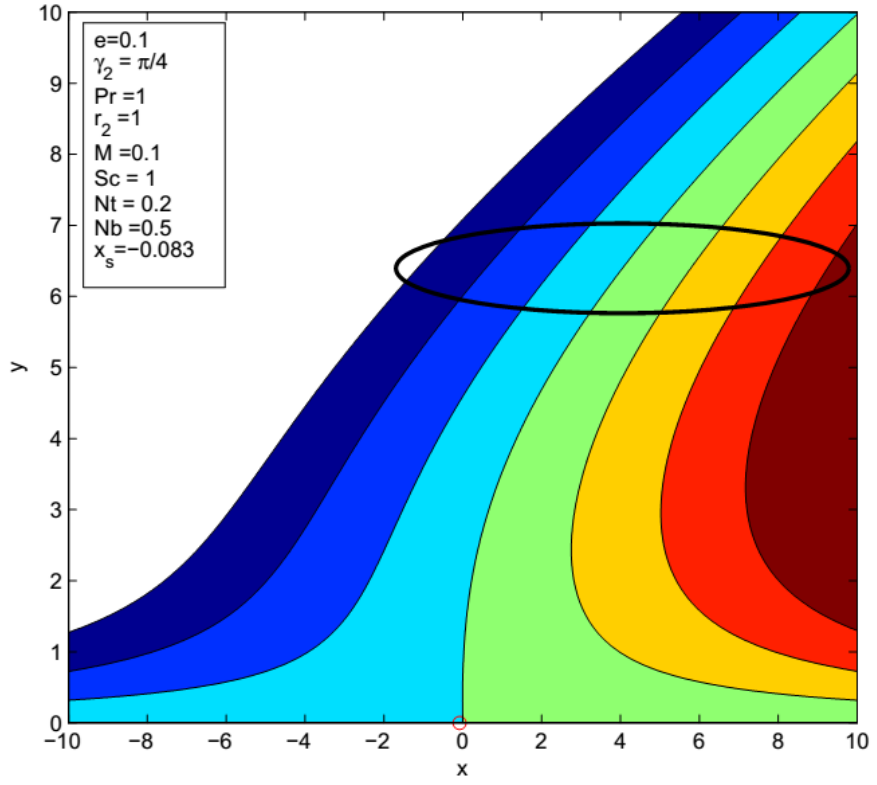

FIGURE 6.22: Stream lines for $e = 0.1$.

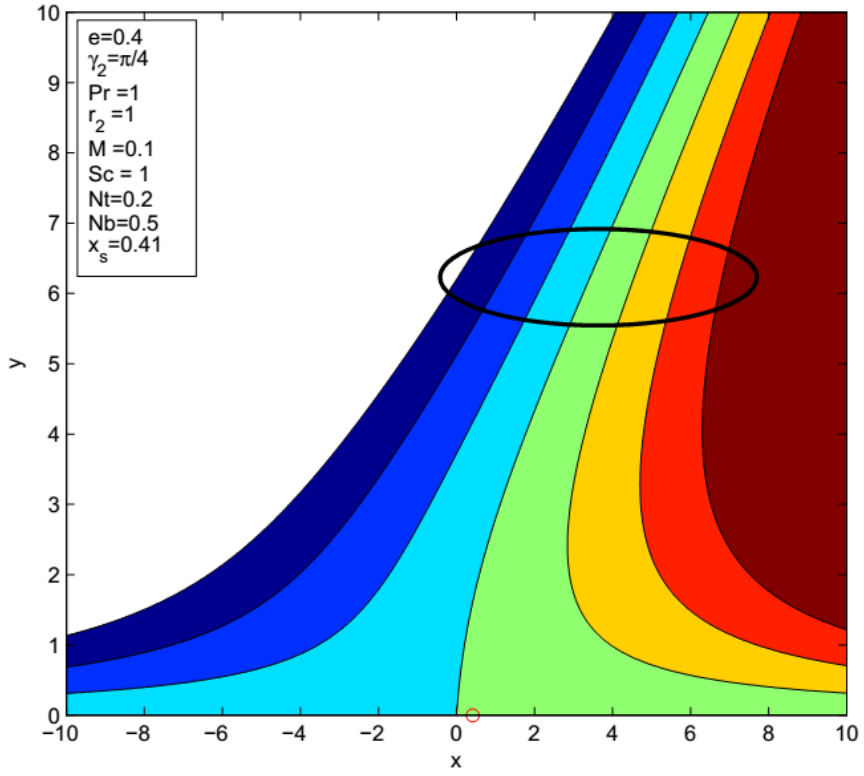

FIGURE 6.23: Stream lines for $e = 0.4$.

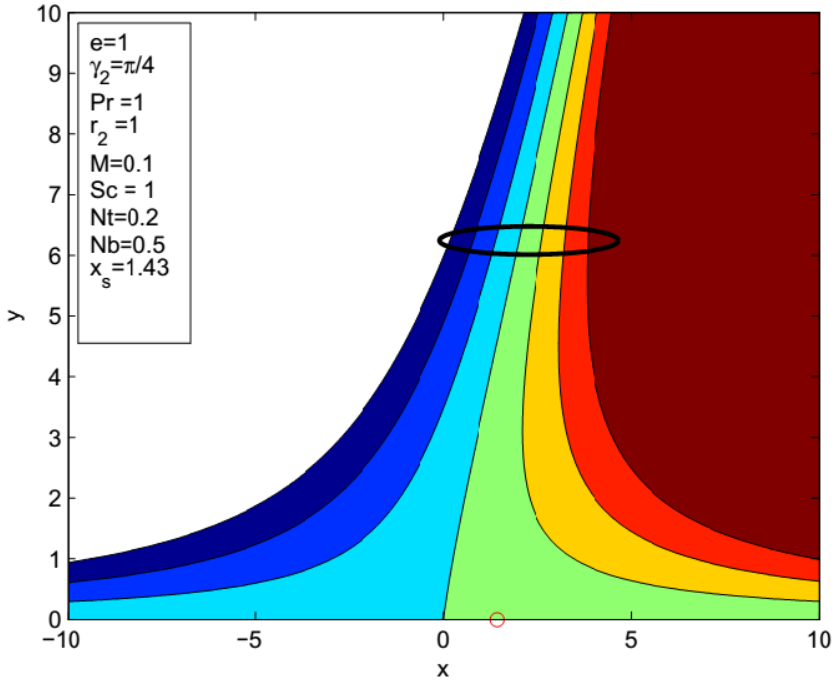

FIGURE 6.24: Stream lines patterns for $e = 1$.

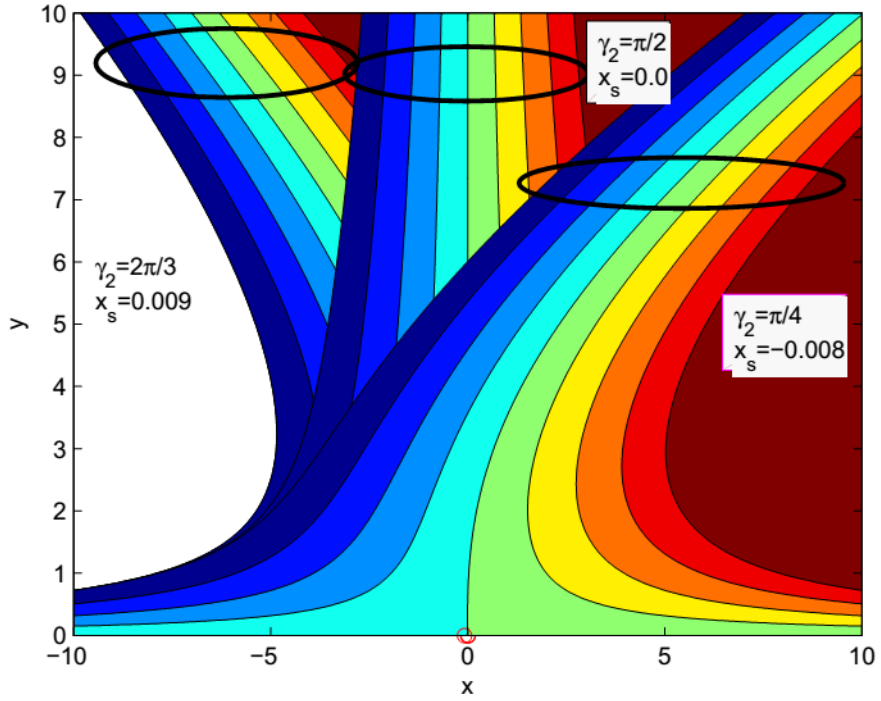

FIGURE 6.25: Stream lines patterns for γ_2.

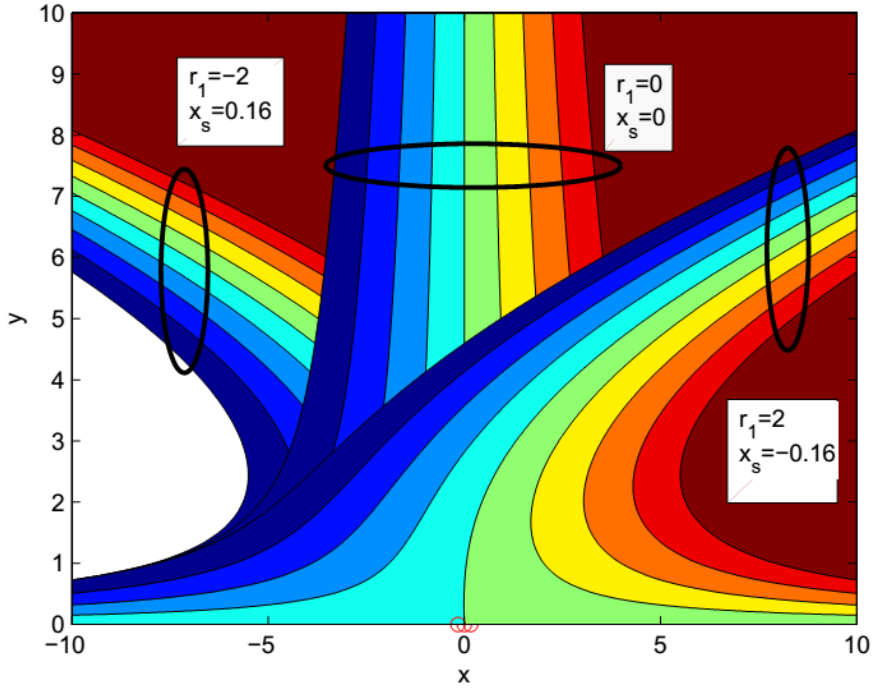

FIGURE 6.26: Stream lines patterns for r_1.

6.5 Concluding Remarks

In the present chapter, the oblique stagnation point along with nanofluid flow for the heat and mass transfer over a linearly stretching sheet in the presence of MHD is addressed. The main points are summarized as follows.

- It is analyzed that the point of zero skin friction along the wall undergoes a shift in the position with the variations in the parameters M, γ_2 and e .
- Nusselt number undergoes the increasing behavior for Biot and Prandtl numbers and decreasing for Magnetic, thermophoresis, Brownian motion and Schmidt number.
- Sherwood number shows an increasing behavior for the Brownian motion and Schmidt number and decreasing profile for Biot, Prandtl, Magnetic and thermophoresis parameters.

Chapter 7

Conclusion

In this dissertation, an analysis of the orthogonal and non orthogonal stagnation point flows for Newtonain, upper convected Maxwell and Williamson fluids over different types of geometries is presented. Partial differential equations are formed by using the law of conservation of mass, Newtons second law of motion and the second law of thermo dynamics. Similarity transformations played a pivotal role for obtaining the ordinary differential equations from the mathematically modeled partial differential equations. In all the cases, these system of differential equations are solved numerically by the classical shooting method together with the RK-4 scheme. Numerical results are further supported by a built-in MATLAB function bvp4c. In all the chapters, results are compared with the previously published articles in limiting cases. The main findings of the thesis are as follows:

- For the upper-convected Maxwell, Newtonian and Williamson fluids, it is observed that with an increase in the magnetic field intensity, velocity profile exhibits a decreasing pattern and an opposite behavior is seen in the thermal boundary layer.
- In case of the upper-convected Maxwell fluid, an increase in the elasticity number and slip coefficients causes a decrease in the velocity phenomenon and an opposite behavior is observed in the temperature profile.
- An enhancement in the stretching ratio parameter results a decrease in the wall shear stress and an increment in the Nusselt number for all the fluid models which are discusssed in this dissertation.

- By increasing the thermal relaxation time, the temperature profile raises up in an UCM fluid as discussed in Chapter number 3.
- The temperature profile reduces in an UCM fluid with an increase in the heat flux relaxation time.
- Concentration profile shows a decreasing pattern for the Schmidt number of an UCM fluid & Newtonian fluids.
- The strength of the homogenous and heterogenous reactions shows a decreasing effect on the concentration distribution in the Willaimson fluid illustrated in Chapter number 5.
- The temperature profile portrays a decreasing pattern in the case of upper-convected Maxwell, Newtonian and Williamson fluids for the increasing values of Prandtl number.
- Speed as well as the skin friction coefficient increases with an enhancement in the curvature parameter in the Willaimson fluid.
- It is analyzed in Chapter number 6 that in case of the non orthogonal stagnation point flows for the Newtonian fluid, the point of zero skin friction along the wall undergoes a shift in the position with the variations in the magnetic parameter M, angle of incidence γ_2 and stretching ratio parameter e.

Bibliography

[1] M. M. Rashidi and E. Erfani, "Analytical method for solving steady MHD convective and slip flow due to a rotating disk with viscous dissipation and Ohmic heating." *Eng. Comp*, vol. 29, p. 562579, 2012.

[2] M. H. Abolbashari, N. Freidoonimehr, F. Nazari, and M. M. Rashidi, "Entropy analysis for an unsteady MHD flow past a stretching permeable surface in nano-fluid." *Powd. tech*, vol. 267, p. 256267, 2014.

[3] M. M. Rashidi, M. Ali, N. Freidoonimehr, B. Rostami, and M. A. Hossain, "Mixed convective heat transfer for MHD viscoelastic fluid flow over a porous wedge with thermal radiation." *Adv. Mech. Eng*, vol. 2014, 2014.

[4] N. Freidoonimehr, M. M. Rashidi, and S. Mahmud, "Unsteady MHD free convective flow past a permeable stretching vertical surface in a nano-fluid." *Int. J. Ther. Sci*, vol. 87, p. 136145, 2015.

[5] M. Turkyilmazoglu, "Magnetic field and slip effects on the flow and heat transfer of stagnation point Jeffrey fluid over deformable surfaces." *Int. J. Heat Mass Tra.*, vol. 71, p. 549556, 2016.

[6] ——, "An analytical treatment for the exact solutions of MHD flow and heat over two-three dimensional deforming bodies." *Int. J. Heat Mass Tra.*, vol. 90, pp. 781–789, 2015.

[7] ——, "Multiple analytic solutions of heat and mass transfer of magnetohydrodynamic slip flow for two types of viscoelastic fluids over a stretching surface." *J. Heat Trans.*, vol. 134, pp. 071 701–1–9, 2012.

[8] ——, "Equivalences and correspondences between the deforming body induced flow and heat in two-three dimensions." *Phy. Fluids*, vol. 28, pp. 043 102–1–10, 2016.

[9] C. Cattaneo, "Sulla conduzione del calore," *Atti Semin. Mat. Fis. Univ. Modena Reggio Emilia*, vol. 3, pp. 83–101, 1948.

[10] C. I. Christov, "On frame indifferent formulation of the Maxwell-Cattaneo model of finite speed heat conduction," *Mech. Res. Commun*, vol. 36, pp. 481–486, 2009.

[11] B. Straughan, "Thermal convection with the Cattaneo-Christov model," *Int. J. Heat Mass Transfer*, vol. 53, pp. 95–98, 2010.

[12] V. Tibullo and V. Zampoli, "A uniqueness result for the Cattaneo-Christov heat conduction model applied to incompressible fluids," *Mech. Res. Commun*, vol. 38, pp. 77–99, 2011.

[13] S. Han, L. Zheng, C. Li, and X. Zhang, "Coupled flow and heat transfer in viscoelastic fluid with Cattaneo-Christov heat flux model," *Appl. Math. Lett.*, vol. 38, pp. 87–93, 2014.

[14] J. A. Khan, M. Mustafa, T. Hayat, and A. Alsaedi, "Numerical study of Cattaneo-Christov heat flux model for viscoelastic flow due to an exponentially stretching surface," *PLOS ONE*, vol. 10(9), p. e0137363, 2015.

[15] J. J. Choi, Z. Rusak, and J. A. Tichy, "Maxwell fluid suction flow in a channel," *Non-Newtonian Fluid Mech*, vol. 85, pp. 165–187, 1999.

[16] Z. Abbas, M. Sajid, and T. Hayat, "MHD boundary-layer flow of an upper-convected Maxwell fluid in a porous channel," *Theor. Comput. Fluid Dyn*, vol. 20, pp. 229–238, 2006.

[17] V. Aliakbar, A. A. Pahlavan, and K. Sadeghy, "The influence of thermal radiation on MHD flow of Maxwellian fluids above stretching sheets," *Commun. Nonlinear Sci. Numer. Simul*, vol. 14, pp. 779–794, 2009.

[18] M. Mustafa, "Cattaneo-Christov heat flux model for rotating flow and heat transfer of upper convected Maxwell fluid," *AIP Advances*, vol. 5, p. 047109, 2015.

[19] M. Kumaria and G. Nath, "Steady mixed convection stagnation-point flow of upper convected Maxwell fluids with magnetic field," *Int. J. Non-Linear Mech*, vol. 44, pp. 1048–1055, 2009.

[20] K. Sadeghy, H. Hajibeygib, and S. M. Taghavia, "Stagnation-point flow of upper-convected Maxwell fluids," *Int. J. Non-Linear Mech*, vol. 41, pp. 1242–1247, 2006.

[21] T. Hayat, M. Awais, M. Qasim, and A. A. Hendi, "Effects of mass transfer on the stagnation point flow of an upper-convected Maxwell (UCM) fluid," *Int. J. Heat Mass Transfer*, vol. 54, pp. 3777–3782, 2011.

[22] T. Hayat, M. Mustafa, S. A. Shehzad, and S. Obaidat, "Melting heat transfer in the stagnation-point flow of an upper-convected Maxwell (UCM) fluid past a stretching sheet," *Int. J. Numer. Meth. Fluids*, vol. 68, pp. 233–243, 2012.

[23] T. Hayat, M. I. Khan, M. Farooq, T. Yasmeen, and A. Alsaedi, "Stagnation point flow with Cattaneo-Christov heat flux and homogeneous-heterogeneous reactions," *J. Mol. Liq*, vol. 220, pp. 49–55, 2016.

[24] A. A. Kendoush, "Theory of stagnation region heat and mass transfer to fluid jets impinging normally on solid surfaces." *Chem. Eng. Proc*, vol. 37, p. 223228, 1998.

[25] I. C. Liu, "A note on heat and mass transfer for a hydromagnetic flow over a stretching sheet." *Int. Com. Heat Mass Trans*, vol. 32, p. 10751084, 2005.

[26] R. Cortell, "Toward an understanding of the motion and mass transfer with chemically reactive species for two classes of viscoelastic fluid over a porous stretching sheet." *Chem. Eng. Proc*, vol. 46, p. 982989, 2007.

[27] J. Sui, L. Zheng, and X. Zhang, "Boundary layer heat and mass transfer with Cattaneo-Christov double-diffusion in upper-convected Maxwell fluid past a stretching sheet with slip velocity." *Int. J. Ther. Sci*, vol. 104, p. 461468, 2016.

[28] Q. Hussain, S. Asghar, T. Hayat, and A. Alsaedi, "Heat transfer analysis in peristaltic flow of MHD Jeffrey fluid with variable thermal conductivity," *Appl. Math. Mech. -Engl. Ed.*, vol. 36(4), pp. 499–516, 2015.

[29] Y. Lin, L. Zheng, and G. Chen, "Unsteady flow and heat transfer of Pseudo-plastic nanoliquid in a finite thinfilm on a stretching surface with variable thermal conductivity and viscous dissipation," *Powder Tech.*, vol. 274, pp. 324–332, 2015.

[30] T. Hayat, A. Shafiq, A. Alsaedi, and S. Asghar, "Effect of inclined magnetic field in flow of third grade fluid with variable thermal conductivity," *AIP Adv.*, vol. 5, p. 087108, 2015.

[31] T. Hayat, M. Waqas, S. A. Shehzad, and A. Alsaedi, "Mixed convection flow of viscoelastic nanofluid by a cylinder with variable thermal conductivity and heat source/sink," *Int. J. Num. Met. Heat Fluid Flow*, vol. 26(1), pp. 214–234, 2016.

[32] X. Si, X. Zhu, L. Zheng, X. Zhang, and P. Lin, "Laminar film condensation of Pseudo-plastic non-Newtonian fluid with variable thermal conductivity on an isothermal vertical plate," *Int. J. Heat Mass Trans.*, vol. 92, pp. 979–986, 2016.

[33] M. Y. Malik, M. Bibi, F. Khan, and T. Salahuddin, "Numerical solution of Williamson fluid flow past a stretching cylinder and heat transfer with variable thermal conductivity and heat generation/absorption," *AIP Adv.*, vol. 6, p. 035101, 2016.

[34] M. G. Reddy, "Unsteady radiative-convective boundary layer flow of a Casson fluid with variable thermal conductivity," *J. Engr. Phy. Thermophy.*, vol. 88(1), pp. 240–251, 2015.

[35] M. Ghalambaza, A. Behseresht, J. Behseresht, and A. Chamkha, "Effects of nanoparticles diameter and concentration on natural convection of the Al_2O_3 water nanofluids considering variable thermal conductivity around a vertical cone in porous media," *Adv. Powder Tech.*, vol. 26, pp. 224–235, 2015.

[36] G. J. Li, J. Ma, and B. W. Li, "Collocation spectral method for the transient conduction-radiation heat transfer with variable thermal conductivity in two-dimensional rectangular enclosure," *J. Heat Trans.*, vol. 137, pp. 032 701–1, 2015.

[37] I. L. Animasaun and N. Sandeep, "Buoyancy induced model for the flow of 36nm Alumina-water nanofluid along upper horizontal surface of a paraboloid of revolution with variable thermal conductivity and viscosity," *Powder Tech.*, 2016.

[38] R. V. Williamson, "The flow of pseudoplastic materials," *Ind. Engr. Chem. Res.*, vol. 11, pp. 1108–1111, 1929.

[39] M. Y. Malik and T. Salahuddin, "Numerical solution of MHD stagnation point flow of Williamson fluid model over a stretching cylinder," *Int. J. Nonlinear Sci. Num. Sim.*, vol. 16(4), pp. 161–164, 2015.

[40] M. Y. Malik, T. Salahuddin, A. Hussain, S. Bilal, and M. Awais, "Homogeneous-heterogeneous reactions in Williamson fluid model over a stretching cylinder by using Keller box method," *AIP Adv.*, vol. 5, p. 107227, 2015.

[41] T. Salahuddin, M. Y. Malik, A. Hussain, S. Bilal, and M. Awais, "MHD flow of Cattaneo-Christov heat flux model for Williamson over a stretching sheet with variable thickness: using numerical approach," *J. Mag. Mag. Mat.*, vol. 5, p. doi.org/10.1016/j.jmmm.2015.11.022, 2015.

[42] T. Hayat, A. Shafiq, and A. Alsaedi, "Hydromagnetic boundary layer flow of Williamson fluid in the presence of thermal radiation and Ohmic dissipation," *Alex. Engr J.*, pp. 1–12, 2016.

[43] B. C. Prasannakumara, B. J. Gireesha, R. S. R. Gorla, and M. R. Krishnamurthy, "Effects of chemical reaction and nonlinear thermal radiation on Williamson nanofluid slip flow over a stretching sheet embedded in a porous medium," *J. Aerosp. Eng.*, vol. 04016019, pp. 1–10, 2016.

[44] T. Hayat, S. Bibi, M. Rafiq, A. Alsaedi, and F. M. Abbasi, "Effect of an inclined magnetic field on peristaltic flow of Williamson fluid in an inclined channel with convective conditions," *J. Mag. Mag. Mat.*, p. doi .org/10.1016/ j .jmmm.2015.10.107, 2015.

[45] M. M. Bhatti and M. M. Rashidi, "Effects of thermo-diffusion and thermal radiation on Williamson nanofluid over a porous shrinking/stretching sheet," *J. Mol. liq.*, p. doi:10.1016/j.molliq.2016.05.049, 2016.

[46] T. Hayat, S. Qayyum, M. Imtiaz, and A. Alsaedi, "Impact of Cattaneo-Christov heat flux in Jeffrey fluid flow with homogeneous/heterogeneous reactions," *PLOS ONE*, vol. 11(2), p. e0148662, 2016.

[47] T. Hayat, M. Imtiaz, A. Alsaedi, and S. Almezal, "On Cattaneo-Christov heat flux in MHD flow of Oldroyd-B fluid with homogeneous-heterogeneous reactions," *J. Mag. Mag. Mat.*, vol. 401, pp. 296–303, 2016.

[48] J. V. R. Reddy, V. Sugunamma, and N. Sandeep, "Effect of nonlinear thermal radiation on MHD flow between rotating plates with homogeneous-heterogeneous reactions," *Int. J. Engr. Res. Africa*, vol. 20, pp. 130–143, 2016.

[49] S. Mansur, A. Ishak, and I. Pop, "MHD homogeneous-heterogeneous reactions in a nanofluid due to a permeable shrinking surface," *J. App. Fluid Mech.*, vol. 9(3), pp. 1073–1079, 2016.

[50] P. K. Kameswaran, S. Shaw, P. Sibanda, and P. V. S. N. Murthy, "Homogeneous-heterogeneous reactions in a nanofluid flow due to a porous stretching sheet," *Int. J. Heat Mass Tran.*, vol. 57(2), p. 465472, 2013.

[51] M. R. Eid, "Chemical reaction effect on MHD boundary-layer flow of two-phase nanofluid model over an exponentially stretching sheet with a heat generation," *J. Mol. Liq.*, vol. 220, p. 718725, 2016.

[52] W. Ibrahim, "The effect of induced magnetic field and convective boundary condition on MHD stagnation point flow and heat transfer of upper-convected Maxwell fluid in the presence of nanoparticle past a stretching sheet," *Prop. Power Res.*, vol. 5(2), p. 164175, 2016.

[53] O. D. Makinde, T. Iskander, F. Mabood, W. A. Khan, and M. S. Tshehla, "MHD Couette-Poiseuille flow of variable viscosity nanofluids in a rotating permeable channel with Hall effects," *J. Mol. Liq.*, vol. 221, p. 778787, 2016.

[54] H. Rosali, A. Ishak, R. Nazar, and I. Pop, "Mixed convection boundary layer flow past a vertical cone embedded in a porous medium subjected to a convective boundary condition," *Prop. Power Res.*, vol. 5(2), p. 118122, 2016.

[55] F. Mabood, S. M. Ibrahim, M. M. Rashidi, M. S. Shadloo, and G. Lorenzini, "Non-uniform heat source/sink and soret effects on MHD non-Darcian convective flow past a stretching sheet in a micropolar fluid with radiation," *Int. J. Heat Mass Tran.*, vol. 93, p. 674682, 2016.

[56] K. Hiemenz, "Die grenzschicht an einem in den gleichfrmigen flessigkeitsstrom eingetauchten geraden kreiszylinder," *Dinglers Polytech. J*, vol. 5, pp. 321–326, 1911.

[57] F. Homann, "Die einfluss grsse zahigkeit bei der strmung um der zylinder und um die kugel." *J. Appl. Math. Mech.*, vol. 16, pp. 153–164, 1936.

[58] J. T. Stuart, "The viscous flow near a stagnation point when the external flow has uniform vorticity," *J. Aerosp. Sci.*, vol. 26, pp. 124–125, 1959.

[59] K. J. Tamada, "Two-dimensional stagnation point flow impinging obliquely on a plane wall," *J. Phys. Soc. Jpn.*, vol. 46, pp. 310–311, 1979.

[60] F. Labropulu, J. M. Dorrepaal, and O. P. Chandna, "Oblique flow impinging on a wall with suction or blowing," *Acta. Mech.*, vol. 115, pp. 15–25, 1996.

[61] Y. Y. Lok, N. Amin, and I. Pop, "Non-orthogonal stagnation point flow towards a stretching sheet," *Int. J. Nonlinear Mech.*, vol. 41, pp. 622–627, 2006.

[62] P. Singh, D. Sinha, and N. S. Tomer, "Oblique stagnation-point Darcy flow towards a stretching sheet," *J. App. Fluid Mech.*, vol. 5, pp. 29–37, 2012.

[63] G. C. Dash, R. S. Tripathya, M. M. Rashidi, and S. R. Mishra, "Numerical approach to boundary layer stagnation-point flow past a stretching/shrinking sheet." *J. Mol. Liq.*, vol. 221, p. 860866, 2016.

[64] F. Mabood, S. Shateyi, M. M. Rashidi, E. Momoniat, and N. Freidoonimehr, "MHD stagnation point flow heat and mass transfer of nanofluids in porous medium with radiation, viscous dissipation and chemical reaction." *Adv. Powd. Tech.*, vol. 27, p. 742749, 2016.

[65] T. Hayat, M. I. Khan, M. Farooq, T. Yasmeen, and A. Alsaedi, "Stagnation point flow with Cattaneo-Christov heat flux and homogeneous-heterogeneous reactions." *J. Mol. Liq.*, vol. 20, p. 4955, 2016.

[66] F. Labropulu, D. Li, and I. Pop, "Non-orthogonal stagnation-point flow towards a stretching surface in a non Newtonian fluid with heat transfer," *Int. J. Therm. Sci.*, vol. 49, pp. 1042–1050, 2010.

[67] T. R. Mahapatra and A. S. Gupta, "Heat transfer in stagnation point flow towards a stretching sheet," *Heat Mass Transfer*, vol. 38, pp. 517–521, 2002.

[68] Y. Y. Lok, J. H. Merkin, and I. Pop, "MHD oblique stagnation-point flow towards a stretching/shrinking surface," *Meccanica*, vol. 50, pp. 2949–2961, 2015.

[69] T. C. Chiam, "Heat transfer with variable conductivity in a stagnation-point flow towards a stretching sheet," *Heat Mass Transfer*, vol. 23, pp. 239–248, 1996.

[70] Z. Y. Guo, D. Y. Li, and B. X. Wang, "A novel concept for convective heat transfer enhancement," *Heat Mass Transfer*, vol. 41, pp. 2221–2225, 1998.

[71] S. Yao, T. Fang, and Y. Zhong, "Heat transfer of a generalized stretching/shrinking wall problem with convective boundary conditions," *Commun. Nonlinear Sci. Numer Simul.*, vol. 16, pp. 752–760, 2011.

[72] T. Grosan, I. Pop, C. Revnic, and D. B. Ingham, "Magnetohydrodynamic oblique stagnation-point flow," *Meccanica*, vol. 44, pp. 565–572, 2009.

[73] P. Singh, N. S. Tomer, S. Kumar, and D. Sinha, "MHD oblique stagnation-point flow towards a stretching sheet with heat transfer," *J. Appl. Math. Mech.*, vol. 6, pp. 94–111, 2010.

[74] S. Nadeem, R. Mehmood, and N. S. Akbar, "Combined effects of magnetic field and partial slip on obliquely striking rheological fluid over a stretching surface," *J. Magn. Magn. Mater.*, vol. 378, pp. 457–462, 2015.

[75] Y. Y. Lok, J. H. Merkin, and I. Pop, "MHD oblique stagnation-point flow towards a stretching/shrinking surface," *Meccanica*, vol. 50, pp. 2949–2961, 2015.

[76] S. U. S. Choi and J. A. Eastman, "Enhancing thermal conductivity of fluids with nanoparticles, processing of ASME," *Int. Mech. Eng. Congr. Expo*, vol. 66, pp. 99–105, 1995.

[77] X. Q. Wang and A. S. Mujumdar, "Heat transfer characteristics of nanofluids: a review," *Int. J. Therm. Sci.*, vol. 46, pp. 1–19, 2007.

[78] J. Buongiorno, "Convective transport in nanofluids," *Trans. ASME*, vol. 128, pp. 240–250, 2006.

[79] D. A. Nield and A. V. Kuznetsov, "The Cheng-Minkowycz problem for natural convective boundary-layer flow in a porous medium saturated by a nanofluid," *Int. J. Heat Mass Tran.*, vol. 52, pp. 5792–5795, 2009.

[80] W. A. Khan and I. Pop, "Boundary-layer flow of a nanofluid past a stretching sheet," *Int. J. Heat Mass Tran.*, vol. 53, pp. 2477–2483, 2010.

[81] R. Haq, S. Nadeem, Z. H. Khan, and N. S. Akbar, "Thermal radiation and slip effects on MHD stagnation point flow of nanofluid over a stretching sheet," *Physica, E*, vol. 65, pp. 17–23, 2015.

[82] S. Nadeem, R. Mehmood, and N. S. Akbar, "Optimized analytical solution for oblique flow of a Casson-nanofluid with convective boundary conditions," *Int. J. Therm. Sci.*, vol. 78, pp. 90–100, 2014.

[83] K. S. N. Raju, "Fluid mechanics, heat transfer, and mass transfer (chemical engineering practice)," *A. John Wiley and sons*, vol. 1.

[84] S. N. Ha, "A nonlinear shooting method for two-point boundary value problems," *Comp. Maths.*, vol. 11, pp. 1411–1420, 2001.

[85] T. Y. Na, "Computational methods in engineering boundary value problems," *Academic Press*, 1979.

[86] L. F. Shampine, M. W. Reichelt, and J. Kierzenka, "Solving boundary value problems for ordinary differential equations in MATLAB with bvp4c," *http://www.mathworks.com/bvp_tutorial*.

[87] M. S. Abel, J. V. Tawade, and M. M. Nandeppanavar, "MHD flow and heat transfer for the upper-convected Maxwell fluid over a stretching sheet." *Meccanica*, vol. 47, p. 385393, 2012.

[88] T. R. Mahapatra and A. S. Gupta, "Heat transfer in stagnation-point flow towards a stretching sheet," *Heat Mass Trans.*, vol. 38, pp. 517–521, 2002.

[89] R. Nazar, N. Amin, D. Filip, and I. Pop, "Unsteady boundary layer flow in the region of the stagnation point on a stretching sheet," *Int. J. Eng. Sci.*, vol. 42, p. 12411253, 2004.

[90] M. Y. Malik and T. Salahuddin, "Numerical solution of MHD stagnation point flow of Williamson fluid model over a stretching cylinder," *Int. J. Nonlinear Sci. Num. Sim.*, pp. 1–4, 2015.

[91] S. Nadeem, R. Mehmood, and N. S. Akbar, "Oblique stagnation point flow of a Casson-nano fluid towards a stretching surface with heat transfer," *J. Comp. Theor. Nanosci.*, vol. 11, pp. 1422–1432, 2014.